University of Stavanger

Faculty of Science and Technology

MASTER'S THESIS

Study program/ Specialization: Master`s degree in structural engineering and materials science – specialization in offshore structures.	Spring semester, 2013 Open / ~~Restricted access~~
Writer: Endre Ulversøy	…… (Writer's signature)
Faculty supervisor: Ove Tobias Gudmestad External supervisor(s): Meric Pakkan (Subsea7)	
Title of thesis: Finite element analysis and experimental testing of lifting capacity for GRP cover.	
Credits (ECTS): 30	
Key words: - Glass Reinforced Plastic (GRP) - Subsea protection cover - Finite element analysis (FEA) - Progressive analysis - Lifting capacity	Pages: 64 + enclosure: 49 Stavanger, 14th June, 2013. Date/year

Front page for master thesis
Faculty of Science and
Technology
Decision made by the Dean October 30th 2009

Abstract

Structures made of glass reinforced plastic (GRP), often abbreviated GRP cover, are used to protect subsea equipment in the oil and gas industry. These structures need to be lifted during fabrication, transportation and during the installation. The present work investigates the lifting capacity of the GRP covers. The aim is to achieve a more accurate analytical estimate of the lifting capacity, with a desire to replace the simplified hand calculations used today. In order to investigate the lifting capacity, a lifting point (reinforced lifting holes made of GRP) is studied with both finite element analysis and experimental tests in a hydraulic tensile bench.

Three different test setups, Case 1, Case 2 and Case 3 are investigated. Case 1 is a representation of a lift through the splash zone during installation, where the GRP cover is in an upright vertical position. Case 2 is an approximation of a horizontal lift with the lifting point located on top of the cover, causing the lifting point to encounter out-of-plane loads. Case 3 is a representation of a horizontal four-point lift, with the lifting point placed on the side walls. The experimental tests were performed in collaboration with Highcomp AS at Westcon Løfteteknikk in Haugesund.

The finite element analysis represents the test setup in the hydraulic tensile bench in order to achieve comparable data. Finite element analysis can reduce cost and time compared with physical experiments. For Case 1, with in-plane loads representing the lifting through the splash zone, the results achieved were within a 2% error margin. For the out-of-plane situation (Case 2) with solid elements, the results were within a 20% error margin. The results from the in-plane and out-of-plane scenarios were used in a capacity evaluation to create a graph which represents all results and takes into account the out-of-plane angle from the lifting slings. This graph is easy to use in design and provides good results. Based on the comparison of the results, it was concluded that the Puck criterion with gradual degradation provides the most accurate estimate for the capacity and that use of this criterion can replace simplified hand calculation and reduce the number of physical experiments in the future.

Based on these findings, an improvement study was conducted for a 30 mm laminate with Puck criterion and gradual degradation with a new lay-up consisting of fibers at [0, 90, +45, -45] degrees, compared to the one used today [0, 90]. The results of the new study showed an increase of over 28% for the capacity in Case 1 and an increase of over 16% compared with Case 2. These are interesting results, leading to the conclusion that by introducing the fiber directions $\pm$ 45 degrees, one can enhance the capacity of the material by about 20%, and it is easy and efficient to implement in a new design of the lifting point used in GRP covers.

Preface

This Master Thesis has been prepared at the Department of Mechanical and Structural Engineering and Material Science at the University of Stavanger (UiS), Norway. The subject was proposed by the Structural department of Subsea 7 in Stavanger in collaboration with the University of Stavanger. First of all I would like to thank my supervisor professor Ove Tobias Gudmestad (Department of Mechanical and Structural Engineering and Material Science) and co-supervisor Senior Engineer Meric Pakkan (Structural Department, Subsea 7). I am very grateful for the support and guidance throughout the thesis. I would also like to thank Pål Myge (Structural Discipline Leader, Subsea 7) for providing me with a computer and an office place at Subsea 7 in Stavanger.

Stavanger, June 14, 2013.

Endre Ulversøy

Nomenclature

Abbreviations

GRP	*Glass reinforced plastic*
FRP	*Fiber reinforced plastic*
DNV	*Det Norske Veritas*
Te	*Tons*
3D	*Three dimensional*
2D	*Two dimensional*
UiS	*University of Stavanger*
FE	*Finite Element*
FEA	*Finite Element Analysis*
FEM	*Finite Element Method*
CLT	*Classical Laminate Theory*

Symbols

In the following list the most used symbols are presented. If the symbols are not mentioned in this list they are explained in the present with the relevant equations.

ε_1	*Strain in principle direction 1*	
ε_2	*Strain in principle direction 2*	
ε_3	*Strain in principle direction 3*	
γ_{12}	*Strain associated with 12 plane*	
γ_{13}	*Strain associated with 13 plane*	
γ_{23}	*Strain associated with 23 plane*	
σ_1	*Stress in principle direction 1*	*N/mm^2 (MPa)*
σ_2	*Stress in principle direction 2*	*N/mm^2 (MPa)*
σ_3	*Stress in principle direction 3*	*N/mm^2 (MPa)*
τ_{12}	*Stress associated with 12 plane*	*N/mm^2 (MPa)*
τ_{13}	*Stress associated with 13 plane*	*N/mm^2 (MPa)*
τ_{23}	*Stress associated with 23 plane*	*N/mm^2 (MPa)*
E_1	*Young modulus in principle direction 1*	*GPa*
E_2	*Young Modulus in principle direction 2*	*GPa*
E_3	*Young Modulus in principle direction 3*	*GPa*
v_{12}	*Poisson`s ratio associated with 12 plane*	
v_{13}	*Poisson`s ratio associated with 13 plane*	
v_{23}	*Poisson`s ratio associated with 23 plane*	
G_{12}	*Shear modulus associated with the 12 plane*	*GPa*
G_{31}	*Shear modulus associated with the 13 plane*	*GPa*
G_{23}	*Shear modulus associated with the 23 plane*	*GPa*

Terms overview

Composites
The definition of the composite material is that it needs to be a combination of two or more materials, and yielding properties have to be better than for the individual material. This report is limited to the composite called Fiber Reinforced Polymer (FRP). FRP composite consists of the two materials, fiber and matrix.

Fiber
The fiber is also called reinforcement and can be made of Glass, Carbon, Kevlar and other materials and provides strength and stiffness. The fiber is strong parallel, but weak transverse to the fiber.

Matrix
The fibres are then combined with resin called the matrix. The matrix provides the transverse strength.

Lamina or Ply
The combination of fiber with matrix is often called lamina or ply. Unidirectional ply is when the fibres are placed in one direction.

Layer
A layer consists of ply in arbitrary directions. For instance, one layer may consist of 50% unidirectional ply in 0 degree direction, and 50% in 90 degree direction.

Laminate
Layer bonded together to form the laminate which is the finished material product.

Stacking sequence or Lay-up
The stacking sequence is an overview of the laminate with plies in arbitrary directions. For example [+45 degree, -45 degree] laminate.

Table of contents

List of Figures

List of Tables

Chapter 1

Introduction

The increase in the development of fields in the oil and gas industry on the Norwegian Continental Shelf has led to a large increase in subsea installations in recent decades. Many of the underwater structures that process and transport oil, need protection from dropped objects and from being hit by fishing gear. In order to protect this equipment, a shell structure made of glass-reinforced plastic (GRP) has been developed, often abbreviated to GRP cover. Typical design criteria for GRP covers are the installation loads, trawler load, dropped objects and forces from currents and waves. Installation loads are associated with lifting. The covers will be lifted during fabrication, transportation and reposition prior to the installation. Installation includes offshore lift, deployment through the splash zone, wet storing and final installation on the seabed. The covers have reinforced lifting holes, (also made of GRP). The soft sling used in the lifting operation is attached through the holes, forming an anchor point. The local reinforced holes are often called lifting points, and are a central part of the GRP cover in terms of installation.

To this day, simplified hand calculations based on experimental failure values have been used to verify the lifting capacity of the lifting points. The simplified hand calculations do not take account for bending moments which occurs in some lifting scenarios. In order to take account for the uncertainty in the simplified method, a material factor of 2.0 is used (meaning the capacity is reduced by 50%). The purpose of this thesis is to use finite element method (FEM) to analyze the behavior of the material during lifting and to ensure lifting capacities, in addition, seek to obtain more accurate results. In the present work, a full-sized lifting point is studied with FEM software called MSC Nastran. The results have been compared with experimental tests. The tests have been performed in collaboration with Highcomp (GRP cover manufacturer) at Westcon Løfteteknikks hydraulic tensile bench in Haugesund. Based on the results, opportunities for improving the lifting points used in GRP cover design have also been investigated.

The benefits of the GRP cover are that it is lightweight, strong and corrosion-resistant. All these features make it suitable for use as protection for underwater equipment. It has led to an increase in the number of GRP covers. Subsea 7 alone designed over 100 covers in 2012. At the same time, virtually all new projects include GRP cover design. There is thus a clear desire and need to analyze the lifting points with more accuracy and understand the behavior of the material to a greater extent.

The thesis is divided into chapters. Chapter 2 provides a background of the GRP cover and the lifting scenarios. Chapter 3 consists of relevant theory for the analysis. Chapter 4 addresses the experimental tests performed, while Chapter 5 includes analyses of the lifting point. The conclusion is presented in

Chapter 6. All the results from the analyses are presented in Appendixes B, C and D along with the test report in Appendix A.

Chapter 2

Background

In the offshore subsea market, protection covers made of GRP are interesting because of their advantages over conventional steel covers. The main advantages are the low weight and the possibility to stack covers on top of each other. Because of the stacking, it is possible to transport a higher number of covers on each trip. Further, because of the low weight, the protection covers are easier to handle, and it is possible to use smaller vessels for installation (Highcomp, 2013). In addition, the glass reinforced plastic is corrosion proof, which is a great advantage when the covers are designed to stay on the seabed for many years under harsh conditions .GRP covers are used to protect small templates with subsea equipment, spools, pipelines and flowlines.

Figure 2.1: Field layout with subsea template and GRP covers, (Highcomp, 2013).

The general requirements for GRP covers on the Norwegian Continental Shelf are:

- Withstand permanent loads such as self- weight, on land and submerged. General structural design should be according to NORSOK N-001 Structural design.

- Covers shall sustain installation loads in accordance with DNV Rules for Planning and Execution of Marine Operations. It involves being able to withstand lifting during fabrication, transfer and installation. Installation includes offshore lift, deployment trough splash zone and the final position on the seabed.

- Covers shall withstand trawling load in accordance with NORSOK U-001. In addition, try to design the covers to be snag-free, which will reduce the forces from trawling loads significantly.

- Protection covers shall be stable in a one-year-return-period storm prior to rock-dump stabilization. During operation, the rock dumped covers shall be stable in a 100- year return period storm. (Rock dumping to provide on bottom stability check against trawling load and severe weather condition.)

- Covers shall withstand dropped objects (Impact load) in accordance with NORSOK U-001

In order to obtain the lifting capacities for the lifting points used in the GRP cover, the tests and analyses need to represent reality in a satisfactory manner. Concentration is on the most common lifting situations, four-point lift and two-point lift. The locations of the lifting points are either on the sidewalls or on top of the cover, leading to a total of three different lifting situations regarding the lifting points, i.e. Case 1, Case 2 and Case 3.

2.1 Description of load scenario for Case 1

Prior to installation through the splash zone, the GRP cover is lifted off the ground from a horizontal to an upright position. This is done in order to reduce the hydrodynamic loads and the risk of slack in the slings. Two of the lifting points in the highest position will take the entire load. For this upright lifting position, the lifting point has to take the force horizontally in the local point in the test arrangement (see Figure 2.3). The test setup is basically a lift point that has been placed in a steel test arrangement fixed to a point. Further, a sling is attached through the holes and the load is applied to the sling gradually. The lifting points used in the tests are full-size models of the reinforced lift points used in GRP covers.

Figure 2.2: Lift setup through splash zone.

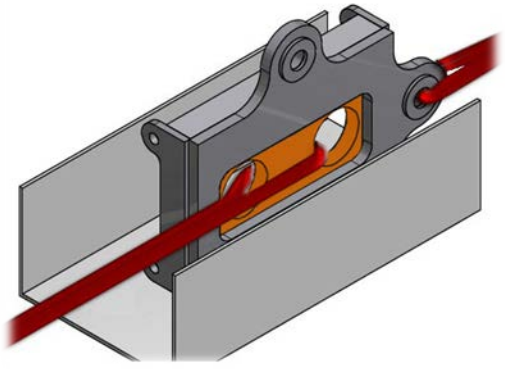

Figure 2.3: Test setup for Case 1.

2.2 Description of load scenario for Case 2

A horizontal lift is performed when the covers are weighed, loaded on to the vessel and placed into the final position on the seabed. In some instances for light covers, the lifting points are placed on top of the cover, as shown in Figure 2.4. The lifting force is applied directly out-of-plane in relation to the lifting point, which is expected to be the weakest direction of the laminate based on the material properties. The out-of-plane loads will cause the lifting points to encounter bending moment. Since the load is acting in the weakest direction compared to the other lifting situations, it is only applicable to light and relatively small covers. The test setup for the out-of-plane test is shown in Figure 2.5. The steel arrangement holds the lifting point in place while being fixed to a point. A sling is attached through the holes and is connected to the hydraulic tensile bench, which gradually applies the load through the sling. With this specific test setup, the lifting point will encounter pure out-of-plane loads.

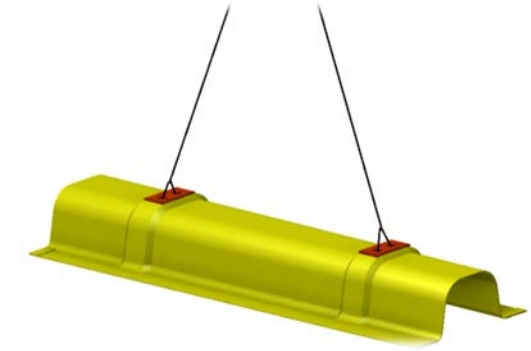

Figure 2.4: Lift point on top of cover.

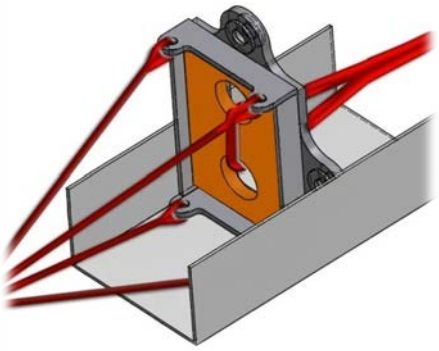

Figure 2.5: Out-of-plane test arrangement.

2.3 Description of load scenario for Case 3

The most common lifting situation for horizontal lifting is a four-point lift situation. A horizontal lift is performed when the covers are weighed, loaded on to the vessel and placed into the final position on the seabed. The total weight of the GRP cover acts on the lifting points (see Figure 2.6). The load is working slightly out-of-plane in relation to the material plane. To represent the same situation, the test setup for Case 3 is arranged in a similar way, meaning that the lifting point will encounter some out-of-plane load. Theoretically, the setup will cause an angle of around 45 degrees with the material plane. This setup is shown in Figure 2.7.

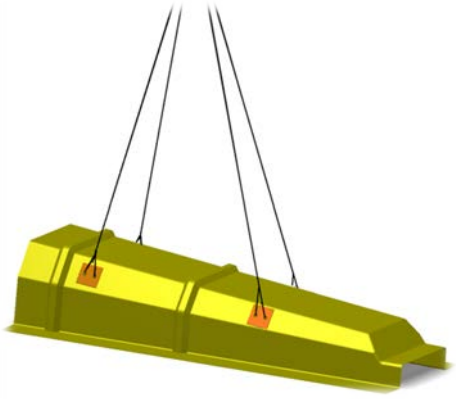

Figure 2.6: Lift point on side of the cover.

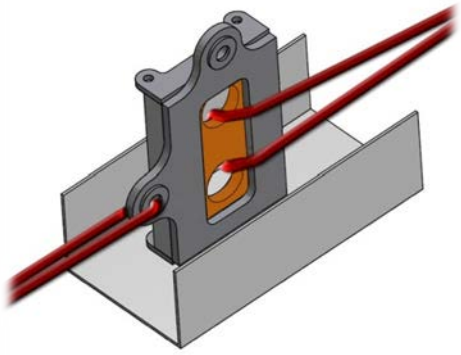

Figure 2.7: Case 3 test arrangement.

2.4 Lifting point used in GRP cover design

The lifting point is designed with two holes that form the basis for attaching a sling. The lifting point is made of the same material as the rest of the cover and appears as a local increase in thickness. The fabrication of the GRP cover starts with creating a mold, and then the main thickness is achieved by adding layers on the mold. Finally, the areas surrounding the lifting holes are reinforced with additional layers. The size of the lifting point is shown in Figure 2.8.

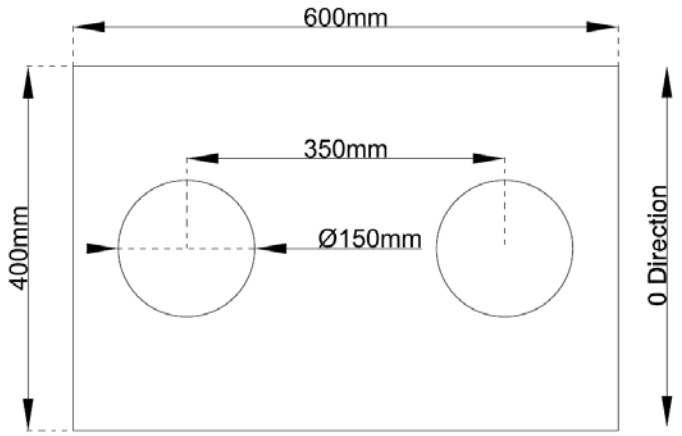

Figure 2.8: Size of lifting point.

The laminate lay-up used in the GRP covers is based on the global forces from the corresponding load cases. The occurring force moves the stiffest route across a structure, and for GRP cover the transverse direction is the most critical (shortest direction). Based on this, a layer consists of 70% of fibers in transverse direction (0 degree), 25% of fibers in the longitudinal direction (90 degrees), with the last 5% consisting of chopped strand material (small fibers in random positions), which provides better adhesion between the layers. Both the main body thickness and the reinforced lifting holes consist of this specific lay-up sequence.

The material laminates were prepared at Highcomp AS and sent to Reichhold AS for testing. The material consists of fiber reinforcement of Formax FGE 394; 0 / 90 degree, with density 1902g/m^2, and polyester type PLT 480-622. The conducted material properties from the material tests are given in Tables 2.1, 2.2 and 2.3.

Table 2.1: Fiber dominated ply properties

Parameter	Value	Unit	Explanation
E_1	28.7	GPa	Modulus of elasticity in the main fiber direction
X_t	660	MPa	Tension stress at break in the main fiber direction
X_c	460	MPa	Compressive stress at break in the main fiber direction

Table 2.2: Matrix dominated ply properties

Parameter	Value	Unit	Explanation
E_2	9.00	GPa	Modulus of elasticity transverse to the main fiber direction
G_{12}	3.00	GPa	Shear modulus in the ply plane

ν_{12}	0.26		Ply major Poisson's ratio
Y_t	34.0	MPa	Tension stress at break normal to the main fiber direction
Y_c	50.0	MPa	Compressive stress at break normal to the main fiber direction
S_{12}	26.0	MPa	Shear stress in ply plane at failure

Table 2.3: Through thickness ply properties

Parameter	Value	Unit	Explanation
E_3	9.00	GPa	Modulus of elasticity normal to the fiber plane
G_{13}	3.00	GPa	Shear modulus normal to the fiber plane, incl. fiber direction.
G_{23}	2.00	GPa	Shear modulus normal to fiber plane, normal to the fiber direction
ν_{13}	0.26		Poisson's ratio normal to fiber plane, incl. fiber direction
ν_{23}	0.48		Poisson's ratio normal to fiber plane, normal to the fiber direction
Z_t	13.0	MPa	Tension stress at break normal to fiber plane
Z_c	61.0	MPa	Compression stress at break normal to fiber plane
S_{13}	14.0	MPa	Shear stress at failure normal to fiber plane, incl. fiber direction
S_{23}	14.0	MPa	Shear stress at failure normal to fiber plane, normal to fiber direction

Chapter 3

Theory

There are three different ways perform analysis of fiber reinforced plastic (FRP) materials: the micro-scale, meso-scale and macro-scale approaches. Each method has its own area of application and complexity. The micro-scale approach provides the most detailed information describing the micro structure of the composite. It involves the size, geometry and location of the fibers within the layer. It is possible to use the micro-scale approach to calculate the mechanical properties of the material. However, the material properties can also be obtained by testing (ANSYS, 2012).

The meso-scale approach is used to analyze strains and stresses. In this method the composite material is regarded as many layers with specified material properties. Stresses and strains can be checked against chosen failure criteria, and it is possible to estimate the strength of the material. This method is essential for this thesis, forming the foundation for stress analysis.

The last method is the macro-scale, in which the composite material is regarded as one big layer with given material properties. It is not possible to perform stress analysis for this method; however, it can be used to examine the deflection, buckling loads and vibration (ANSYS, 2012).

This chapter is divided into two main parts. The first section consists of the mechanics of orthotropic materials, which explains how the lamina material stiffness is obtained. The second part is about the failure analysis, including the development and theory behind the failure.

3.1 Mechanics of orthotropic materials

In reality the fiber reinforced material has different properties at any given point and is called heterogeneous material. Heterogeneous materials are difficult to analyze because of all the differences in the material, but we can simplify this and say that the material properties are the average value at all points, and then the material characteristic becomes the same as homogenous material (the same properties at any given point).

Fibers have different properties parallel with the fibers compared to the transverse direction (normal to the fibers). The result of this is that the material has different properties in two main directions and is called an orthotropic material.

3.2 Cartesian coordinate system

In the coordinate system there are three planes that define the three main directions, X_1, X_2 and X_3. In addition, at each plane there are three stresses, σ_{ij}. The first number in the stress notation (i) corresponds to the direction; normal of the plane it is working on. The second notation for the stress (j) corresponds to the direction of the stress. An overview of the coordinate system in a 3D stress situation is shown in Figure 3.1.

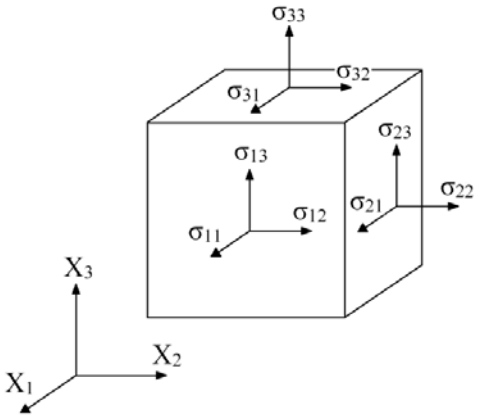

Figure 3.1: 3D stress illustration (Wikipedia, 2013).

3.2.1 Stress

The stress is defined as the force per unit area acting on the plane passing the point. Stress has the designation N/mm^2 or MPa. The stress tensor can be expressed as a matrix (Barbero, 2008). An alternative notation, which is often used in the mechanics of the material, is also shown in Equation (3.1):

$$[\sigma] = \begin{bmatrix} \sigma_{11} & \sigma_{12} & \sigma_{13} \\ \sigma_{12} & \sigma_{22} & \sigma_{23} \\ \sigma_{13} & \sigma_{23} & \sigma_{33} \end{bmatrix} = \begin{bmatrix} \sigma_1 & \tau_{12} & \tau_{31} \\ \tau_{12} & \sigma_2 & \tau_{23} \\ \tau_{31} & \tau_{23} & \sigma_3 \end{bmatrix} \tag{3.1}$$

3.2.2 Strain

The engineering strain is defined as a ratio of total deformation to the initial dimension of the material body in which the forces are applied (Wikipedia, 2013). When the material body is stretched, the strain is positive, and during compression the notation is negative. In other words, the strain is a change of length divided by the original length in the material direction. The strain tensor can be expressed as a matrix, as in Equation (3.2) (Barbero, 2008). In the mechanics of the material, the alternative expression is also shown in this equation, which is used further in the thesis.

$$[\varepsilon] = \begin{bmatrix} \varepsilon_{11} & \varepsilon_{12} & \varepsilon_{13} \\ \varepsilon_{12} & \varepsilon_{22} & \varepsilon_{23} \\ \varepsilon_{13} & \varepsilon_{23} & \varepsilon_{33} \end{bmatrix} = \begin{bmatrix} \varepsilon_1 & \gamma_{12} & \gamma_{31} \\ \gamma_{12} & \varepsilon_2 & \gamma_{23} \\ \gamma_{31} & \gamma_{23} & \varepsilon_3 \end{bmatrix} \tag{3.2}$$

3.2.3 Hooke's law

One of the key assumptions for the material mechanics is that it follows Hooke's Law. Hooke's law describes the relationship between strain and stress in linear elasticity. For small strain, the law states that the stress is proportional to the strain. In the simplest form, Hooke's law can be expressed as in Equation (3.3) for the case of a stress applied unidirectional to an isotropic solid (Chawla, 1987).

$$\sigma = \varepsilon \cdot E \tag{3.3}$$

For an orthotropic material in 3D, Hooke's law is more complex. The relationship between the strain and stress is expressed in Equations (3.4) and (3.5).For the 3D state for an orthotropic material, there are nine constants that need to be described. A compliance matrix gives the relationship between the strain and stress and is expressed as (Barbero, 2008):

$$\begin{Bmatrix} \varepsilon_1 \\ \varepsilon_2 \\ \varepsilon_3 \\ \gamma_{23} \\ \gamma_{31} \\ \gamma_{12} \end{Bmatrix} = \begin{bmatrix} S_{11} & S_{12} & S_{13} & 0 & 0 & 0 \\ S_{12} & S_{22} & S_{23} & 0 & 0 & 0 \\ S_{13} & S_{23} & S_{33} & 0 & 0 & 0 \\ 0 & 0 & 0 & S_{44} & 0 & 0 \\ 0 & 0 & 0 & 0 & S_{55} & 0 \\ 0 & 0 & 0 & 0 & 0 & S_{66} \end{bmatrix} \begin{Bmatrix} \sigma_1 \\ \sigma_2 \\ \sigma_3 \\ \tau_{23} \\ \tau_{31} \\ \tau_{12} \end{Bmatrix} \tag{3.4}$$

The inverted compliance matrix [S] = $[C]^{-1}$ is called the stiffness matrix for the lamina and is expressed as:

$$\begin{Bmatrix} \sigma_1 \\ \sigma_2 \\ \sigma_3 \\ \tau_{23} \\ \tau_{31} \\ \tau_{12} \end{Bmatrix} = \begin{bmatrix} C_{11} & C_{12} & C_{13} & 0 & 0 & 0 \\ C_{12} & C_{22} & C_{23} & 0 & 0 & 0 \\ C_{13} & C_{23} & C_{33} & 0 & 0 & 0 \\ 0 & 0 & 0 & C_{44} & 0 & 0 \\ 0 & 0 & 0 & 0 & C_{55} & 0 \\ 0 & 0 & 0 & 0 & 0 & C_{66} \end{bmatrix} \begin{Bmatrix} \varepsilon_1 \\ \varepsilon_2 \\ \varepsilon_3 \\ \gamma_{23} \\ \gamma_{31} \\ \gamma_{12} \end{Bmatrix} \tag{3.5}$$

3.2.4 Engineering constants

In order to describe the orthotropic material, the nine constants need to be described as the engineering constants E1, E2, E3, ν_{12}, ν_{13}, ν_{23}, G_{12}, G_{13}, and G_{23}. Both Young's modulus E and Poisson's ratio ν are results from tensile testing, while the shear modulus G is measured from a shear test. Young's modulus is the ratio between applied stress and strain in the same direction, while Poisson's ratio is the ratio between longitudinal and transverse strain (Chawla, 1987).

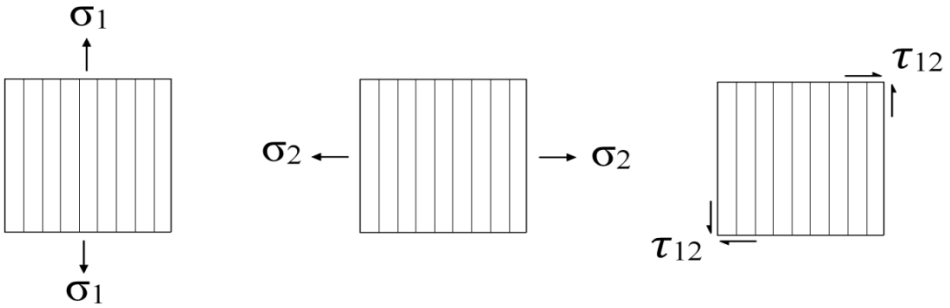

Figure 3.2: Simple states of stress used to define lamina engineering constants (Gibson, 1994).

Simple states of stress are used to define lamina engineering constants. The definition of the engineering constants is based on Hooke's Law described in the previous section. By considering a uniaxial tensile test with an applied normal stress σ_1 along the fiber direction (see Figure 3.2 a) and assuming all other stresses to be equal to zero (Equation (3.9)), it has been experimentally observed that the engineering constants associated with 123 can be expressed empirically (Gibson, 1994). These connections are expressed in Equations (3.6), (3.7) and (3.8).

$$\varepsilon_1 = \frac{\sigma_1}{E_1} \tag{3.6}$$

$$\varepsilon_2 = -\nu_{21}\varepsilon_1 = -\nu_{21}\frac{\sigma_1}{E_1} \tag{3.7}$$

$$\varepsilon_3 = -\nu_{13}\varepsilon_1 = -\nu_{13}\frac{\sigma_1}{E_1} \tag{3.8}$$

$$\gamma_{12} = \gamma_{23} = \gamma_{13} = 0 \tag{3.9}$$

Considering a similar experiment with a normal stress $\sigma_2$acting normal to the fiber direction (Figure 3.2 b) and assuming all other stresses are equal to zero (Equation 3.13), the experimental observation states that the resulting strain normal to the fiber can be expressed as in Equations (3.10), (3.11) and (3.12) (Gibson, 1994).

$$\varepsilon_2 = \frac{\sigma_2}{E_2} \tag{3.10}$$

$$\varepsilon_1 = -\nu_{21}\varepsilon_2 = -\nu_{21}\frac{\sigma_2}{E_2} \tag{3.11}$$

$$\varepsilon_3 = -\nu_{23}\varepsilon_1 = -\nu_{23}\frac{\sigma_2}{E_2} \tag{3.12}$$

$$\gamma_{12} = \gamma_{23} = \gamma_{13} = 0 \tag{3.13}$$

In addition, considering a pure shear test, where $\sigma_{12}=\tau_{12}$ is applied in the 12-plane of the material (Figure 3.2 c), the experimental observation shows that the resulting strain can be expressed as in Equation (3.14),and assuming all other stresses are equal to zero (Equation 3.15) (Gibson, 1994).

$$\gamma_{12} = \frac{\tau_{12}}{G_{12}} \tag{3.14}$$

$$\varepsilon_1 = \varepsilon_2 = \varepsilon_3 = \gamma_{13} = \gamma_{23} = 0 \tag{3.15}$$

Based on the previous equations for the general 3D state of stress, consisting of all normal and shear stresses that are associated with the three axes as shown in Figure 3.1, the resulting set of equations can be expressed in the compliance matrix [S] (Eq.(3.16)). The compliance matrix gives the relationship between the strain and stress for a 3D orthotropic material.

Compliance matrix [S] which gives the relationship between stress and strain $\varepsilon = [S]\sigma$

$$[S] = \begin{bmatrix} \frac{1}{E_1} & -\frac{\nu_{21}}{E_2} & -\frac{\nu_{31}}{E_3} & 0 & 0 & 0 \\ -\frac{\nu_{12}}{E_1} & \frac{1}{E_2} & -\frac{\nu_{31}}{E_3} & 0 & 0 & 0 \\ -\frac{\nu_{31}}{E_1} & -\frac{\nu_{23}}{E_2} & \frac{1}{E_3} & 0 & 0 & 0 \\ 0 & 0 & 0 & \frac{1}{G_{23}} & 0 & 0 \\ 0 & 0 & 0 & 0 & \frac{1}{G_{31}} & 0 \\ 0 & 0 & 0 & 0 & 0 & \frac{1}{G_{12}} \end{bmatrix} \tag{3.16}$$

To compute the failure analysis, the stiffness of the material is of great importance. The stiffness of the orthotropic material can be computed as the inverted compliance matrix as shown in Equation (3.17). The stiffness matrix [C] is known as the lamina stiffness matrix and is expressed in Equation (3.18) (Barbero, 2008).

$$\sigma = [S]^{-1}\varepsilon \text{equals } \sigma = [C]\varepsilon \tag{3.17}$$

The stiffness matrix [C] gives the relationship between stress and strain $\sigma = [C]$

$$[C] = \begin{bmatrix} \frac{1-\nu_{23}\nu_{32}}{E_2E_3\Delta} & \frac{\nu_{12}+\nu_{32}\nu_{13}}{E_1E_3\Delta} & \frac{\nu_{13}+\nu_{12}\nu_{23}}{E_1E_2\Delta} & 0 & 0 & 0 \\ \frac{\nu_{12}+\nu_{32}\nu_{13}}{E_1E_3\Delta} & \frac{1-\nu_{13}\nu_{31}}{E_1E_3\Delta} & \frac{\nu_{23}+\nu_{21}\nu_{13}}{E_1E_2\Delta} & 0 & 0 & 0 \\ \frac{\nu_{13}+\nu_{12}\nu_{23}}{E_1E_2\Delta} & \frac{\nu_{23}+\nu_{21}\nu_{13}}{E_1E_2\Delta} & \frac{1-\nu_{12}\nu_{21}}{E_1E_2\Delta} & 0 & 0 & 0 \\ 0 & 0 & 0 & G_{23} & 0 & 0 \\ 0 & 0 & 0 & 0 & G_{31} & 0 \\ 0 & 0 & 0 & 0 & 0 & G_{12} \end{bmatrix} \tag{3.18}$$

Where:

$$\Delta = \frac{1-\nu_{12}\nu_{21}-\nu_{23}\nu_{32}-\nu_{31}\nu_{13}-2\nu_{21}\nu_{32}\nu_{13}}{E_1E_3E_3} \tag{3.19}$$

3.2.5 Plane stress

Often it is assumed that the 3rd direction is equal to zero. This assumption is valid when the length and width of a structure is a lot greater than the thickness and the load is not applied in the thickness direction, which is often the case for most composite structures. These structures can often be characterized as a shell, (Okutan, 2001).

In this thesis both situations occur. If there is a load applied in the thickness direction it cannot be assumed to be plane stress. However, if the load is acting in-plane of the material and the thickness is relatively small compared to the width and length of the structure, this assumption is valid. When the 3rd direction is assumed to be equal to zero, the stresses in Equation (3.20) are equal to zero.

$$\sigma_3 = \tau_{23} = \tau_{31} = 0 \tag{3.20}$$

Hence the compliance matrix [S] is reduced as shown in Equation (3.21).

$$[S]_{plane\ stress} = \begin{bmatrix} \frac{1}{E_1} & -\frac{\nu_{21}}{E_2} & 0 \\ -\frac{\nu_{12}}{E_1} & \frac{1}{E_2} & 0 \\ 0 & 0 & \frac{1}{G_{12}} \end{bmatrix} \tag{3.21}$$

3.3 Failure analysis

By examining failure, one can estimate how much the material can withstand and how the failure occurs. A very important aspect of composite material used in structural applications is to understand the failure mode. The analysis models should be able to predict where the failure takes place and how it evolves. For fiber reinforced composites, the main failure modes are described below based on Pinho et al. (2005):

Fiber tensile failure can release large amounts of energy and can act as more explosive, which typically leads to a catastrophic failure.

Fiber compression failure is a complex failure mode which is affected by matrix shear behavior and material imperfection such as voids and fiber misalignment, which can cause fiber micro-buckling.

From the **matrix tensile failure** mode, normally some fiber splitting at the fracture surface can be observed, and is typically normal to the load direction.

Matrix compression failure occurs at an angle with the applied load; this is more accurately a shear matrix failure and can be seen from the shear nature of the failure process.

Composite materials are made of lamina stacked together to create a laminate. **Delamination failure** mode is when the lamina tends to split from the laminate.

3.3.1 Failure criteria

Failure criteria are used to explain whether a layer (ply) has failed due to the applied loads. In composite material design, there are numerous failure criteria available. In this thesis, two failure criteria were selected: the Puck failure criterion and the Hashin failure criterion. Both criteria have the ability to take into account the 3Delement, which includes the out-of-plane components of stress. In addition, a major feature of both these criteria is that they can distinguish between fiber and matrix failure. With this feature, it is possible to know the failure mode of the structure, and it is easier to have control over the failure propagation, including more control over the degradation of the material after the first ply failure (discussed later in Section 3.4.1).

For composite structures, failure criteria based on strength are commonly used to predict failure. Many criteria have been derived based on stresses and measurements from experiments to predict failure (semi-empirical formulas). Hashin and Puck have been credited for creating failure criteria based on the failure mechanism (Mohite, 2012).

The difference between Hashin and Puck in the matrix cracking is that Hashin only distinguishes between transverse tension (Mode A) and compression (Mode B), while Puck additionally checks the possibility of an inclined fracture plane (Mode C) (Mohite, 2012). All three modes are shown in Figure 3.3.

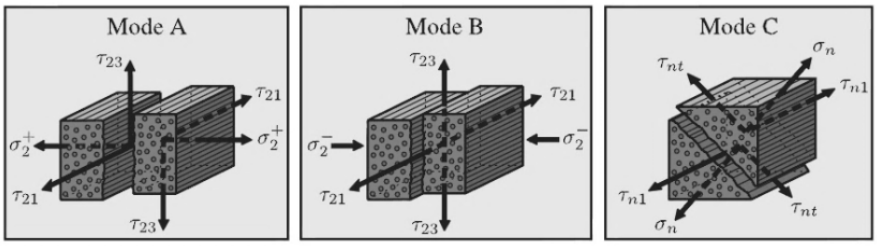

Figure 3.3: Matrix cracking failure modes (Lauterbach et al., 2009).

The allowable strength for the lamina is defined as X, Y, and Z, respectively in the three main directions 1, 2 and 3. There are limits both for tensile and compression denoted by t, and c. In addition, the allowable shear strength is denoted by S_{12}, S_{13}, and S_{23}.

X_t,X_c	Respectively allowable tensile and compression strength in 1st direction	N/mm^2
Y_t,Y_c	Respectively allowable tensile and compression strength in 2nd direction	N/mm^2
Z_t,Z_c	Respectively allowable tensile and compression strength in 3rd direction	N/mm^2
S_{12}	Allowable shear strength in the 12-plane	N/mm^2
S_{13}	Allowable shear strength in the 13 -plane	N/mm^2
S_{23}	Allowable shear strength in the 23-plane	N/mm^2

3.3.2 Puck failure criterion

One of the reasons for the choice of the puck criteria is that it can distinguish between fiber failures (FF) and inter-fiber failure (IFF). The inter-fiber failure is essentially matrix cracking. The criteria are divided into two parts for the situation with 3D problems and for that withn2D plane stress problems. For plane stress there are three modes of fracture. Mode A is a check for transverse tension, Mode B a test for compression and the last Mode C is a check for the possibility of an inclined fracture plane. For 3D problems, the criterion is divided into fiber failure (FF) and inter-fiber failure (IFF) (Barbero, 2008).

The fiber fracture criterion for 2D and 3D failure analysis is described in Equation (3.22); refer to Knops (2008).

$$f_{E,FF} = \frac{1}{\pm X_{t,c}}\left[\sigma_1 - \left(\nu_{21} - \nu_{21} m_{of}\frac{E_1}{E_{1f}}\right)(\sigma_2 + \sigma_3)\right] \; with \begin{cases} +X_t \; for \; value \geq 0 \\ -X_c \; for \; value \; < 0 \end{cases} \tag{3.22}$$

where:

M_{of}	Stress magnification factor, typically 1.3 for glass fiber (Perillo et al., 2011)	
E_1	Longitudinal Young's Modulus of the lamina parallel to the fibers	N/mm^2
E_{1f}	Longitudinal Young's Modulus of the fibers	N/mm^2

2D Puck inter-fiber criterion

The failure criterion for Mode A is active when there is positive transverse stress, and this is defined as in Equation (3.23); refer to Barbero (2008).

$$f_{IFF,A} = \sqrt{\left(\frac{\sigma_{12}}{S_{12}}\right)^2 + \left(1 - p_{6t}\frac{Y_t}{S_{12}}\right)^2 \left(\frac{\sigma_2}{Y_t}\right)^2} + p_{6t}\frac{\sigma_2}{S_{12}} \qquad if\ \sigma_2 \geq 0 \tag{3.23}$$

where:

p_{6t} Fitting parameter, 0.3 for glass fiber (Barbero, 2008)
p_{6c} Fitting parameter, 0.2 for glass fiber (Barbero, 2008)

The failure criteria for Mode B and Mode C are both active under negative transverse stress. What determines the choice of mode depends on the relationship between the in-plane shear stress and the transversal shear stress, S_{1A}/S_{2A} (Barbero, 2008).

$$\frac{S_{1A}}{S_{2A}} \tag{3.24}$$

The relationship in Equation (3.24) is further described by Equations (3.25), (3.26) and (3.27).

$$S_{1A} = \frac{S_{12}}{2_{p6c}}\left[\sqrt{1 + 2_{p6c}\frac{Y_c}{S_{12}}} - 1\right] \tag{3.25}$$

$$S_{2A} = S_{12}\sqrt{1 + 2_{p2c}} \tag{3.26}$$

$$p_{2c} = p_{6c}\frac{S_{1A}}{S_{12}} \tag{3.27}$$

The failure criterion for Mode B is defined in Equation (3.28); refer to Barbero (2008).

$$f_{IFF,B} = \frac{1}{S_{12}}\left[\sqrt{{\sigma_{12}}^2 + (p_{6c}\sigma_2)^2} + p_{6c}\sigma_2\right] \quad if \begin{cases} \sigma_2 & < & 0 \\ \dfrac{\sigma_2}{\sigma_{12}} & \leq & \dfrac{S_{1A}}{S_{2A}} \end{cases} \tag{3.28}$$

The failure criterion for Mode C is defined in Equation (3.29); refer to Barbero (2008).

$$f_{IFF,C} = \frac{Y_C}{\sigma_2}\left[\left(\frac{\sigma_{12}}{2(1+p_{2c})S_{12}}\right)^2 + \left(\frac{\sigma_2}{Y_C}\right)^2\right] \quad if \begin{cases} \sigma_2 & < & 0 \\ \dfrac{\sigma_2}{\sigma_{12}} & \geq & \dfrac{S_{1A}}{S_{2A}} \end{cases} \tag{3.29}$$

3D Puck Failure Criterion

It is assumed that fracture is only created by the stresses acting on the fracture plane. The working normal and shear stress on the fracture plane can be described by tensor transformation given in Equations (3.30)-(3.32); refer to Deuschle (2010).

$$\sigma_n(\theta) = \sigma_2 cos^2(\theta) + \sigma_3 sin^2(\theta) + 2\tau_{23} sin(\theta) cos(\theta) \tag{3.30}$$

$$\tau_{nt}(\theta) = (\sigma_3 - \sigma_2) sin(\theta) cos(\theta) + \tau_{23}\left(cos^2(\theta) - sin^2(\theta)\right) \tag{3.31}$$

$$\tau_{nl}(\theta) = \tau_{31}\, sin(\theta) + \tau_{21}\, cos(\theta) \tag{3.32}$$

where:

θ	Angle between the fracture plane and the material plane	*Degree*
$\sigma_n(\theta)$	Stress normal to the fracture plane	*N/mm²*
$\tau_{nl}(\theta)$	Shear stresses in the fracture plane, parallel to the fiber direction	*N/mm²*
$\tau_{nt}(\theta)$	Shear stresses in the fracture plane, perpendicular to the fiber direction	*N/mm²*

The inter-fiber failure criterion is only a function of the stresses acting on the fracture plane (Perillo et al., 2011):

$$f_{IFF} = \begin{cases} \sqrt{\left[\left(\frac{1}{Y_{t,c}} - \frac{P^{+}_{\perp\psi}}{S_{23}}\right)\sigma_n(\theta)\right]^2 + \left(\frac{\tau_{nt}(\theta)}{S_{12}}\right)^2 + \left(\frac{\tau_{nl}(\theta)}{S_{13}}\right)^2} + \frac{P^{+}_{\perp\psi}}{S_{23}}\sigma_n(\theta) & for\ \sigma_n \geq 0 \\ \sqrt{\left(\frac{\tau_{nt}(\theta)}{S_{12}}\right)^2 + \left(\frac{\tau_{nl}(\theta)}{S_{13}}\right)^2 \left[\left(\frac{P^{-}_{\perp\psi}}{S_{23}}\right)\sigma_n(\theta)\right]^2} + \frac{P^{-}_{\perp\psi}}{S_{23}}\sigma_n(\theta) & for\ \sigma_n \leq 0 \end{cases} \tag{3.33}$$

where:

$P^{+}_{\perp\psi}$	slope parameter representing internal friction effects for tension
$P^{-}_{\perp\psi}$	slope parameter representing internal friction effects for compression

The connection between the slope parameters and the allowable stresses is given in Equations (3.34) and (3.35), and the angle connection in Equations (3.36) and (3.37).

$$\frac{P^{+}_{\perp\psi}}{S_{23}} = \frac{P^{+}_{\perp\perp}}{S_{22}}(cos\ \alpha)^2 + \frac{P^{+}_{\perp\parallel}}{S_{21}}(sin\ \alpha)^2 \tag{3.34}$$

$$\frac{P^{-}_{\perp\psi}}{S_{23}} = \frac{P^{-}_{\perp\perp}}{S_{22}}(cos\ \alpha)^2 + \frac{P^{-}_{\perp\parallel}}{S_{21}}(sin\ \alpha)^2 \tag{3.35}$$

$$(cos\ \alpha)^2 = \frac{{\tau_{nt}}^2(\theta)}{{\tau_{nt}}^2(\theta) + {\tau_{nl}}^2(\theta)} \tag{3.36}$$

$$(sin\ \alpha)^2 = \frac{{\tau_{nl}}^2(\theta)}{{\tau_{nt}}^2(\theta) + {\tau_{nl}}^2(\theta)} \tag{3.37}$$

$$S_{22} = \frac{Y_c}{2(1 + P_{\perp\perp}^-)} \tag{3.38}$$

To be able to describe the equations above, additional parameters are needed to describe the failure criterion. Puck recommended some parameters, which are given in Table 3.1.

Table 3.1 : Puck recommended parameters (Perillo et al., 2011).

Puck parameters for glass fiber	$P_{\perp\parallel}^+$	$P_{\perp\parallel}^-$	$P_{\perp\perp}^+$	$P_{\perp\perp}^-$
	0.30	0.25	0.2-0.25	0.2-0.25

3.3.3 Hashin failure criterion

Hashin proposed a criterion based on experimental observations of tensile failure specimens in 1973.It implies that the criterion is created on a logical basis, rather than on micromechanics. The Hashin failure criterion also distinguishes between fiber failure and matrix cracking, and, following an improvement in 1998, the criterion could distinguish between tension and compression. The equation below is based on Pinho et al. (2005).

Fiber failure

Tensile fiber failure for $\sigma_1 \geq 0$

$$\left(\frac{\sigma_1}{X_t}\right)^2 + \frac{{\tau_{12}}^2 + {\tau_{13}}^2}{{S_{12}}^2} = \begin{cases} \geq 1\ \ failure \\ < 1\ no\ failure \end{cases} \tag{3.39}$$

Compressive fiber failure for $\sigma_1 < 0$

$$\left(\frac{\sigma_1}{X_c}\right)^2 = \begin{cases} \geq 1\ \ failure \\ < 1\ no\ failure \end{cases} \tag{3.40}$$

Matrix failure

Tensile matrix failure for $\sigma_2 + \sigma_3 > 0$

$$\frac{(\sigma_2 + \sigma_3)^2}{{Y_t}^2} + \frac{{\tau_{23}}^2 + \sigma_2\sigma_3}{{S_{23}}^2} + \frac{{\tau_{12}}^2 + {\tau_{13}}^2}{{S_{12}}^2} = \begin{cases} \geq 1\ \ failure \\ < 1\ no\ failure \end{cases} \tag{3.41}$$

Compressive matrix failure for $\sigma_2 + \sigma_3 < 0$

$$\left[\left(\frac{Y_c}{2S_{23}}\right)^2 - 1\right]\frac{\sigma_2 + \sigma_3}{Y_c} + \frac{(\sigma_2 + \sigma_3)^2}{4{S_{23}}^2} + \frac{{\tau_{23}}^2 - \sigma_2\sigma_3}{{S_{23}}^2} + \frac{{\tau_{12}}^2 + {\tau_{13}}^2}{{S_{12}}^2} = \begin{cases} \geq 1\ \ failure \\ < 1\ no\ failure \end{cases} \tag{3.42}$$

Interlaminar failure
Tensile interlaminar failure for $\sigma_3 > 0$

$$\left(\frac{\sigma_3}{Z_t}\right)^2 = \begin{cases} \geq 1 \ failure \\ < 1 \ no \ failure \end{cases} \tag{3.43}$$

Compression interlaminar failure for $\sigma_3 < 0$

$$\left(\frac{\sigma_3}{Z_c}\right)^2 = \begin{cases} \geq 1 \ failure \\ < 1 \ no \ failure \end{cases} \tag{3.44}$$

3.4 First ply failure

A common method to predict strength of a laminate is first ply failure, which states that when the first ply failure occurs, then the structure has failed. It is a rather simple approach to laminate design. Firstly, the stresses in each lamina are determined by using FEM or Classical Laminate Theory (CLT). Secondly, the stresses in the lamina are checked against a failure criterion. There are many failure criteria available, such as Maximum Stress/Strain Criterion, Tsai-Hill, Tsai-Wu, Puck, Hashin, Cutze and many more. However, there is still to this day no universal agreement on which of the failure criteria is the best (Gibson, 1994).

Like the Von Mises criterion for steel, the first ply failure is numerically easy to find because the criterion determine whether or not the lamina fails for any given situation. One of the assumptions is that the lamina is assumed to be a homogenized material; in other words, the matrix and fiber properties are often melted together. This can lead to inaccurate analytical results compared to actual response. However, recently there have been determined new failure criteria that address this problem by dividing the failure criteria into failure mode of fibers and failure mode of matrix. Such criteria are Hashin, Puck, and LARC02 (Milligan, 2012).

For the lifting analysis, a global check is often performed with first ply failure; the advantage is fast and efficient analysis, and, in addition, it is considered to be conservative. With GRP covers, the structures are often relatively large and demand computer time to perform analysis. First ply failure tells something about when the failure starts, but it cannot provide any information on whether the whole structure will fail, or whether it can handle more load after the first ply failure occurs. In this thesis the focus is on how the material behaves after the first ply failure occurs; this will be discussed in the next section.

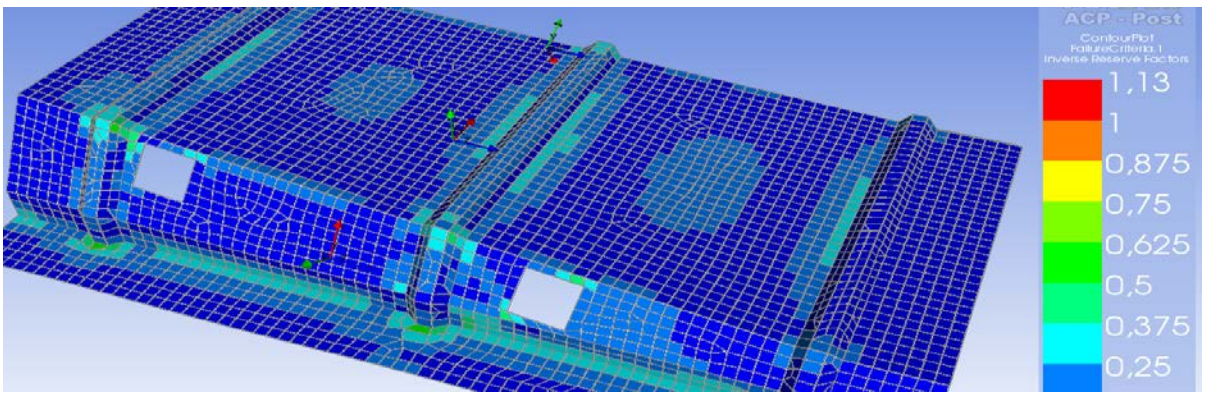

Figure 3.4: Finite element results of first ply failure for GRP cover during a four-point lift.

3.5 Progressive ply failure

Progressive failure analysis is basically an analysis of what happens to the material after first ply failure. In many situations the composite material can withstand further load after first ply failure. To be able to more accurately determine the strength estimates for the material, knowledge about what happens after first ply failure is of great importance (Milligan, 2012).

The progressive analysis can be described in a few main steps (Perillo et al., 2011).

1. Define material properties and boundary condition for the composite model.
2. Calculate stresses and strains at every integration point for each element with FEA.
3. Check the calculated stresses and strain against a specified failure criterion.
4. In the case of failure at the integration points, the local material properties need to be degraded.

The applied load/displacement is divided into small increments, and, step by step, the stress and strain are calculated for the increment and then checked against a failure criterion. In the case where a failure has occurred, then the local material properties will be degraded before the same increment is checked again, with the new local degraded material properties. This process will go on in a loop till the total load/displacement is achieved. The process is shown in a progressive failure analysis scheme in Figure 3.5.

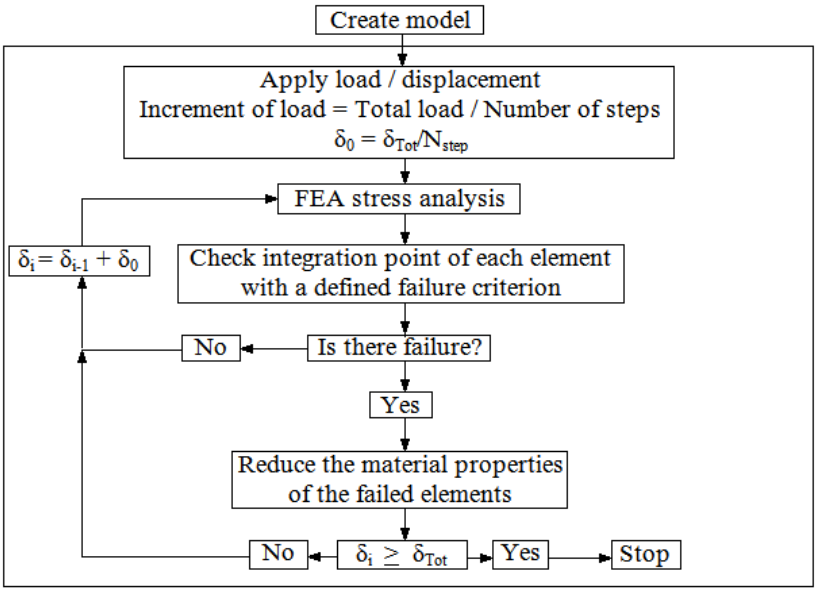

Figure 3.5: Progressive failure analysis scheme (Perillo et al., 2011).

For progressive damage modeling, the finite element analysis has shown great potential (Okutan, 2001).In finite element analysis, the composite structure is meshed in appropriate elements. Then the material properties are assigned to the elements. Additionally, the applied loads cause the occurrence of stress and strains in the model. Both the material properties and the stress and strain values are divided into integration points of an element in the model.

Within an element, the integration point is a point at which the integrals are evaluated numerically. An important note is that displacements are most accurate at the nodes, while stresses and strains tend to be most accurate at the integration points (www.eng-tips.com, 2013).

As mentioned, at each increment there is an FE stress analysis. The combination of stresses that causes the highest values will be identified and checked against the failure criterion. The element with the highest value will be the first to fail, and the material properties of the failed element will be reduced. The failed element with reduced stiffness will not be able to carry the same amount of load as the surrounding elements. In the finite element model, the internal loads will be redistributed into the full stiffness element surrounding the failed element. With an increase of load, this will cause new elements to fail, and the process continues until the structure cannot carry more loads. This will cause the complete model to fail, and thus we have ultimate failure. The progressive failure process is inherently non-linear because of the stiffness degradation, and the linear elasticity ends, (Milligan, 2012). This principle is shown in Figure 3.6, demonstrating the progressive failure analysis for a composite cantilever beam.

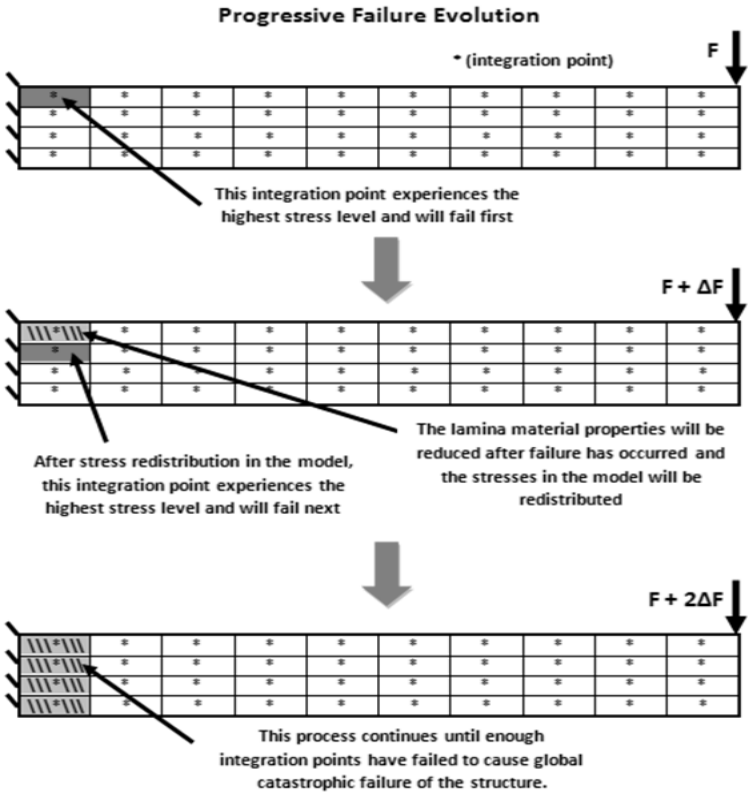

Figure 3.6: Principle for progressive failure analysis with finite element method (Milligan, 2012).

In comparison, the first failed element that occurs in a progressive analysis is equal to the first ply failure. Often the surrounding elements can support more load before they fail, and thus the structure can withstand more load before ultimate failure. Therefore, in many instances, the first ply failure may be very conservative approximation of the actual strength in the composite structure.

Important information in a progressive failure analysis is how the failure will propagate through the structure and figure out the highest load the structure can support before ultimate failure. This

information would help to create better design, and to be able to optimize and create safe and secure structures in composite.

3.5.1 Degradation material models

An important part of the progressive analysis is how the material properties are reduced after a local failure. In recent years many degradation models have been proposed (Perillo et al., 2011). In this thesis two normal degradation models, gradual and immediate degradation are examined. The two models have a different approach to reducing the material properties of the composite material. Choice of the degradation should be dictated by material behavior.

Puck and Hashin failure criteria can distinguish between fiber and matrix failure, with either tensile and compression failure, leading to a truly selective degradation. This means that if the matrix fails, the fiber properties do not change and it is the same if fiber failure occurs, the matrix properties do no change. According to the failure mode, the selective local material properties are reduced. The specific degradation is similar for both Hashin and Puck, since them both distinguish between matrix and fiber failure. If fiber failure is found, the Young's Modulus E_1 and E_3 are reduced. If matrix failure is found, the Young's Modulus E_2 and the shear modulus G_{12}, G_{23}, G_{31} are reduced.

In the FEA software MSC Nastran, additional factors are introduced to give further control. For instance, it can be selected to attain less degradation of matrix properties in compression than in tension. It is important to be aware that in FEA software the material properties cannot be set equal to zero for numerical reasons (convergence problems). Because of this issue, a reduction factor has been introduced. By multiplying the original value with the reduction factor, the material properties would degrade.

Immediate stiffness degradation

For the immediate degradation model, the material properties are instantaneously degraded approximate to zero after local failure. This model would fit the behavior of brittle materials (Perillo et al., 2011). When failure occurs, the respective material properties are degraded to a fraction of the original value. In MSC Nastran, the residual stiffness factor is defaulted to 1%. This means that the reduction is set to 1% of the original value.

Gradual stiffness degradation

For the gradual stiffness degradation, the material properties are reduced to the state when the highest failure index is just below one. The failure index is basically applied stress in the elements divided by the allowable stress. If the failure index is below one, the element is fine, while in the situation when the failure index is above one, the element is said to have failed. After a failure, the material properties are reduced so that the largest failure index is equal to one, which means that the properties will be reduced by a small amount each increment, and would therefore experience the properties gradually being degraded close to zero. The stiffness cannot be reduced to less than 1% because of numerical problems.

3.6 Finite element analysis software

According to Offshore Standard DNV Composite components, the selection of finite elements software package shall be based on the following:

1. Software availability
2. Necessary model size
3. Analysis option required
4. Validated software for intended analysis.

In addition important options should be available in the chosen FE analysis software for this thesis:

1. Layered solid elements for orthotropic materials behavior
2. Layered shell elements
3. Options characterizing large displacements and large strain (for geometrically non-linear analysis)
4. Material models describing the behavior of laminates beyond first ply failure.
5. Robust incremental procedures for non-linear analysis

MSC Nastran supports the entire list of requirements that the DNV standard for composite components demands, especially the key components for composite design, such as layered solid elements with orthotropic behavior, layered shell elements, large displacement/strain, and the ability to describe the behavior of laminates beyond first ply failure.

In other words, the FEA software MSC Nastran is a complete tool for composite design. One of the key features for complex analysis is to handle 3D problems and progressive failure analysis. These features have recently been implemented in much of the commercial FEA software. MSC Nastran first supported progressive analysis in 2010, while ANSYS had that option in the latest version (14.5, 2012). In other words, the implemented analysis tool is very new in the commercial analysis software. In addition, MSC Nastran allows the use of the latest failure criteria such as Hashin and Puck, which can also divide the failure between fiber and matrix cracking. The latest version of MSC Nastran also exists in a student version that is free for non-commercial use. Therefore, MSC Nastran a natural choice for the basis of finite element analysis in this thesis.

Chapter 4

Experimental Tests

The DNV standard for composite components states that all test specimens shall represent the actual structure and that the production methods and materials shall be exactly the same. In addition, the load cases shall be tested in a realistic manner. The purpose of the load test of the glass reinforced plastic (GRP) lift point is to establish the breaking capacity. The lift points are tested to represent the reality in the best way possible, as described in chapter 2. The tests will help to document the lifting capacity of the local lift points. This will lead to lifting points being designed with less uncertainty than before. It will affect the design of lifting points for all new projects in Subsea 7. The different tests performed look at the normal lifting setups used for GRP cover during onshore, transport and installation. The full test report is presented in Appendix A.

The goal of the tests is to have documentation of the tested ultimate failure capacity representing the real lifting situation. The result can confirm that the lift point is strong enough. In addition, the test data can be used for comparison of analytical solutions, such as finite element analysis results.

The testing is divided into three test setups, representing the three most common lifting situations. The main situations are four-point and two-point lift. The four-point lift is used when lifting onshore, and the transfer of various means of transport. While the two-point lift is common when installing through the splash zone. Additionally, you have a situation where the lifting point is located on top of the cover, which in some cases are used for relative small and light covers.

4.1 Experimental test setup

The test arrangement is located in a hydraulic tensile bench at Westcon Løfteteknikk AS in Haugesund. The tensile bench has a maximum pull value of 60 tons. The test arrangement is fixed at one end, and the lift point is connected to the hydraulic pulling device with a sling, to represent the same situation it would expect during the actual lifting. The hydraulic pulling device is connected to measurement instrument. This instrument shows how much load is applied to the lift point at any given time during the test. In addition, the instrument has a separate marker which represents the maximum load the GRP point encountered during the test. The maximum load is the break load for the lift point involving ultimate failure. This maximum load is the key parameter attained from the different test setups.

Figure 4.1: Hydraulic tensile bench with the Case 3 test setup.

4.2 Recommended improvements

Firstly, it is recommended to carry out more tests of each individual thickness of each test setup. By doing several tests, it would be possible to see whether the results are consistent and collect characteristic values for each laminate thickness for each test performed. It would make the results more valuable for strength estimate and when comparing the result with analytical solutions.

Secondly, the test setup worked well, but in some cases the sharp edges from the steel arrangement affected the sling. This was improved by using rubber between the steel and the strap. On another occasion it may be possible to improve the test setup so that the sling is not affected by the steel.

The final recommended improvement is to perform the test in a hydraulic tensile bench with a higher maximum cap for tensile load. The 60-ton hydraulic bench did not cause ultimate failure in the 40mm laminate during testing for Case 1.

4.3 Results from experimental tests

Three tests were conducted with different setups, Case 1, Case 2 and Case 3. Case 1 is a representation of a lift through the splash zone, where GRP cover is in an upright vertical position. Case 2 is an approximation of a horizontal lift with the lifting point located on top of the cover, causing the lifting point to encounter out-of-plane loads. Case 3 is a representation of a horizontal four-point lift where the lifting point is placed on the side walls.

Table 4.1: Tested break load for all cases.

Test setup	Break load [*Te*] for 20mm laminate	Break load [*Te*] for 30mm laminate	Break load [*Te*] for 40mm laminate
Case 1	45.0	56.0	N/A
Case 2	12.0	19.0	22.0
Case 3	20.0	28.0	38.0

The results are presented in Table 4.1 and in Figure 4.2. The only value that was not found was for 40mm laminate in Case 1. Given that the hydraulic tensile bench had a maximum pulling capacity of 60 tons, the bench was unable to cause ultimate failure on the lifting in the Case 1 setup.

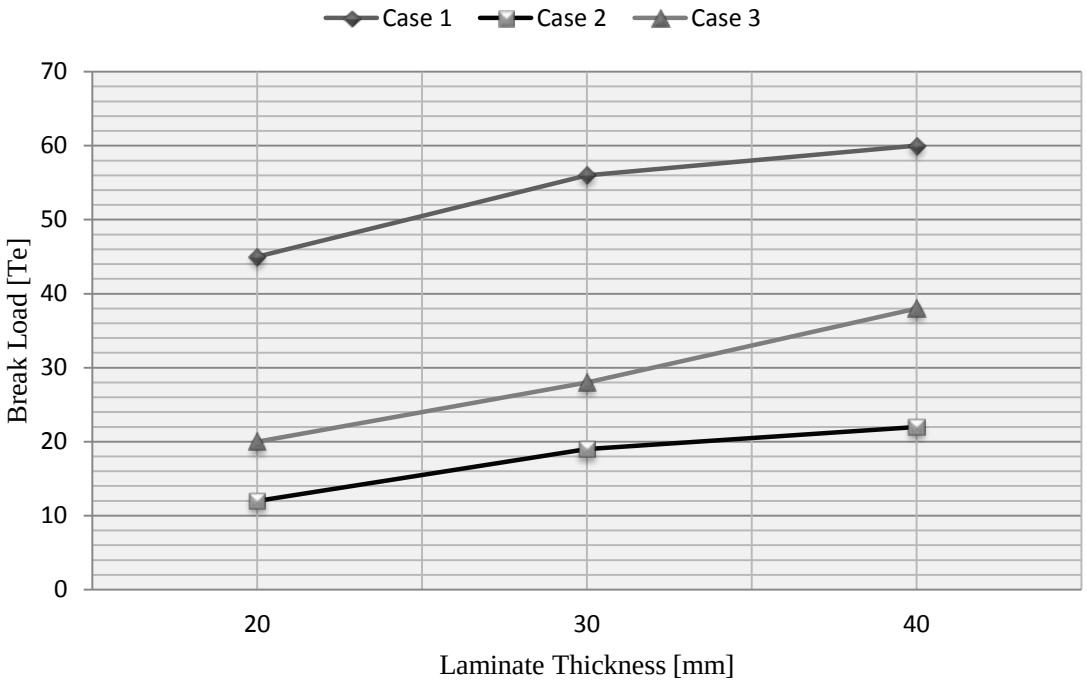

Figure 4.2: All the test results presented in a graph.

The ultimate failure that occurred for Case 1 is shown in Figure 4.3a. The sling caused the mid-section of the GRP lift point (Section between the two holes) to break free in the in the in-plane direction. The failure began developing on the edges of the sling, progressing to ultimate failure from the initial failure at the edges.

The ultimate failure that occurred for Case 2 is shown in Figure 4.3b. The sling caused the whole mid-section of the GRP lift point (section between the two holes) to be ripped out in the out-of-plane direction. Ultimate failure through thickness started on the edges of the sling that was attached around the holes.

The ultimate failure that occurred for Case 3 is shown in Figure 4.3c. The sling caused ultimate failure at the centre of the mid-section. The failure seems to be caused by out-of-plane failure, since the fibers are pointing out of the plane of the material.

a) Case 1 ultimate failure b) Case 2 ultimate failure c) Case 3 ultimate failure

Figure 4.3: Ultimate failure mechanism for the lifting point in the three test setups.

Chapter 5

Analysis

In the coming section, several finite element analyses of the problems discussed in the previous sections (Case 1 and Case 2) are performed. The aim is to virtually model the tested situation in the best way possible, in order to achieve comparable results. According to DNV, the recommended way to perform analysis of composite structures is to use the finite element method, which is considered the most accurate. The challenge is to make a model that represents the situations of reality in an optimal way. For instance, in FE models the supports are idealized as hinged, or completely rigid, whereas the actual supports are often somewhere in between. Thus, the supports must be treated with care. There are several requirements for finite element analysis of composite structures used in the offshore industry. The requirements help to give an indication of how the analysis should be carried out. The purpose is to obtain better results and reduce the risk of errors.

Overview of requirements according to DNV composite components C501:

1. Element types shall be chosen on the basis of the physics of the problem.
2. The choice of mesh should be based on a systematic iterative process, which includes mesh refinements in areas with large stress/strain gradients.

Model behavior shall be checked against behavior of the structure. The following modeling aspects shall be treated carefully:

3. Loads
4. Boundary conditions
5. Important and unimportant actions
6. Isotropic, orthotropic or anisotropic material
7. Non-linearity (due to geometrical and material properties)

For non-linear problems, the following special considerations shall be taken into account:

8. The analyst shall make several trial runs in order to discover and remove any mistake.
9. The analyst shall start with a simple model, possibly the linear form of the problem, and then add non-linarites one by one.

5.1 Finite element analysis of Case 1

The model is designed to represent the real test setup for Case 1. The dimensions of the lifting points are exactly the same size as in the tests. The lifting point is placed in a steel arrangement, which is attached to a fixed point on the bench. During the test, a sling was attached through the lifting holes and connected to the hydraulic tensile hook where the load is applied. In the finite element model, the support for the lift point is fixed at one end, with additional constraints in the out-of-plane direction at the opposite corners. The supports represent the inside of the steel arrangement. The load is applied to the material by the attached sling. This is modeled with multi-point constraints, connecting several points at the mid-section to a single point. A load or displacement is then applied to the single point, representing the load applied from the tensile bench. The width of the real sling is modeled as the total width of the multi-point constraint. The entire finite element model of the lifting point, with supports and attached loads, is shown in Figure 5.1.

In Chapter 3 there is a full description of the theory of progressive failure. A short summary of procedure is given here. The progressive analysis works by dividing the total load into smaller increments. An increment is then checked, by finding the stresses and strains acting in the model, and these values are checked against a given failure criterion. In the case of failure, the local material properties will be degraded and the lifting point is checked again. If no new failure occurs, then the load is increased incrementally and the same procedure can continue. This goes on until it reaches a point where the material achieves the total load, or becomes too weak to withstand higher load.

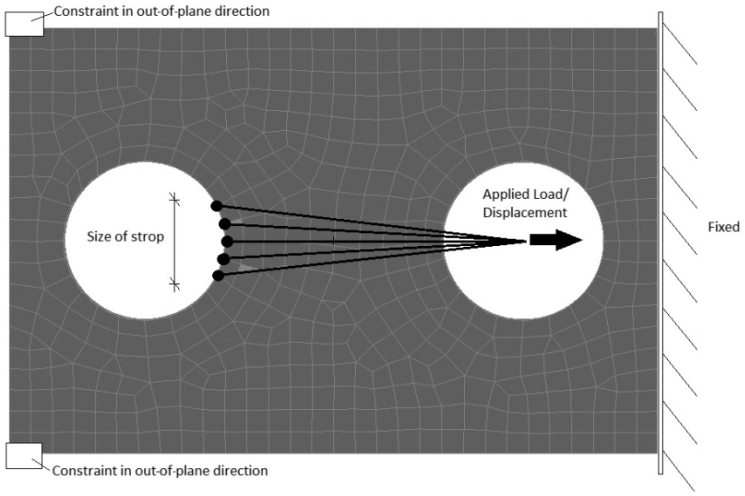

Figure 5.1: Finite element model of Case 1.

5.1.1 Finite element model and boundary conditions for Case 1

The lifting point is modeled with shell elements for the analysis of Case 1. Shell elements provide a good assumption when the thickness is small compared to the length and width, and the loads act in the material plane (Chawla, 1987). DNV composite C501 states that shell elements can be chosen in finite element analysis when the stresses in the out-of-plane direction can be neglected.

Attaining a square mesh with IsoMesh setting is advised for non-linear progressive analysis, according to the MSC Nastran manual (MSC, 2012). It is desirable to achieve a uniform mesh with sufficient elements in the middle-section of the lifting point to ensure efficient finite element results.

The material model is based on the values attained from the material tests at Reinhold AS. The ply material properties are 2D orthotropic with the same lay-up as the lifting points used in the tests. One layer is based on 70% fibers parallel in the 0 degree direction, 25% fibers in the 90 degree direction, and finally, 5% chopped strand material (CSM) to obtain improved adhesion between the layers. One layer is 1.5mm, and to obtain 20, 30 and 40mm laminates, there are respectively 14, 20, and 27 layers.

Four different progressive analyses are performed:

- Puck failure criterion with gradual stiffness degradation
- Puck failure criterion with immediate stiffness degradation
- Hashin failure criterion with gradual stiffness degradation
- Hashin failure criterion with immediate stiffness degradation

The analysis is based on the implicit non-linearity because of the degradation of the material properties. The maximum time step is set to 0.05 (of a total time 1.0),meaning that the material is checked at maximum 5% of the total load at each step, before increasing another maximum 5%. An overview of the finite element settings used in the analysis is given in Table 5.1.

Table 5.1: Finite element analysis settings for Case 2.

Parameter	Setting
Version	MCS Nastran 2012.2
Number of elements	493
Number of nodes	559
Mesh type	IsoMesh
Element property	Shell 2D
Ply material properties	2D orthotropic
Increment type	Adaptive
Total time	1.0
Max time step	0.05
Solver parameter	Implicit non-linear
Non-linear formulation	Large strain

5.1.2 Result of Case 1

All results from all the analysis of Case 1 are collected in Appendix B; a list of results for Case 1 are presented in Table 5.2.The result is the peak value for the graph from Figure 5.2, which indicates the maximum load the GRP lift point can withstand before ultimate failure.

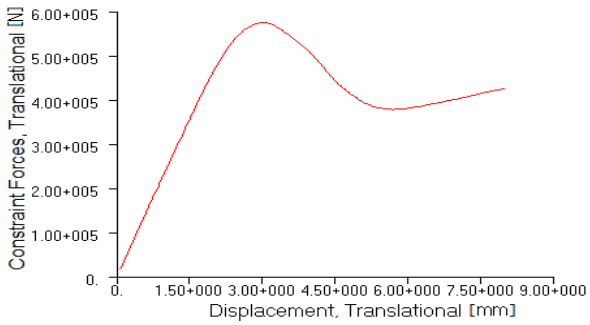

Figure 5.2: Puck failure criterion with gradual degradation for 30mm laminate.

A constraint force is the total force the laminate can withstand and is given in Newton [*N*]; 590 000N is approximately the same as 59 tons (simplified with gravity equal to 10m/s^2). The displacement is given in millimeters [*mm*], representing the applied load. From Figure 5.2, one can see that the local degradation of the material causes the material to be weaker. The peak value of the graph indicates the maximum load the GRP lift point can withstand before ultimate failure. In the tested situation, the load applied is always being increased, causing ultimate failure. However, in the analytical solution, after the peak value has been accomplished, the material can still withstand a reduced load but would fail with an increase of load, as in the tests.

Table 5.2: Finite element analysis results of break load for Case 1.

Failure criteria and degradation model	Break load [*Te*] for 20mm laminate	Break load [*Te*] for 30mm laminate	Break load [*Te*] for 30mm laminate
Hashin with Gradual	36.0	51.0	68.0
Hashin with Immediate	27.0	36.0	48.0
Puck with Gradual	45.0	59.0	77.0
Puck with Immediate	28.0	39.0	51.0

The result from the finite element results for Case 1, summarized in Table 5.2, is presented in Figure 5.3. The graph includes the breaking capacity for the three laminate thicknesses, 20, 30 and 40mm.

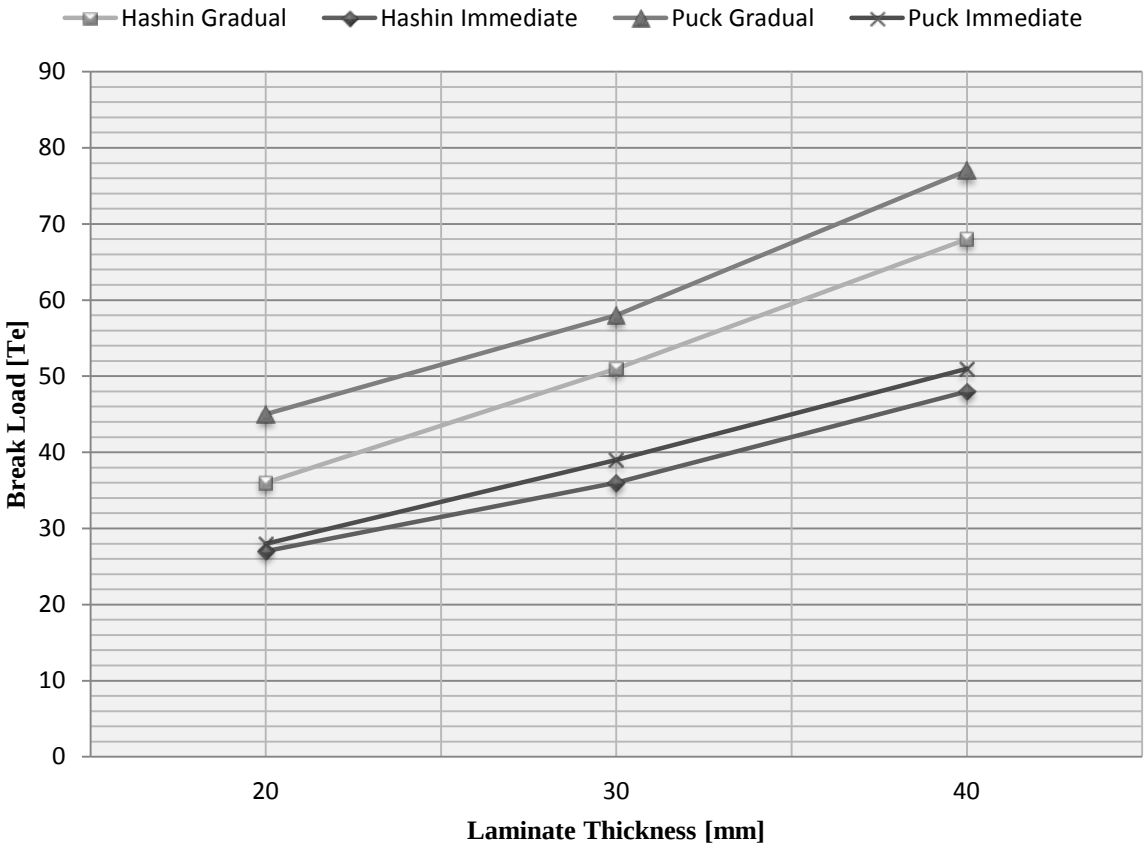

Figure 5.3: Finite element results of Case 1.

5.1.3 Damage propagation in Case 1

Figure 5.4 below shows when and how the material begins to develop a failure. It entails both the matrix and fiber failure, in other words, the total progressive damage model. By increasing the load, the failure begins to develop locally on the edges of the sling at the hole. It thereafter progresses further into the material, until ultimate failure occurs. Total failure through the thickness is shown as a red color. An overall red presentation between the lifting holes indicates that the material properties are fully degraded and cannot take on higher loads.

The current analysis presented below is Puck failure criterion together with the gradual stiffness degradation for 30mm laminate. This criterion and degradation model was best suited when compared to the tested values (all results are presented in Appendix B).

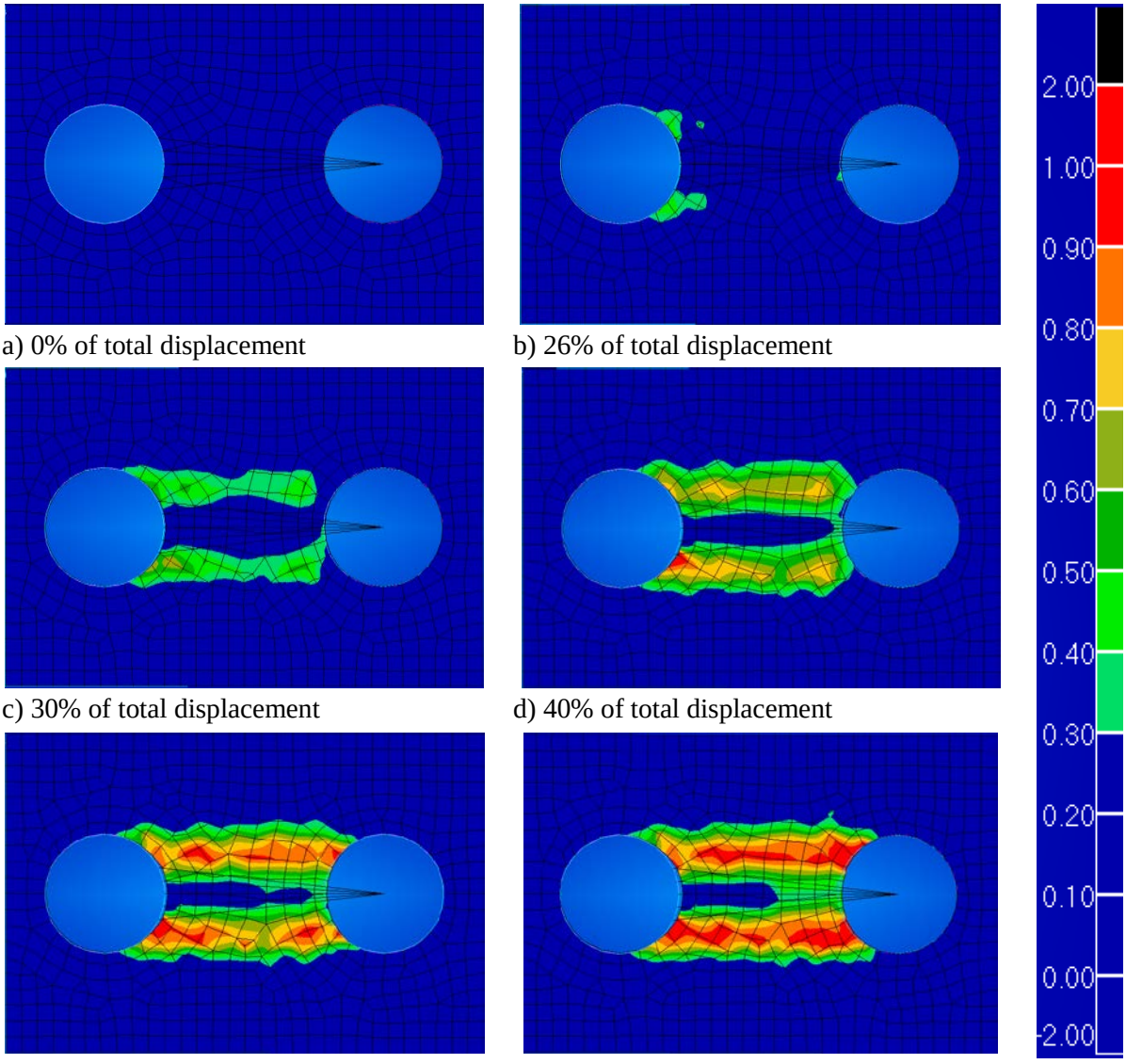

a) 0% of total displacement b) 26% of total displacement

c) 30% of total displacement d) 40% of total displacement

e) 51% of total displacement f) 61% of total displacement g)

Figure 5.4: Damage propagation in the FE analysis for Case 1.

5.1.4 General discussion of the result for Case 1

Consistently, the results of the Puck failure criterion give a higher estimate of the maximum capacity compared to those of the Hashin failure criterion. This applies to both the immediate and gradual stiffness degradations. Both criteria follow the same linear increase with increasing thickness of the laminate, respectively, 20, 30 and 40mm laminate thicknesses.

As expected, the immediate has a steeper curve than the gradual degradation. This was anticipated because the stiffness is reduced to nearly zero for immediate, whereas gradual stiffness is reduced to the last functional stiffness, prior to any failure (the process is described in further detail in Section 3.4.1, Degradation models).In every case, the results from immediate degradation provide a smaller maximum capacity.

5.1.5 Comparing finite element analysis and test results for Case 1

When comparing the test results and the analytical results, the Puck failure criterion with gradual stiffness degradation stands out from the rest. This criterion is within 2% error margin, which is a very good result. However, the hydraulic tensile bench was not strong enough to cause ultimate failure in the 40mm laminate lifting point, entailing that only two values are compared, which makes the results slightly weaker. Regardless, based on the two remaining results that were compared, the finite element model seems to give very accurate results.

For both the criteria and both degradation models, an increase in laminate thickness provides a fairly linear increase of capacity. It appeared in all the analysis that was performed. One benefit of having a linear increase in capacity with an increase/decrease of laminate thickness is that it is possible to expect an ultimate failure value. This will be beneficial for tests that are undertaken in the future. For instance, if a test result is very different from the expected result, it may help to indicate whether there is a problem with the test or the materials involved.

Due to the linear increase based on the two laminate thicknesses, 20 and 30mm, it is possible to assume that the capacity for 40mm would be around 65 to 75 tons, according to the test results. Based on the analytical results, the Puck failure criterion estimates an ultimate failure value of 77 tons. Both the estimated value from the test and the analytical results are within the same range of values for the ultimate failure load for the 40mm lifting point.

The comparison of the results shows that gradual provides a much better approximation to the actual maximum capacity than the immediate degradation. Based on the results, it appears that immediate is a conservative degradation model for this situation with the specific material properties. Immediate is a model that will fit well when the material is very brittle and thus breaks suddenly, while a gradual development behaves more like a ductile material. During the increase of load in the hydraulic tensile bench, it was possible to hear sounds of the material deforming before the ultimate failure occurred, which indicates that the material in reality has a more gradual degradation model. This observation corresponds well with the analytical results, which indicate that the gradual approach should give better results compared to immediate degradation.

Another exciting result concerns how the ultimate failure developed during the test. The central section between the two holes in the lifting point was torn out as a whole piece. Interestingly, the same type of failure developed in the finite element analysis, where the material fails on either side of the sling, thus showing that a central section is being torn out of the lifting point. These findings support the obtained finite element results being consistent with reality. The same failure development appears for both Puck and Hashin failure criteria. The only difference between them is that the ultimate failure occurs at different maximum loads.

5.2 Finite element analysis of Case 2

Case 2 is the setup with pure out-of-plane loads applied to the lifting point. It entails that a sling is attached through the holes, around the mid-section and pointing directly out of the plane in relation to the material. For the finite element analysis, the lifting point is simplified by looking at the mid-section of the lifting point. This is shown as the dark area in Figure 5.5. The strength to withhold the applied out-of-plane forces will mainly be shouldered by the mid-section. Therefore, one can assume that the simplification can provide relatively similar results. The advantage of the simplification is in saving a lot of computer time. Due to major stresses acting in an out-of-plane direction in this situation, the lifting point must be modeled with solid elements (to take account of the stresses in the3rddirection). Use of solid elements increases the number of nodes in the analysis, which simultaneously increases the complexity and time required to carry out an analysis.

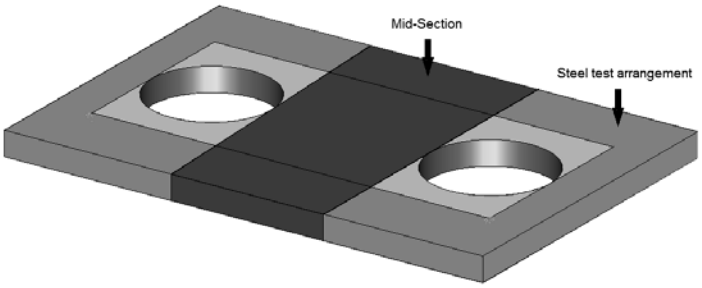

Figure 5.5: Overview over the mid-section in the lifting point.

The model is designed to represent the real test setup for Case 2. The dimensions of the lifting points are exactly the same size as in the tests but, for the analysis, are simplified to represent the mid-section. The lifting point is placed in a steel arrangement, which is attached to a fixed point on the bench. During the test, a sling was attached through the lifting holes and connected to the hydraulic tensile hook where the load is applied in the out-of-plane direction. In the finite element model, the support for the lift point is fixed at the edge of the steel arrangement in the out-of-plane direction. The load is applied to the material by the attached sling through the holes. This is modeled with multi-point constraints, connecting several points to a single point, representing the sling with corresponding sling-size. A load or displacement is then applied to the single point, representing the load applied from the tensile bench. The entire finite element model of the mid-section of the lifting point, with supports and attached loads, is shown in Figure 5.6.

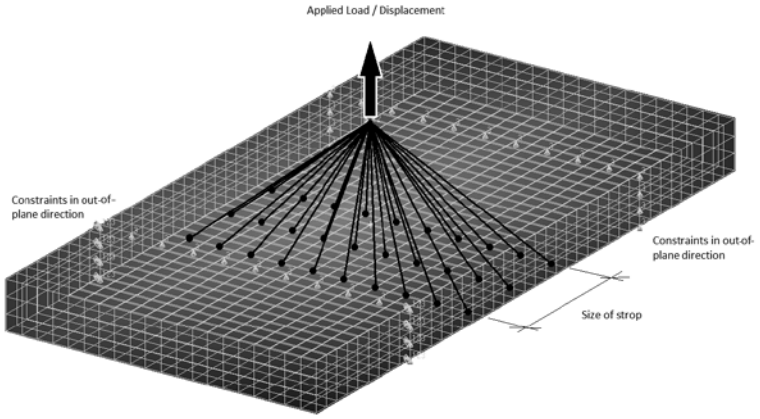

Figure 5.6: Finite element analysis model for mid-section.

5.2.1 Finite element model and boundary conditions

For Case 2 the load is applied in the out-of-plane direction, and thus the plane stress with shell elements fails. Solid elements take account of stresses in all directions and thus provide better results. The disadvantage of solid elements is that the finite element analysis is time-consuming because of more elements and nodes. In order to reduce the computer time, the model is slightly simplified as described in the previous section.

The mesh is completely square and, according to DNV composite design, at least two elements in the thickness direction must be obtained. For the laminate thicknesses of 20 and 30mm, there are three elements in the thickness direction and for the 40mm laminate, four elements.

The laminate properties are of the same order as in the previous analysis (Case 1). The difference between the shell and solid element is that there are several parameters describing the additional out-of-plane direction. It involves both the engineering constants as well as the attained failure values in that direction. The ply material properties are 3D orthotropic with the same lay-up as the lifting points used in the tests and the finite element analysis for Case 1,meaning that one layer of 1.5mm is based on 70% fibers parallel in the 0 degree direction, 25% fibers in the 90 degree direction, and finally, 5% chopped strand material (CSM).

Four different progressive analyses are performed:

- Puck failure criterion with gradual stiffness degradation
- Puck failure criterion with immediate stiffness degradation
- Hashin failure criterion with gradual stiffness degradation
- Hashin failure criterion with immediate stiffness degradation

The analysis is based on the implicit non-linearity because of the degradation of the material properties. The maximum time step is set to 0.05 (of a total time 1.0),meaning the material is checked at a maximum 5% of the total load at each step, before increasing another maximum 5%. An overview of the finite element settings used in the analysis is given in Table 5.3.

Table 5.3: Finite element analysis settings for Case 2.

Parameter	Setting
Version	MSC Nastran 2012.2
Number of elements	2400 (3200 for 40mm)
Number of nodes	3446 (4307 for 40mm)
Mesh type	IsoMesh
Element property	Solid 3D
Ply material properties	3D orthotropic
Increment type	Adaptive
Total time	1.0
Max time step	0.05
Solver parameter	Implicit non-linear
Non-linear formulation	Large strain

5.2.2 Result of Case 2

The results of all the analysis of Case 2 are collected in Appendix C; a list of results for Case 1 are presented in Table 5.4.The result is the peak value for the graph from Figure 5.7, which indicates the maximum load the GRP lift point can withstand before ultimate failure.

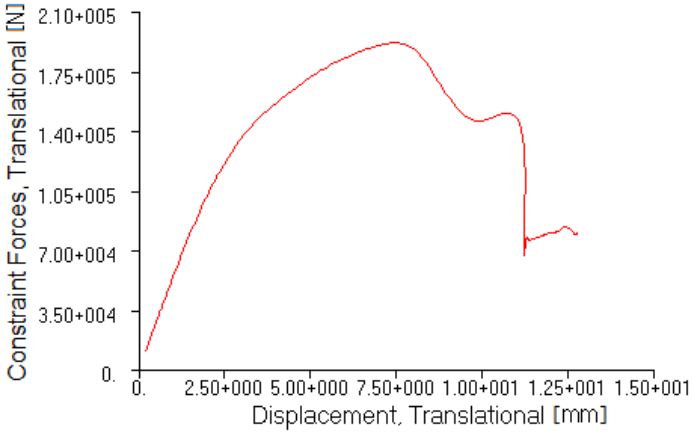

Figure 5.7: Hashin failure criterion with gradual degradation for 30mm laminate.

A constraint force is the total force the laminate can withstand and is given in Newton [*N*]; 210 000N is approximately the same as 21 tons (simplified with gravity equal to 10m/s^2). The displacement is given in millimeters [*mm*], representing the applied load. From Figure 5.7 one can see that the local degradation of the material causes the material to be weaker. The peak value of the graph indicates the maximum load the GRP lift point can withstand before ultimate failure. In the tested situation, the load applied is always being increased, causing ultimate failure. However, in the analytical solution, after the peak value has been accomplished, the material can still withstand a reduced load but would fail with an increase of load, as in the tests.

Table 5.4: Finite element results of break load for Case 2.

Failure criteria and degradation model	Break load [*Te*] for 20mm laminate	Break load [*Te*] for 30mm laminate	Break load [*Te*] for 30mm laminate
Hashin and Gradual	9.5	19.3	26.1
Hashin and Immediate	5.4	11.0	17.4
Puck and Gradual	8.3	18.9	26.0
Puck and Immediate	4.8	12.0	16.8

The result from the finite element results for Case 2, summarized in Table 5.4 is presented in Figure 5.8. The graph includes the breaking capacity for the three laminate thicknesses, 20, 30 and 40mm.

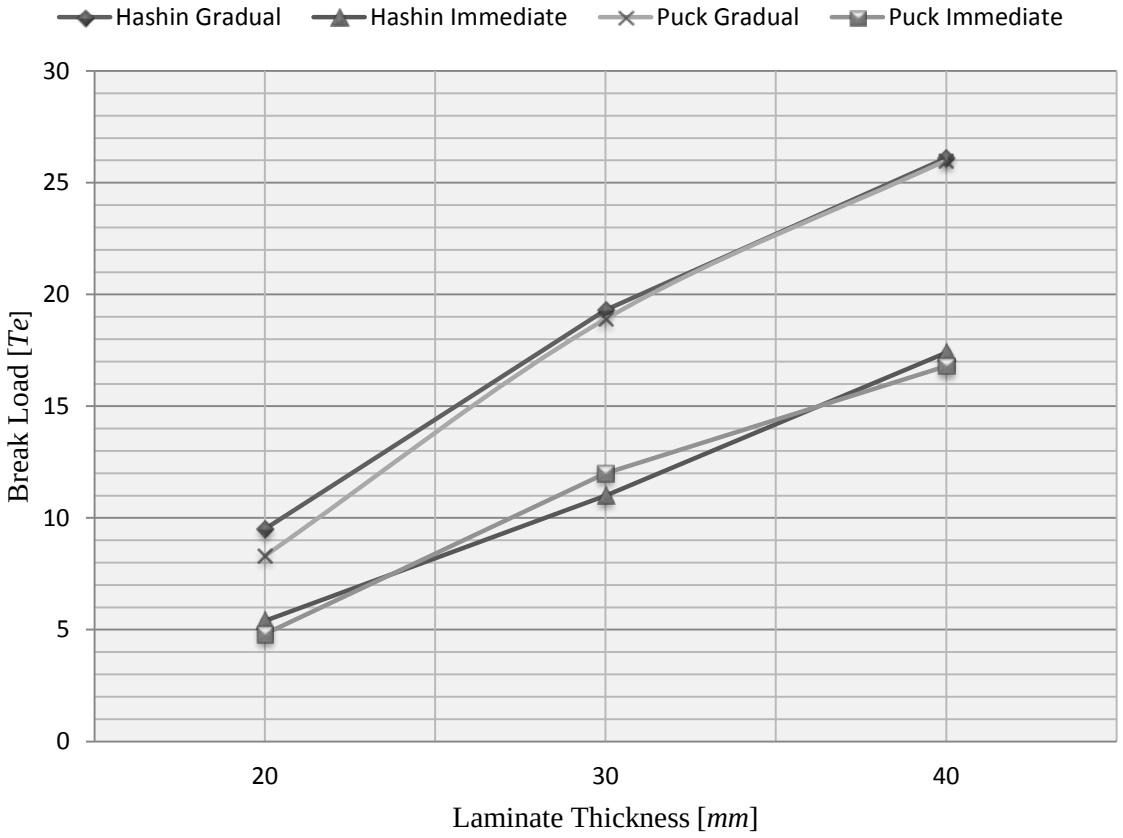

Figure 5.8: Finite element analysis results of Case 2.

5.2.3 Damage propagation of Case 2

Figure 5.9 below shows when and how the material begins to develop a failure. It entails both the matrix and fiber failure, in other words, the total progressive damage model. By increasing the load, the failure begins to develop locally on the top of the mid-section. It thereafter progresses further into the thickness of the material at each side of the sling model (multi-point constraint), until the ultimate failure occurs. Total failure through the thickness is shown as a red color. An overall red presentation through the thickness indicates that the material properties are fully degraded and cannot take on higher loads.

The current analysis presented below is the Hashin failure criterion together with the gradual stiffness degradation for 30mm laminate. This criterion and degradation model was best suited, when compared to the tested values (all results are presented in Appendix C).

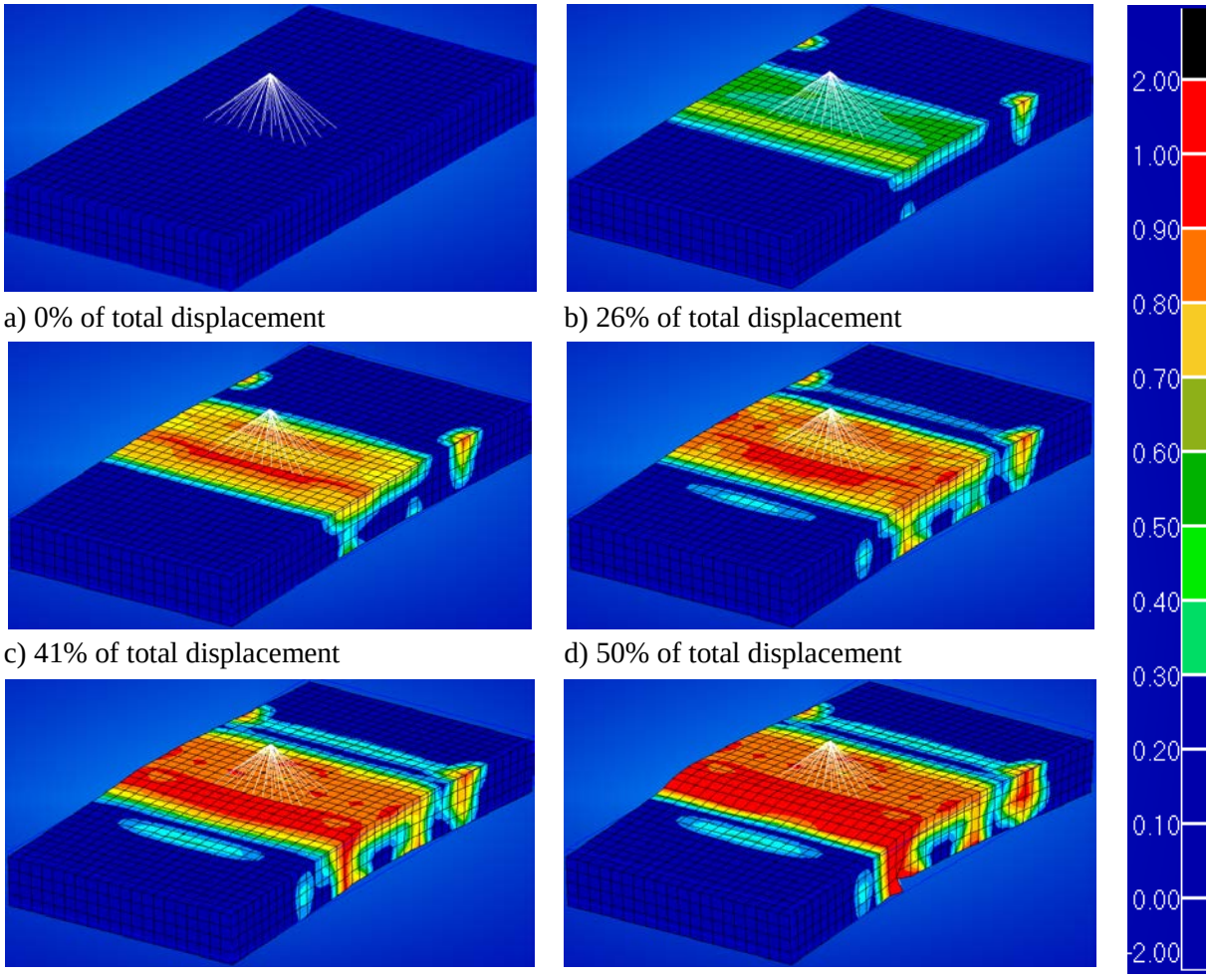

a) 0% of total displacement
b) 26% of total displacement
c) 41% of total displacement
d) 50% of total displacement
e) 65% of total displacement
f) 100% of total displacement
g)

Figure 5.9: Damage propagation in FE analysis of Case 2.

5.2.4 General discussion of the results

The finite element result from Case 2 shows very little deviation between the Hashin and Puck criteria, for both the immediate and gradual degradation. Both the criteria increase approximately linearly with increase in the laminate thickness. As expected, also for Case 2, the immediate has a steeper curve

than the gradual degradation. This was anticipated because the stiffness is reduced to nearly zero for immediate, whereas gradual stiffness is reduced to the last functional stiffness, prior to any failure. For each analysis, compared to the tested result the immediate degradation provides smaller maximum capacity.

5.2.5 Comparing finite element analysis and test results for Case 2

The result of the tests compared with the finite element analyses show an error margin of 21%. This is a higher error margin than that achieved for Case 1. A possible explanation is that there is more uncertainty in the finite element analysis for Case 2. The analysis is slightly simplified. In addition, the solid element used for Case 2 could cause more uncertainty. However, even with an error rate of around 20%, the finite element result provides a good indication of the maximum breaking load in the out-of-plane direction. As expected, the results from Case 2 show that the gradual degradation gives the best assumption of material breaking capacity. It is consistent with the results of Case 1, which also described the most similar analytical result compared to the tested result as the gradual degradation model.

As noted in the Test Report (Appendix A), the results of the tested 40mm laminate thickness are lower than expected. All the other tests, as well as the analytical results, show an approximately linear increase in capacity in accordance with the increase of the thickness. In addition, the analytical result provided a higher estimate of ultimate failure, which reinforces the suspicions that the tested capacity for the 40mm laminate is lower than projected. It is possible that it may have been an error source of some kind, causing inaccuracies in the test result. For the laminate thickness of 20mm, the finite element results are underestimated compared to the tests, while the results for 30mm had only one error rate of 2%. However, overall there is greater uncertainty among the results compared to Case 2.

The failure propagation begins locally on the top layers of the laminate, before it progresses further into the thickness of the material at each side of the constraints. For the Hashin failure criterion with gradual stiffness degradation, the ultimate failure occurred through the thickness at one end only, while, as for the other three combinations (Puck gradual, Puck immediate, and Hashin immediate), the ultimate failure through thickness occurred on both sides at the supports of the steel arrangement. The same type of failure also developed on the lifting point during the tests, where a middle section is torn out, and total failure occurs on both sides at the edge of the steel arrangement. The ultimate failure for the test of Case 2 is shown in Figure 5.10, and the Puck criterion with gradual degradation is shown in Figure 5.11.

Figure 5.10: Tested failure of Case 2.

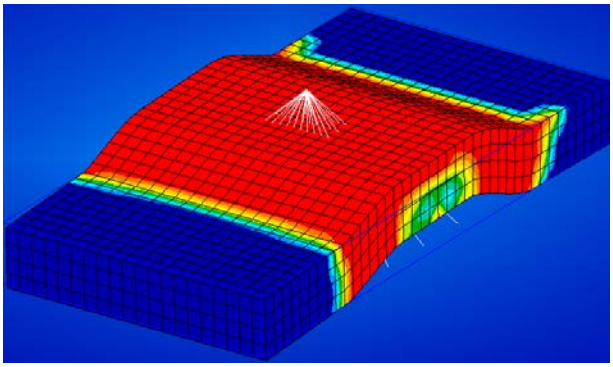

Figure 5.11: Analysed failure of Case 2.

5.3 Geometric approach in Case 3

The layout of Case 3 involves a sling that goes through the lifting holes and is connected to the hydraulic tensile bench. At the same time, the lifting point is kept inside a steel arrangement which is fixed to the bench. The sling forms an angle of approximately 45 degrees through the lifting holes, (see Figure 5.12). The angle of approximately 45 degrees implies that the lifting point will encounter load both in the out-of-plane and in-plane direction. From the previous tests, we have seen that the material is much stronger in-plane, than out-of-plane. On this basis it has been decided to take into account the out-of-plane capacity in a geometric consideration. The angle which is formed between the sling and the plane of the material is essential. The total load ($F_{.pull}$) which is applied to the sling will be decomposed to provide a load in the out-of-plane direction, and a load in the in-plane direction. By taking into account the known out-of-plane capacity and the angle, one can find the maximum sling load (F.pull) the material can withstand before ultimate failure. The out-of-plane capacity is taken from the finite element results in Case 2.

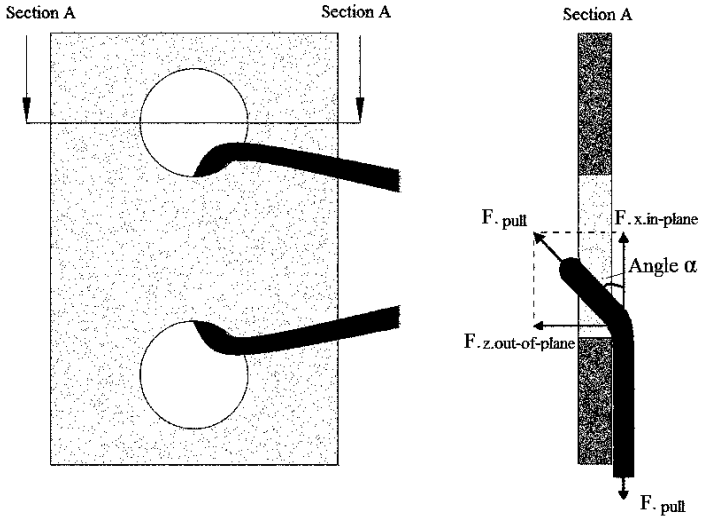

Figure 5.12: An overview of the geometric approach in Case 3.

The total force applied to the sling $F_{.pull}$, is decomposed into the force $F.z_{\text{-out-of-plane}}$, and $F.x_{\text{- in plane}}$. From the finite element results in Case 2, a maximum capacity has been established in the out-of-plane direction. In addition to the angle, these results will determine the maximum capacity in relation to the load applied to the sling, F.pull.

The advantage of using a geometric approach is that it is possible to find the maximum capacity of the lifting point at different sling angles. It helps to make the results very applicable for design. The lifting points can be placed at different angles on the GRP cover wall,depending on the requirements and design of GRP covers, in addition to different rigging design (lift design).This means that the angle the slings create can differ in many covers. By making a capacity function based on this angle, one can very easily determine the breaking capacity of any cover. The capacity function is based on the most accurate analytical results from Case 1 and Case 2. All calculations are presented in Appendix D.

Maximum in-plane capacity: F.p

Maximum out-of-plane capacity: F.z

Lift point capacity function: $F_{(\theta)} = \min(\frac{F.z}{Sin(\theta)}, \frac{F.p}{Cos(\theta)})$

5.3.1 Out-of-plane angle in Case 3

Looking at the test setup, the angle the sling formed was approximately 45 degrees. In addition to visually measuring the angle, it is also possible to calculate the angle based on the result of the tests. The angle calculation is based on the tested capacity for Case 3, against the tested capacity in Case 2. The angle is found by using geometrical considerations:

$$Sin\ (\theta) = \frac{Tested\ result\ Case\ 2}{Tested\ result\ Case\ 3}$$

Table 5.5: Calculated angle from the experimental tests.

Laminate thickness [mm]	Tested result [Te] from Case2	Tested result [Te] from Case3	Corresponding angleθ [°] from tests
20.0	12.0	20.0	37 °
30.0	19.0	28.0	43 °
40.0	22.0	38.0	36 °

The angle that emerges from the tests is between 36 and 43 degrees, close to the expected value of approximately 45 degrees. These results indicate that using a geometric method for achieving the ultimate failure when the sling forms an angle is applicable, but with a slightly higher degree of uncertainty.

5.3.2 Results from geometric approach for Case 3

All the results are presented in Appendix D. A summary of the results for some specific angles is presented in Table 5.6. The result from the capacity function appears in the form of a graph based on the angle, in-plane and out-of-plane capacity, and shows the ultimate break load for any given angle. The beauty of the graph is that it contains a lot of information but is able to present it in a very delicate way. By using this graph for a specific laminate thickness, one can find the capacity for any given angle and for any situation. It leads to a fast and effective way to find the capacity.

Table 5.6: Results for a representation of angles in the range of 35 to 45 degrees.

Laminate thickness [mm]	Break load [Te] at angle θ = 35°	Break load [Te] at angle θ = 40 °	Break load [Te] at angle θ = 45 °
20.0	16.6	14.8	13.4
30.0	33.6	30.0	27.3
40.0	45.5	40.6	36.9

The graph in Figure 5.13 of the laminate with 20mm thickness provides a slightly lower assumption of the analytical load in relation to the tested value. The reason for this is some inaccuracy in the finite element results of Case 2. It is important to be aware that if there are any inaccuracies in the results

from Case1 and Case 2, they will be passed onto the results of Case 3. The graph shows smaller estimates of capacity than in the test. This is displayed in this graph and allows the results to be conservative. Based on the graph, we get a value in the range of 13 to 17 tons for Case 3, which is slightly lower than the tested value of 20tons.

The dotted line is a correction that takes away the unrealistic increase in capacity at low angles. The problem is solved by a linear increase in capacity at the lowest angles.

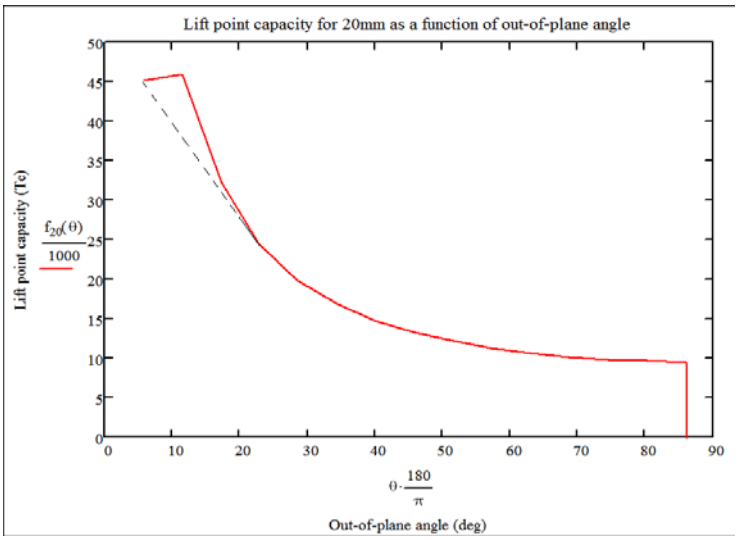

Figure 5.13: Capacity function for 20mm lifting point as a function of out-of-plane angle.

Figure 5.14 shows the 30mm results are almost identical to the actual tested results, which is very good considering they are based on the finite element method. The analytical value of the angle 45 degrees is 28 tons, which is also the tested value for Case 3.

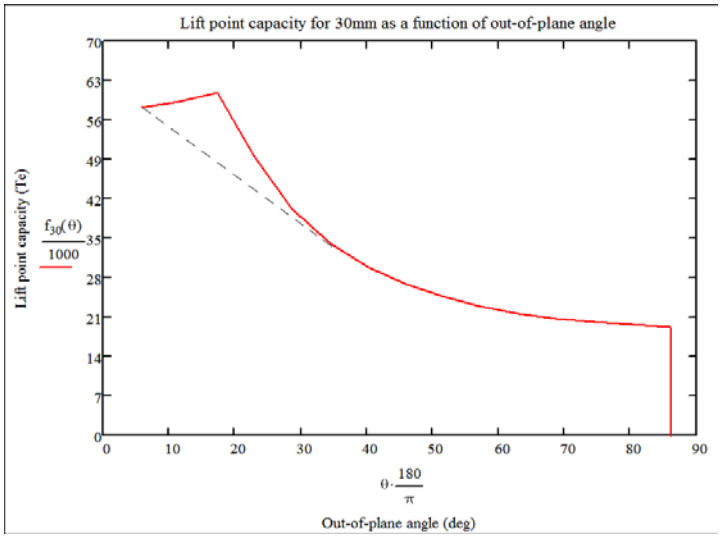

Figure 5.14: Capacity function for 30mm lifting point as a function of out-of-plane angle.

The results from 40mm laminate are interesting. As described earlier, inaccuracy from the finite element results of Cases 1 and 2 will influence the results for Case 3.For the 40 mm lifting point, the out-of-plane capacity achieved in finite element analysis for Case 2 was higher than the tested

capacity. However, the results for the 40mm provide a very good approximation for the result for Case 3 (based on Case 2) with an analytical value of 38 tons compared with 38 tons in the test. This helps to reinforce the suspicion that the tested result of the tested capacity of the 40mm laminate was not as high as it should have been.

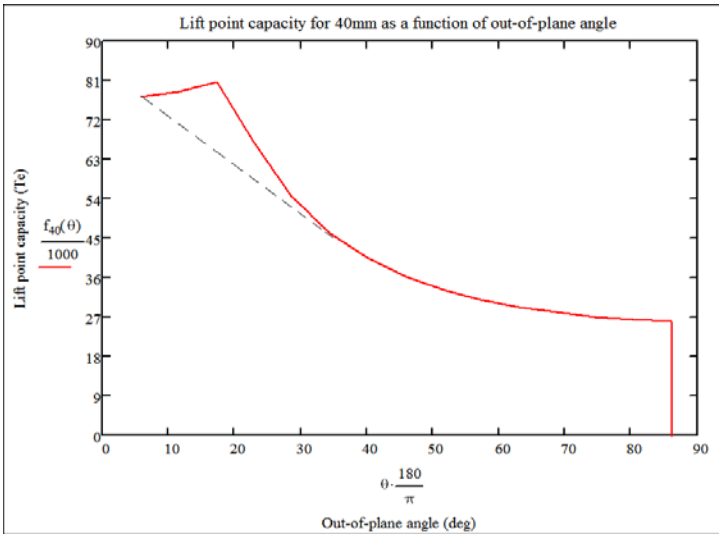

Figure 5.15: Capacity function for 40mm lifting point as a function of out-of-plane angle.

5.4 Improvement study

In the previous sections the experimental tests have been compared with the finite element results. From this, it has been found that the Puck failure criterion with gradual degradation has consistently provided good results compared to the tests. Based on these findings, it was decided to explore the possibility to enhance the capacity of the lifting point in an improvement study. The desire is to look at a new type of laminate lay-up. The current lay-up is based on the forces acting globally on the cover, where the transverse forces are most critical (hence the 70% fibers in the direction 0). Due to the lifting points being essentially extra layers contributing to a local increase in the thickness, it is possible to use a more specified lay-up for the additional layers for the lifting point.

As previously mentioned, the fibers are very strong in the parallel fiber direction. This forms the basis for the new fiber lay-up. The proposal for another lay-up is selected from a setup of fibers in multiple angles. In order to withstand the forces acting locally in the lifting point, multiple angles will help withstand all acting forces such as compression, tension, and shear forces. Therefore the $\pm$ 45 degree direction ply is introduced. This includes maintaining fibers in these fiber directions:

[0, 90, 45, -45]

The new layer contains:

- 30% fibers in 0 degree direction
- 30% fibers in 90 degree direction
- 20% fibers in +45degree direction
- 20% fibers in -45 degree direction

The new analysis is based on the Puck failure criterion with gradual stiffness degradation of 30mm laminate (respectively 20 layers). An analysis is performed for Case 1 and Case 2, with the same parameters as before, the only differencebeingthe new fiber lay-up.

Table 5.7: Finite element analysis settings for improvement study.

Parameter	Setting for Case 1	Setting for Case 2
Version	MCS Nastran 2012.2	MSC Nastran 2012.2
Laminate thickness	30 mm	30mm
Number of elements	493	2400
Number of nodes	559	3446
Mesh type	IsoMesh	IsoMesh
Element property	Shell 2D	Solid 3D
Ply material properties	2D orthotropic	3D orthotropic
Increment type	Adaptive	Adaptive
Total time	1.0	1.0
Max time step	0.05	0.05
Solver parameter	Implicit non-linear	Implicit non-linear
Non-linear formulation	Large strain	Large strain

5.4.1 Results from improvement study

Case 1

The result from the finite element analysis for Case 1 with the new layout is given in Figure 5.16. The graph gives a peak value at 77 tons. This is an increase of over 28% compared to the same test with the initial setup, (initial peak value of 60 tons). Looking at the graph, it appears that even with gradual stiffness degradation, the graph shows a more “immediate” development by having a steeper curve than in the previous case. It may indicate a slightly different behavior of the material with the new lay-up. Regardless, the new lay-up with layers involving the additional angles of 45-degree laminates seems to improve the results for Case 1 convincingly.

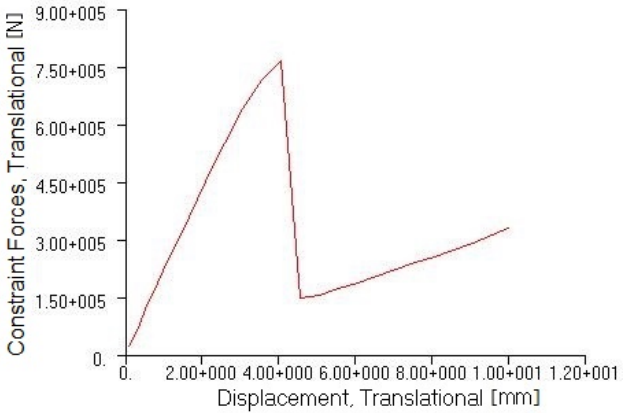

Figure 5.16: Puck gradual 30mm with new lay-up.

Case 2

The result from finite element analysis for Case 2 with the new layout is given in Figure 5.17. The graph gives a peak value at 22 tons. This is an increase of over 16% compared to the same test with the initial setup (initial peak value of 18.9 tons). The curve is similar to the original analysis, but with a higher peak value.

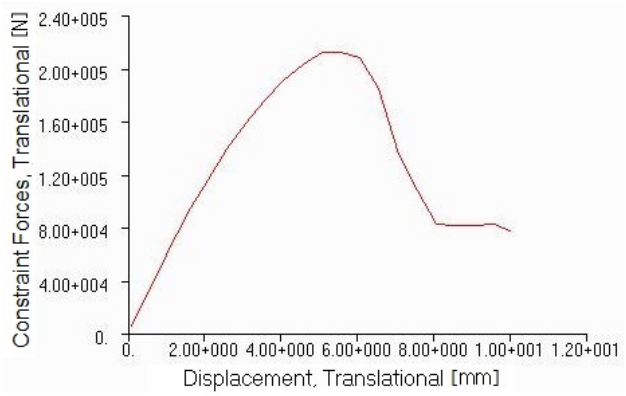

Figure 5.17: Puck gradual 30mm out-of-plane with new lay-up.

Chapter 6

Conclusion

Three normal lifting situations (Case 1, Case 2 and Case 3) have been studied in order to verify the lifting capabilities for the GRP cover with the finite element method, with a desire to replace the simplified hand calculations used today. This involves the ability to analyze the lifting point with greater accuracy and to understand to a greater extent the behavior of the material.

Case 1 is based on the lifting situation through the splash zone with the cover in an upright position. In the test setup, load is applied to act in-plane of the lifting point. By comparing the test results with the analytical results, the Puck failure criterion with gradual stiffness degradation is within 2% error margin, which is considered to be very accurate. However, it is to be noted that the hydraulic tensile bench failed to cause ultimate failure for the 40mm laminate because of a load limitation of 60 tons. For all the failure criteria with different material degradation models, the result consistently showed a linear increase in capacity with an increase of thickness. Interestingly, the damage propagation and failure mode attained in the finite element analysis matched very well with the test for Case 1, meaning that both results showed that the central section of the lifting point was torn out as a separate piece, helping to support the analytical results obtained.

Case 2 is based on the situation with a lift point on top of a cover in a horizontal lift, causing the force to act directly in the out-of-plane direction of the material. The finite element model was slightly simplified by only looking at the mid-section of the lifting point. The solid element is used to take into account the stresses acting in the out-of-plane direction. The result from Case 2 shows practically no deviation between the Hashin and Puck failure criteria, but the Hashin failure criterion with gradual material degradation is a few percent more accurate. Compared to the tests, an error margin of 21% is obtained. As noted in the Test Report (Appendix A), the tested ultimate failure capacity of the 40mm laminate in Case 2 was lower than expected, based on an approximately linear increase of capacity compared to an increase of thickness (from the analytical results). The tested failure propagation showed that the sling caused the whole mid-section of the GRP lift point (section between the two holes) to be ripped out in the out-of-plane direction. Ultimate failure through thickness occurred on the edges of the sling surrounding the holes, causing the mid-section to be ripped out of the lifting point. Regardless, the Hashin failure criterion with gradual degradation anticipated failure to only occur on one side of the lifting holes. Interestingly, the Puck failure criterion predicted the same failure propagation that occurred during the tests.

The result with the immediate stiffness degradation model consistently showed a lower capacity estimate than the tested results, leading to the conclusion that this model is seen as conservative in each analysis. The cause for the inaccuracy in the results for 40mm laminate in Case 2 may be caused by the simplification, or the fact that there is more uncertainty with the use of solid elements to take account of the stresses acting in the out-of-plane direction of the lifting point. In order to arrive at a conclusion, further tests must be carried out to achieve characteristic tested values.

Case 3 is based on the situation with a lift point on the sidewall of a GRP cover in a horizontal lift, causing the sling to form an angle to the material plane. Based on the angle, the forces acting on the lift point can be decomposed to act in the material plane and out-of-plane. The results from Cases 1 and 2 conclude that the out-of-plane direction is considered to be the weakest. Therefore, the decomposed force acting in the out-of-plane direction is checked against the finite element result from Case 2. A capacity function was made in order to show the capacity based on the angle the slings forms in relation the material plane. The function can be viewed in a graph, containing all the information needed to be able to predict the capacity for any situation given the laminate thickness. Regardless, it is important to be aware that, if there are any inaccuracies in the finite element results for Cases 1 and 2, they will be passed onto the graph.

An interesting discovery was made for the 40mm laminate in Case 3. The capacity function predicted a very accurate ultimate failure load compared to the tested result. The analytical result is a product of the finite element result from Case 2, which provided a higher estimate than the test in the specific case. However, for Case 3, the result was accurate, even though in Case 2 the analytical result was 20% higher than for the test. This contributes to a suspicion that the 40mm laminate in the test for Case 2 did not reach its full potential. There may have been a defect in the material or another error source. Regardless, more testing of each laminate thickness should be conducted in order to achieve characteristic values, which will reduce the speculation of the tested capacity.

The purpose of the analysis is to see whether one can estimate the capacity of the lifting points analytically, leading to a reduction of tests that need to be performed and a replacement of the simplified hand calculation method used today. Based on the results in this thesis, it is concluded that the Puck failure criterion with gradual stiffness is considered to be the most accurate. The finite element results provide a good estimate in the strength, but with slightly more uncertainty in the out-of-plane situations. The capacity function provides a graph representing all the results in a simple and efficient matter, with good results. The error margin of 20% would represent a material factor of 1.2, however, a material factor of 1.5 would be reasonable to ensure the lifting capacity (compared to the material factor of 2.0 used in the hand calculation). One can conclude that the obtained method in this thesis provides sufficient results, and could replace the simplified hand calculation used today.

Based on the findings in this thesis, the possibility to improve the laminate lay-up sequence was investigated. An improvement study was conducted using the Puck failure criterion with gradual stiffness degradation with the same settings as used in the previous finite element analysis. The new laminate lay-up included the fiber direction [0, 90, +45, - 45] (compared to the standard lay-up of [0, 90]). The analysis was performed for a 30mm laminate. The result for the new study showed an increase of over 28% in the capacity in Case 1 and an increase of over 16% compared with Case 2. These are great results, leading to the conclusion that by introducing the fiber directions $\pm$ 45 degrees, one can enhance the capacity of the material by about 20%. This new finding is easy and efficient to implement in new designs of lifting points in GRP covers. It entails ordering a separate fiber composition for the layers used to locally reinforce the lifting points.

6.1 Future work

Firstly, a recommended improvement of the tested result is to carry out more tests in order to achieve characteristic values. It would be possible to see whether the results are consistent and it would make the results more valuable for strength estimate and when comparing the result with analytical solutions.

Secondly it would be interesting to look into snap-load (dynamic load) during the lifting through the splash zone. During the installation the cover is tilted and is fitted with ballast in order to reduce the hydrodynamic loads, in addition, reduce the possibility to encounter snap-load. Regardless, if it in some unlikely scenario should occur slack in the sling causing a snap-load, it would be interesting to look at the effect it has on the lifting point.

References

ANSYS (2012).*Composite introduction (for ACP 14.5)*, ANSYS Inc., Pennsylvania, USA

Barbero, E. J. (2008). *Finite Element Analysis of Composite Materials*. CRC Press, West Virginia, USA.

Chawla, K. K. (1987). *Composite Materials Science and Engineering*. Springer-Verlag, Germany.

Deuschle, H. M. (2010). *3D Failure Analysis of UD Fibre Reinforced Composite: Puck's Theory within FEA*. PhD, University of Stuttgart, accessed 2nd April 2013 at: http://d-nb.info/1010526227/34

DNV-OS-C501 (2010). DNV Offshore Standard, Composite Components.

Eng-tips (2013). Finite element tips and tricks on an online forum, accessed 14th April 2013 at: www.eng-tips.com

Gibson, R. F. (1994). *Principles of Composite Material Mechanics*. McGraw-Hill Inc., USA.

Highcomp (2013). GRP cover manufacturer in Norway, accessed 3rd March 2013 at: www.highcomp.no

Knops, M. (2008). *Analysis of Failure in Fiber Polymer Laminates*. Springer, Heidelberg, Berlin.

Lauterbach S., Balzani C., Wagner W. (2009). *Failure Analysis on Shell-like Composite Laminates using the Puck Criteria*. Karlsruhe, Germany, accessed 14th March 2013 at: http://onlinelibrary.wiley.com/doi/10.1002/pamm.200910089/pdf

Milligan, D. (2012). Composites engineering jargon explained – progressive failure, USA, accessed 2nd April 2013 at: info.firehole.com

Mohite, P.M. (2012). *Hashin's Failure Criteria for Unidirectional Fibre Composites*. Department of Aerospace Engineering, Kanpur, accessed at 14th March 2013 at: home.iitk.ac.in/~mohite/Hashin_Failure_Criteria.doc

MSC Software (2012*). Interface to MSC Nastran, Preference Guide, Volume 1: Structural Analysis*. Santa Ana, USA.

Okutan, B. (2001). *Stress and Failure Analysis of Laminated Composite Pinned Joints*. PhD, Izmir, accessed 12th March 2013 at: web.deu.edu.tr/ansys/tezler/doktora/d1.pdf

Perillo, G., Vedvik, N. P., and Echtermeyer, A. T. (2011). *Numerical Application of Three-dimensional Failure Criteria for Laminated Composite Materials*. NTNU, Norway, accessed 14th March 2013 at: www.simulia-china.com/download/global/2011/Perillo.pdf

Pinho, S. T., Davila, C. G., Camanho, P. P., Iannucci, L., Robinson, P. (2005). *Failure Models and Criteria for FRP under In-Plane or Three-dimensional Stress States including Shear Non-linearity*.Nasa Langley Research Center, Hampton, accessed 2nd March 2013 at: http://ntrs.nasa.gov/archive/nasa/casi.ntrs.nasa.gov/20050110223_2005093402.pdf

Wikipedia (2013). Deformation (Mechanics) – Strain, accessed 19th of February 2013 at: en.wikipedia.org/wiki/Derformation_(mechanics)

Appendix A

Test Report

Tensile test of GRP lifting point

Test report prepared by Endre Ulversøy, 2013

Revision Sheet

Release No.	Date	Revision Description
Rev. 0	30/04/13	First edition

Table of Contents

1. General Information

1.1 Purpose

The purpose of the load test of the glass reinforced plastic (GRP) lift point is to establish the breaking capacity. The lifting points are tested to represent the reality in the best way possible.

1.2 Scope

The tests will help to document the lifting capacity of the local lift points. This will lead to lifting points being designed with less uncertainty than before. It will affect the design of lifting points for all new projects in Subsea 7. The different tests performed look at the normal lifting setups used for GRP cover during onshore, transport and installation.

The goal of the tests is to have documentation of the tested ultimate failure capacity representing the real lifting situation. The result can confirm that the lift point is strong enough. In addition, the test data can be used for comparison of analytical solutions, such as finite element analysis results.

The testing is divided into three test setups, representing the three most common lifting situations. The main situations are four-point and two-point lift. The four-point lift is used when lifting onshore, and the transfer of various means of transport. While the two-point lift is common when installing through the splash zone. Additionally, you have a situation where the lifting point is located on top of the cover, as an alternative used in some projects for light covers.

1.3 System Overview

A brief system overview, including the main persons involved:

- Responsible organization — Subsea 7
- System name or title — Tensile tests of GRP lifting points
- Location — Westcon Løfteteknikk AS at Haugesund
- Report — Endre Ulversøy
- Subsea 7 — Arne Skeie
- Subsea 7 — Karl Erik Suphellen
- Westcon Løfteteknikk AS — Svein-Terje Warvik
- Westcon Løfteteknikk AS — Roar Røssehaug
- Highcomp AS — Fredrik Faye

1.4 Error sources

When performing a test, it is important to be aware of the potential error sources that could influence the test results. To reduce the effect of potential error, the fabrication of the material need to be done with care, with the same environmental condition for all test specimens. In addition, the load cells need to be calibrating to be able to show the correct break capacity.

Possible error sources:

- Calibrating the test equipment properly.
- Differences in environment during fabrication of the lifting points, causing different material properties.
- Misalignment in test setup.

1.5 Security Considerations

During testing it is important with proper safety equipment. When performing tensile test of GRP lifting point both safety glasses and helmet was mandatory. There is a possibility for a rather sudden failure when applying load. When failure occurs, parts of the specimen can be accelerated and can cause damage. In addition, during the test a safety cover on the hydraulic tensile bench had to stay open because of the size of the test arrangement, causing the participants to be extra cautious with the safety equipment and keeping a reasonable distance during the testing.

1.6 Acronyms and Abbreviations

Provide a list of the acronyms and abbreviations used in this document and the meaning of each.

CSM	*Chopped Strand Material*
GRP	*Glass Reinforced Plastic*
WCL	*Westcon Løfteteknikk AS*
Te	*Tons*

2. Experimental Tests

2.1 Lift point

Test of lift point

- 3 off 20mm thick lift points
- 3 off 30mm thick lift points
- 3 off 40mm thick lift points

Material lay-up:

- 70% fibres in 0-direction
- 25% fibres in 90-direction
- 5% CSM

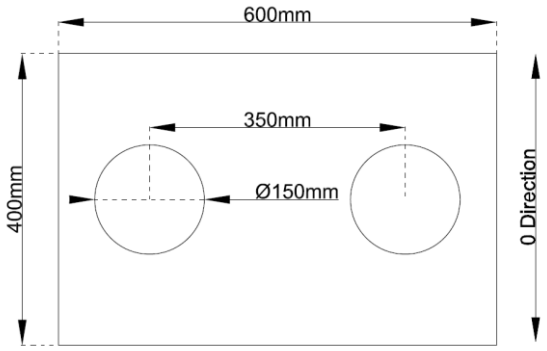

Figure A.1: Size of lift point

The size of the lift point is based on a full scaled representation of the actual lifting points used in GRP cover design.

2.2 Material properties

The material laminates were prepared at Highcomp AS and sent to Reichhold AS for testing. The material consists of fiber reinforcement of Formax FGE 394; 0 / 90 degree, with density 1902g/m^2, and polyester type PLT. 480-622. The conducted material properties from the material tests are given in the tables A.1, A.2 and A3.

Table A.1: Fiber dominated ply properties.

Parameter	Value	Unit	Explanation
E_1	28.7	GPa	Modulus of elasticity in main fiber direction
X_t	660	MPa	Tension stress at break in the main fiber direction
X_c	460	MPa	Compressive stress at break in the main fiber direction

Table A.2: Matrix dominated ply properties.

Parameter	Value	Unit	Explanation
E_2	9.00	GPa	Modulus of elasticity transverse to main fiber direction
G_{12}	3.00	GPa	Shear modulus in the ply plane
ν_{12}	0.26		Ply major Poisson`s ratio
Y_t	34.0	MPa	Tension stress at break normal to the main fiber direction
Y_c	50.0	MPa	Compressive stress at break normal to the main fiber direction
S_{12}	26.0	MPa	Shear stress in ply plane at failure

TableA.3: Through thickness ply properties.

Parameter	Value	Unit	Explanation
E_3	9.00	*GPa*	Modulus of elasticity normal to the fiber plane
G_{13}	3.00	*GPa*	Shear modulus normal to the fiber plane, incl. fiber direction.
G_{23}	2.00	*GPa*	Shear modulus normal to fiber plane, normal to the fiber direction.
ν_{13}	0.26		Poisson`s ratio normal to fiber plane, incl. fiber direction.
ν_{23}	0.48		Poisson`s ratio normal to fiber plane, normal to the fiber direction.
Z_t	13.0	*MPa*	Tension stress at break normal to fiber plane
Z_c	61.0	*MPa*	Compression stress at break normal to fiber plane
S_{13}	14.0	*MPa*	Shear stress at failure normal to fiber plane, incl. fiber direction.
S_{23}	14.0	*MPa*	Shear stress at failure normal to fiber plane, normal to fiber direction.

2.3 Experimental test setup

The test arrangement is located in a hydraulic tensile bench at Westcon Løfteteknikk AS in Haugesund. The tensile bench has a maximum pull value of 60 tons. The test arrangement is fixed at one end, and the lift point is connected to the hydraulic pulling device with a sling (size of approximately 70mm width), to represent the same situation it would expect during the actual lifting. The hydraulic pulling device is connected to measurement instrument. This instrument shows how much load is applied to the lift point at any given time during the test. In addition, the instrument has a separate marker which represents the maximum load the GRP point encountered during the test. The maximum load is the break load for the lift point involving ultimate failure. This maximum load is the key parameter attained from the different test setups.

Figure A.2: Hydraulic tensile bench with the Case 3 test setup.

2.4 Test setup for Case 1

The test of Case 1 is an approximation of the lift situation when installing through splash zone, where the cover is upraised in a vertically position. The lifting point is placed inside and supported by a steel arrangement specially made for the testing. This steel arrangement is attached to a fixed point on the bench. A normal sling was attached through the lifting holes and connected to the hydraulic tensile hook where the load is applied gradually. The sling transmits the forces in the plane of the material. Figure A.3 gives an overview of the test setup during the testing of Case 1. Three laminate thicknesses of the lifting point were tested, (20, 30 and 40mm). The load was applied gradually with increments of 4-5 tons, after each increment the material was checked for any local failure.

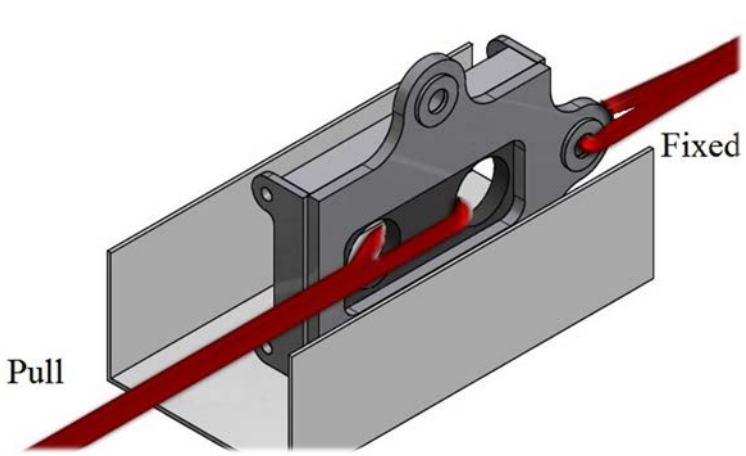

Figure A.3: Test setup for Case 1

2.4.1 Expected Outcome

It is expected that the lift point should be relative strong in this setup, since the load is applied in plane of the material (Strong compared to out-of-plane direction). In addition, it is expected that the results increases linearly when with the increase of the thickness of the tested laminates.

2.4.2 Practical Functionality

The test setup for Case 1 is a good representation of the operational environment the lifting point would encounter during actual lifting, meaning the sling is attached in the same manner, and in the same direction relative to the lifting point.

2.4.3 Results of Case 1

The results of the tests for Case 1 can be found in Table A.4 and in Figure A.4. Results are consistent with the expected outcome. This entails that the GRP material is relatively strong when load is applied in-plane. In addition, the GRP material has an approximately linear increase of capacity by increasing the thickness. Given that the hydraulic tensile bench had a maximum pulling capacity of 60 tons, the bench was unable to cause ultimate failure on the lifting point with 40mm laminate thickness. An expected break load for the 40mm laminate lifting point based on the other results from the tests would be of approximately 70 tons.

Table A.4: Tested result of break load for Case 1

Thickness of lift point *[mm]*	Break load *[Te]*
20.0	45.0
30.0	56.0
40.0	N/A

Comments to the test results for Case 1:

- For the 30 mm laminate thickness test, the lift point started to make cracking sounds at 52 tons.
- The lift point with 40mm laminate thickness was pulled to 60 tons (maximum pulling capacity of hydraulic tensile bench), with no visual damage on the material.

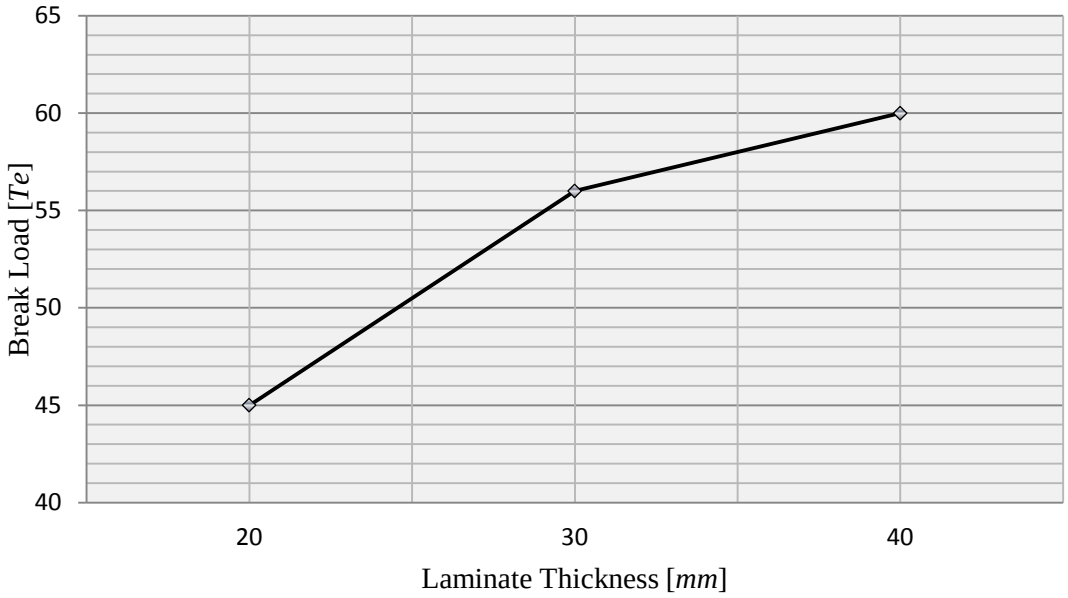

Figure A.4: Tested Break load results presented in a graph for Case 1

The ultimate failure that occurred is shown in the Figure A.5. The sling caused the mid-section of the GRP lift point (Section between the two holes) to break free in the in the in-plane direction. Meaning the failure developed on the edges of the sling, causing the mid-section to be ripped out of the lifting point.

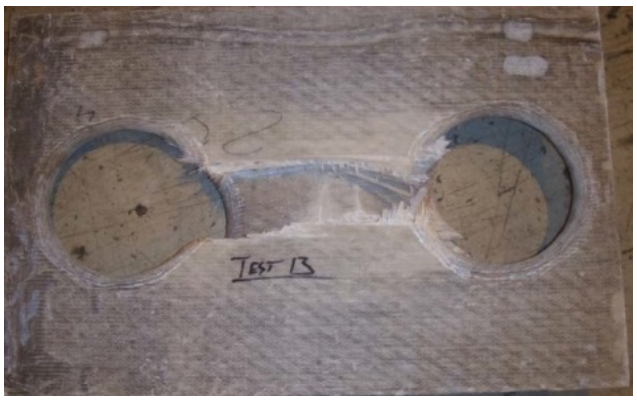

Figure A.5: Case 1 ultimate failure

2.5 Test setup for Case 2

Horizontal lift is performed when the covers are weighed, loaded on to the vessel and placed into final position on the seabed. In some instances for light covers the lifting points are placed on top of the cover. The lifting force is applied directly out-of-plane locally for the lifting points, which is seen as the weakest direction of the laminate. Since the load is acting in the weakest direction compared to the other lifting situations it is only applicable to light and relative small covers. The test setup for Case 2 is shown in Figure A.6. The lifting point is supported by steel arrangement which is fixed to the bench, while the load is applied through a sling that goes around the lifting holes. The load will apply directly out-of-plane of the material. Three laminate thicknesses of the lifting point were tested, (20, 30 and 40mm). The load was applied gradually with increments of 4-5 tons, after each increment the material was checked for any local failure.

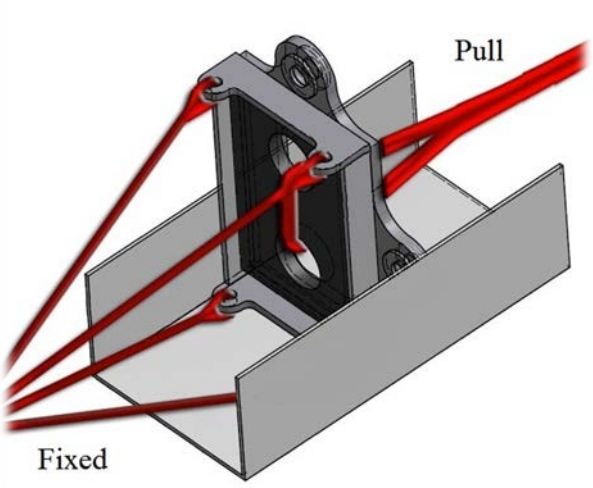

Figure A.6: Test setup for Case 2

2.5.1 Expected Outcome

It is expected to encounter the lowest break load for Case 2, due to pure out-of-plane load. In addition, it is expected that the results will increase linearly with the increase of the thickness of the laminates.

2.5.2 Practical Functionality

In the lifting situation with a horizontal lift and the lifting point placed on top of the GRP cover would the setup for Case 2 be a good representation. Meaning the sling is attached in the same manner, and in the same direction relative to the lifting point as it would encounter during the actual lifting, (out-of-plane).

2.5.3 Results of Case 2

The results of the tests for Case 2 can be found in Table A.5 and in Figure A.7. Most of the results are according to the expected outcome. The GRP material is weak when load is acting in the out-of-plane direction. However, the test results did not show a linear development. The result for the 40mm laminate did not increased as much as expected.

Table A.5: Tested result of break load for Case 2.

Thickness of lift point [mm]	Break load [Te]
20.0	12.0
30.0	19.0
40.0	22.0

Comments to the test result for Case 2:

- The 30mm laminate started to make cracking sounds at around 18 tons.

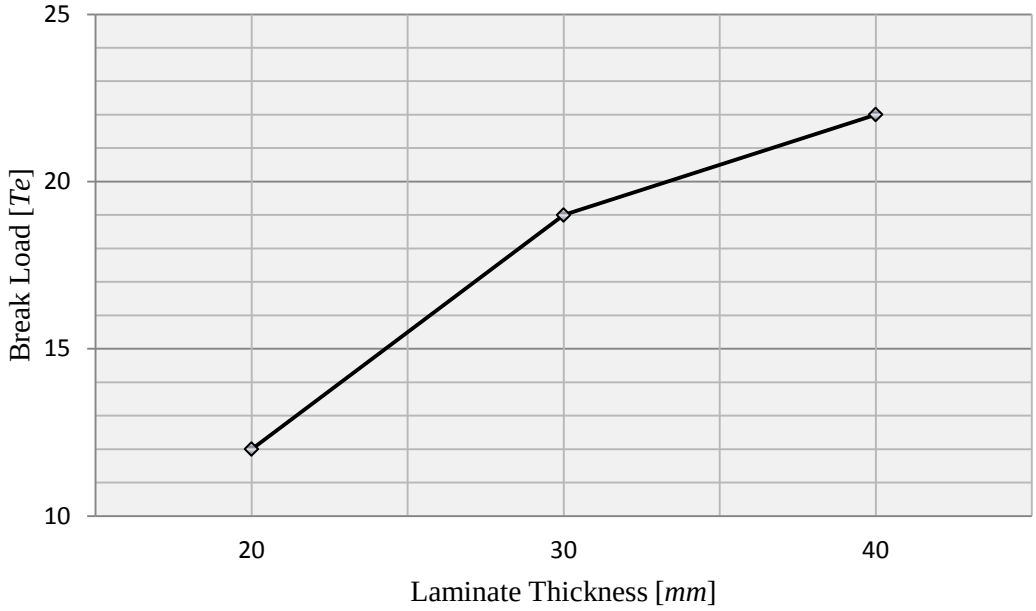

Figure A.7: Tested result of Case 2 represented in a graph.

The ultimate failure that occurred in the test setup for Case 2 is shown in the Figure A.8. The sling caused the whole mid-section of the GRP lift point (section between the two holes) to be ripped out in the out-of-plane direction. Ultimate failure through thickness occurred on the edges of the sling surround the holes, causing the mid-section to be ripped out of the lifting point.

Figure A.8: Ultimate failure mode of Case 2.

2.6 Test setup for Case 3

The most common lifting situation for horizontal lifting is a four-point lift situation. As with the Case 2, horizontal lift is performed when the covers are weighed, loaded on to the vessel and placed into final position on the seabed. The load is working slightly out-of-plane regarding the local lifting point plane. For case 3 the test setup is arranged so that the lift point is placed within the steel arrangement that is fixed to the bench. The sling is fitted around the holes and fastened to the hydraulic pulling device. The sling forms an angle when going through the holes, causing the lifting point to encounter some out-of-plane load. This setup is shown in Figure A.6.Three laminate thicknesses of the lifting point were tested, (20, 30 and 40mm). The load was applied gradually with increments of 4-5 tons, after each increment the material was checked for any local failure.

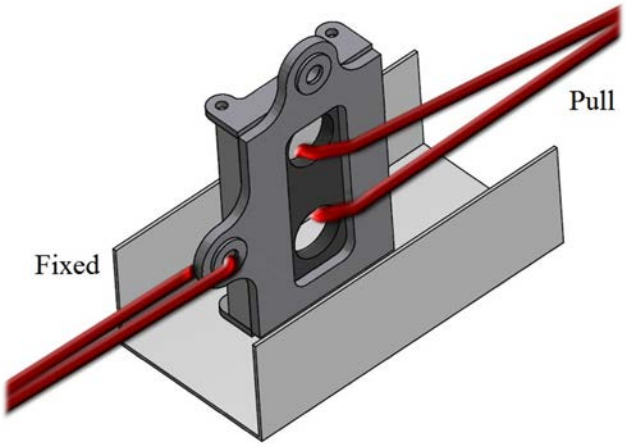

Figure A.9: Test setup for Case 3.

2.6.1 Expected Outcome

Since the sling forms an angle in relation the plane of the material, it is expected that this setup should be weaker than the result for Case 1. In addition, it is expected that the results will increases linearly with the increase of the thickness of the tested laminates.

2.6.2 Practical Functionality

The Case 3 test setup is a good representation for the lifting situation with a horizontal lift and the lifting point placed on the side wall of the GRP. Meaning the sling is attached in the same manner, and in the same direction relative to the lifting point as it would encounter during the actual lifting.

One issue with the test setup used for Case 3 is that the steel arrangement supporting the lifting point featured a relative sharp edge where the sling passes going through the holes. The sharp edge could cause he strop to fail prematurely. During the testing it was solved temporary by installing a protection rubber, reducing the sharp edge.

2.6.3 Results of Case 3

The results of the tests for Case 1 can be found in Table A.6 and in Figure A.10. Results are consistent with the expected outcome. This entails that the GRP material is weaker compared to the result for Case 1, and at the same time is higher than the result for Case 2. It supports the intuition that the sling

forms an angle relative to the material plane, causing the lifting point to encounter both in-plane and out-of-plane load. In addition, as expected the GRP material has an approximately linear increase of capacity with an increase in the thickness.

Table A.6: Tested result of break load for Case 3.

Thickness of lift point [*mm*]	Break load [*Te*]
20.0	20.0
30.0	28.0
40.0	38.0

Comments to the test result for Case 3:

- The 30mm laminate started to make cracking sounds at around 25 tons.

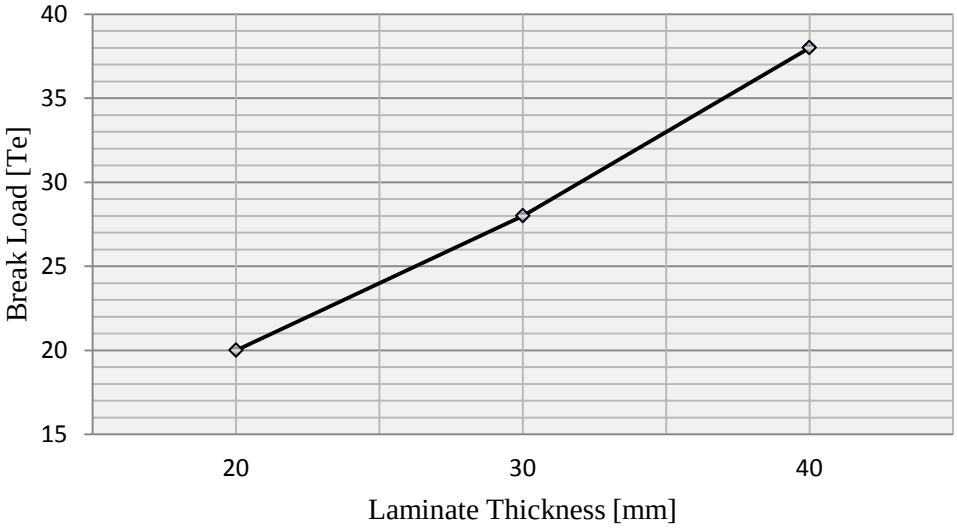

Figure A.10: Tested result of Case 3 presented in a graph.

The ultimate failure that occurred in the test setup for Case 3 is shown in the Figure A.11. The sling caused through thickness failure in the middle of the mid-section. The failure seems to be caused by out-of-plane failure, since the fibres are pointing out of the plane of the material.

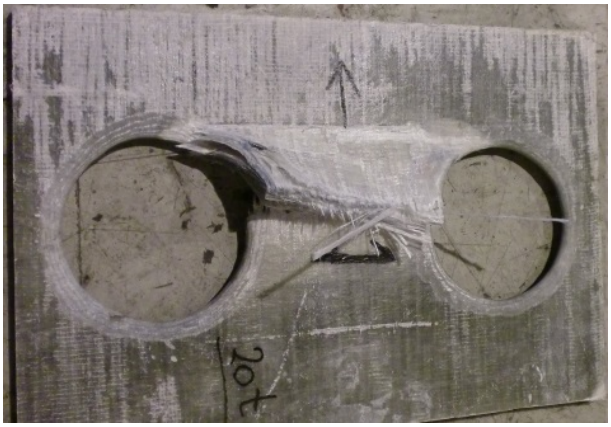

Figure A.11: Case 3 ultimate failure

3. Summary and Conclusion

3.1 Summary

Three tests were conducted with different setups, Case 1, Case 2 and Case 3. Case 1 is a representation of a lift through the splash zone, where GRP cover is in an upright vertical position. Case 2 is an approximation of a horizontal lift with the lifting point located on top of the cover, causing the lifting point to encounter out-of-plane loads. Case 3 is a representation of a horizontal four-point lift where the lifting point is placed on the side walls.

Table A.7: Tested break load for all cases.

Test Setup	Break load [*Te*] for 20 mm laminate	Break load [*Te*] for 30 mm laminate	Break load [*Te*] for 40 mm laminate
Case 1	45.0	56.0	N/A
Case 2	12.0	19.0	22.0
Case 3	20.0	28.0	38.0

The results are presented in Table A.7 and in Figure A.12. The only value that was not found was for 40mm laminate in Case 1. Given that the hydraulic tensile bench had a maximum pulling capacity of 60 tons, the bench was unable to cause ultimate failure on the lifting in the Case 1 setup.

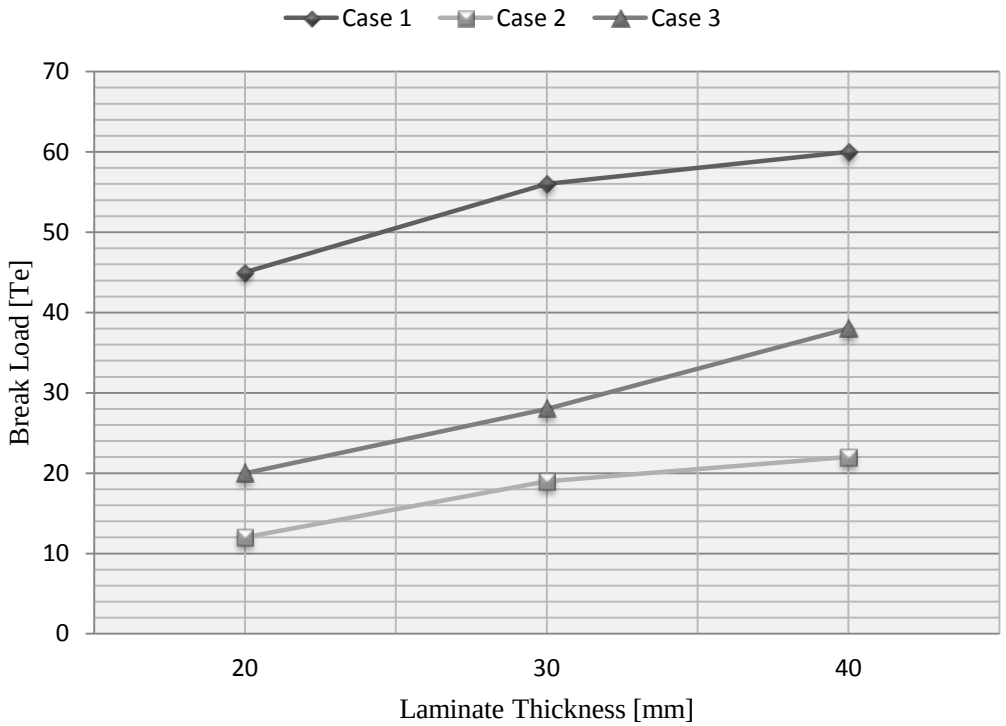

Figure A.12: All the result from test presented in a graph.

3.2 Conclusion

The tests were performed as planned without any changes, and have generally been as expected. The results showed an approximately linear increase in capacity of the lifting point by increasing the laminate thicknesses, respectively, 20, 30 and 40mm. There was only one result that was not as expected, the break load for the 40mm laminate in Case 3 resulted in a capacity of 22Tons, which was a relatively small increase compared with the results from the other tests (30mm laminate break load of 19 Tons). It is possible that there may have been a defect in materials or another error source described in Section 1.4.

3.3 Recommended Improvements

Firstly, it is recommended to carry out more tests of each individual thickness of each test setup. By doing several tests, it would be possible to see whether the results are consistent and collect characteristic values for each laminate thickness for each test performed. It would make the results more valuable for strength estimate and when comparing the result with analytical solutions.

Secondly, the test setup worked well, but in some cases the sharp edges from the steel arrangement affected the sling. This was improved by using rubber between the steel and the strap. On another occasion it may be possible to improve the test setup so that the sling is not affected by the steel.

The final recommended improvement is to perform the test in a hydraulic tensile bench with a higher maximum cap for tensile load. The 60-ton hydraulic bench did not cause ultimate failure in the 40mm laminate during testing for Case 1.

Appendix B

Case 1

Finite element analysis

Failure criterion and degradation model:

- Hashin failure criterion with gradual degradation
- Hashin failure criterion with immediate degradation
- Puck failure criterion with gradual degradation
- Puck failure criterion with immediate degradation

20mm laminate

Hashin failure criterion

Gradual degradation

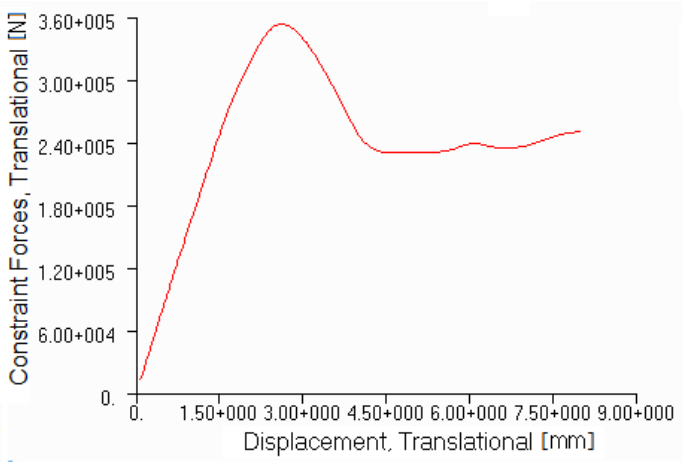

Figure B.1: Constraint force verses displacement for Hashin failure criterion with gradual degradation.

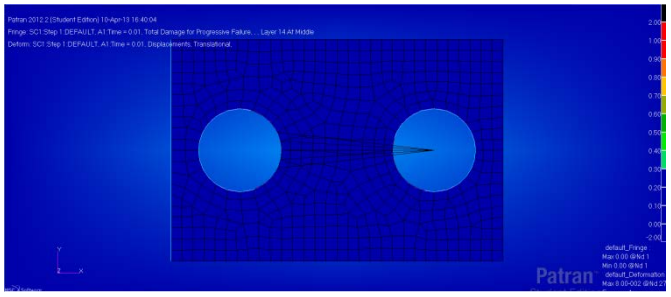

a) 0 % of total displacement

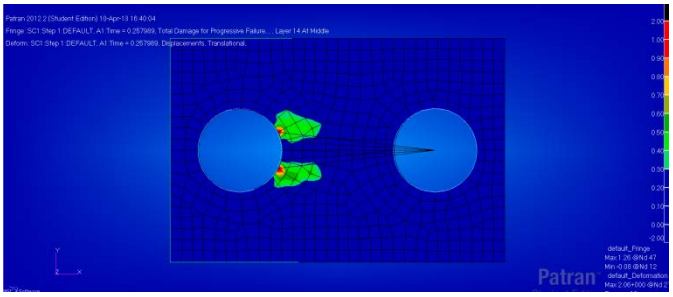

b) 25% of total displacement

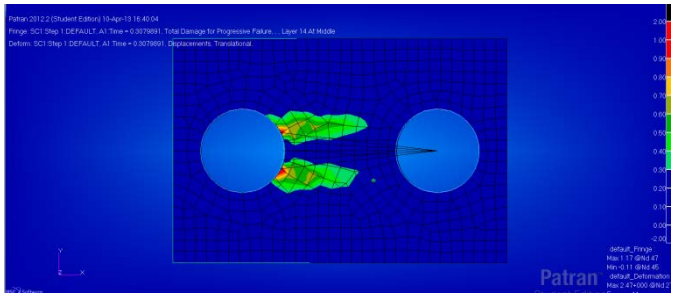

c) 30 % of total displacement

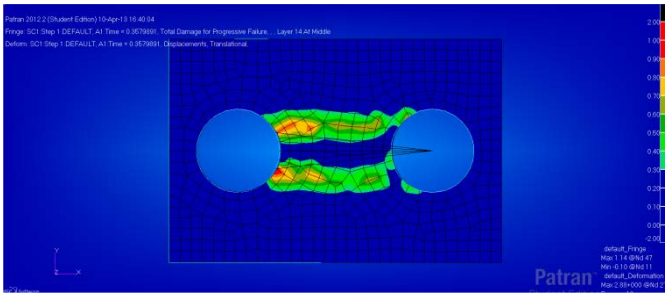

d) 35% of total displacement

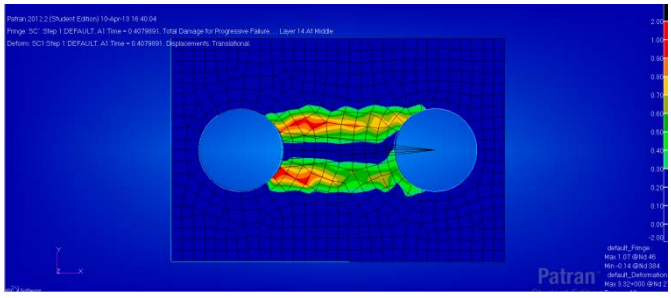

e) 40% of total displacement

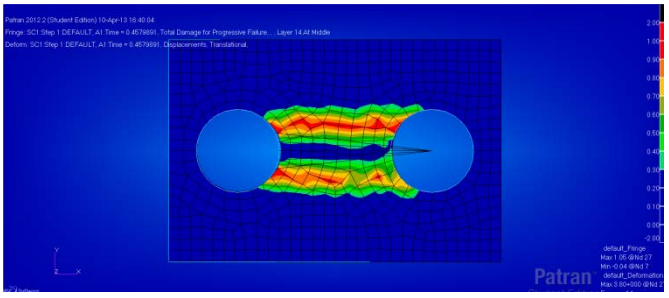

f) 45% of total displacement

Figure B.2: Damage propagation for Hashin failure criterion with gradual stiffness degradation.

20mm laminate

Hashin failure criterion

Immediate degradation

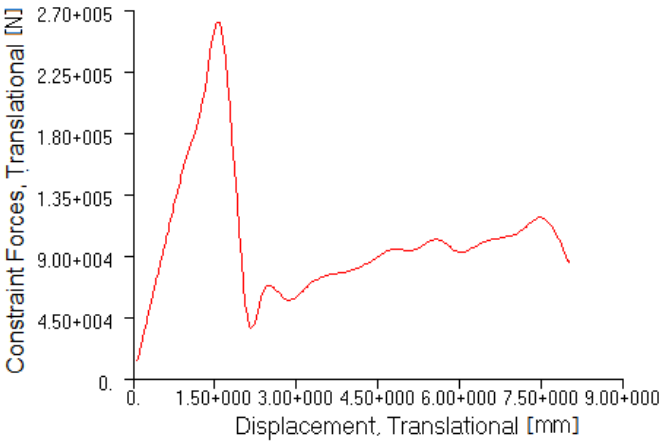

Figure B.3: Constraint force verses displacement for Hashin failure criterion with immediate degradation.

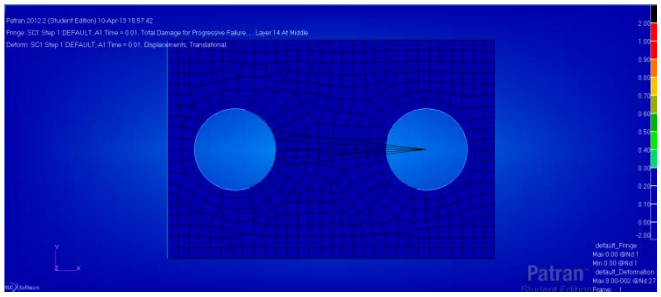

a) 0 % of total displacement

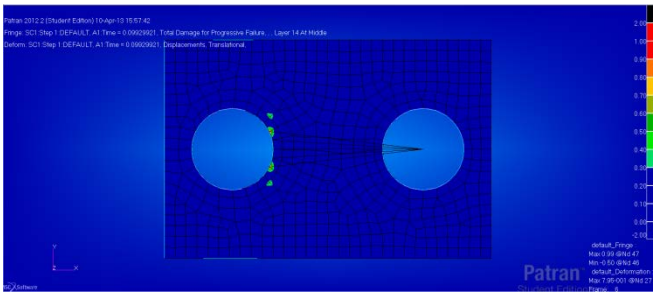

b) 10 % of total displacement

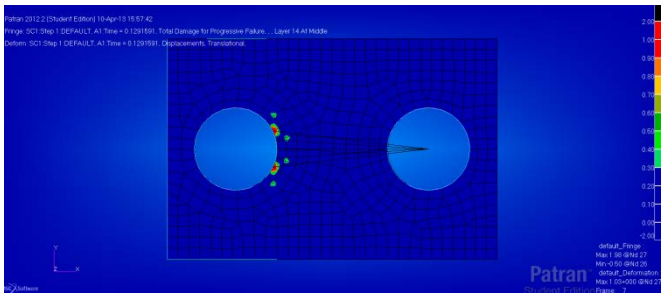

c) 13 % of total displacement

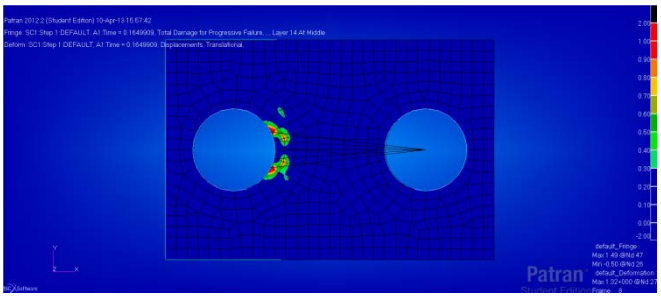

d) 17 % of total displacement

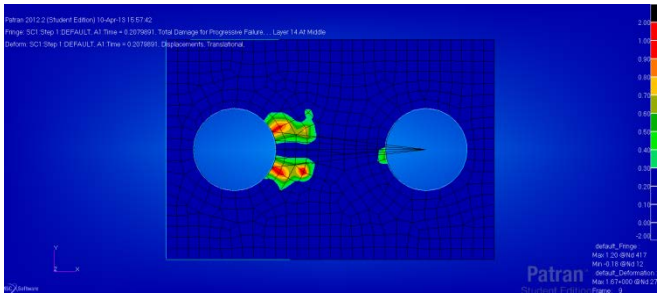

e) 20 % of total displacement

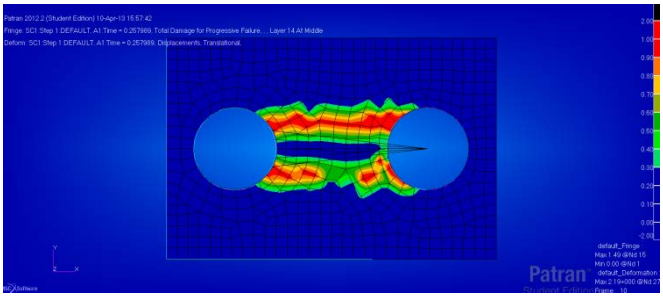

f) 26 % of total displacement

Figure B.4: Damage propagation for Hashin failure criterion with immediate stiffness degradation.

20mm laminate

Puck failure criterion

Gradual degradation

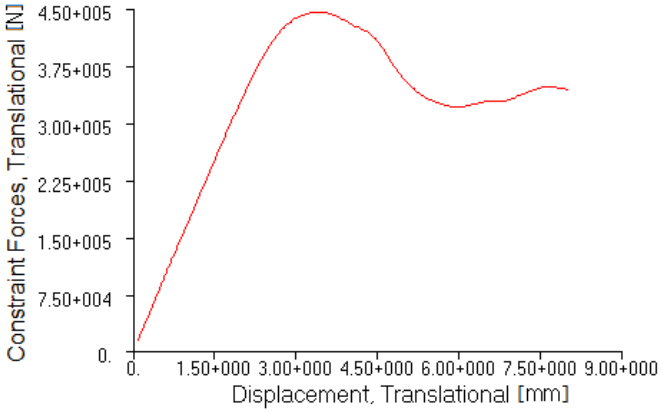

Figure B.5: Constraint force verses displacement for Puck failure criterion with gradual degradation.

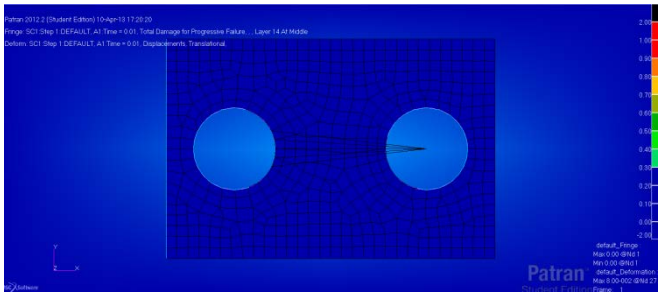

a) 0 % of total displacement

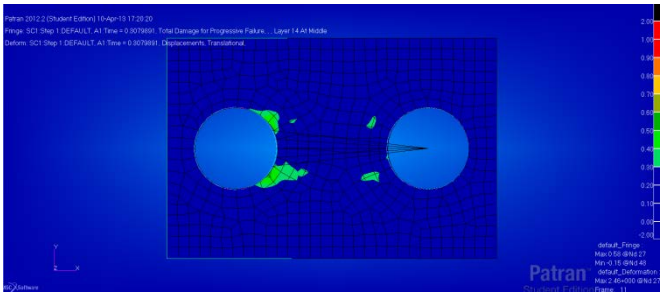

b) 30 % of total displacement

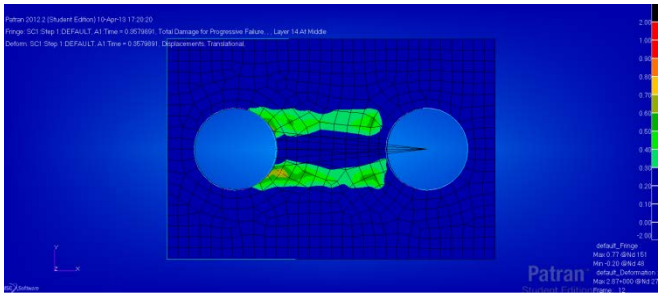

c) 35 % of total displacement

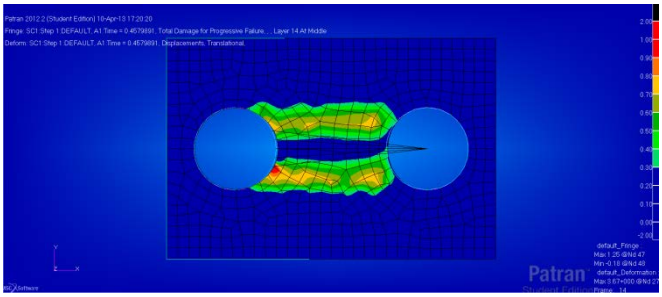

d) 45 % of total displacement

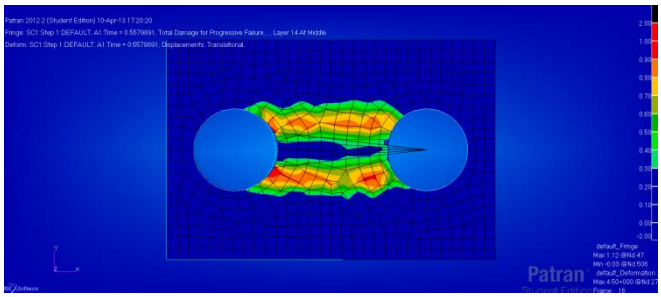

e) 55 % of total displacement

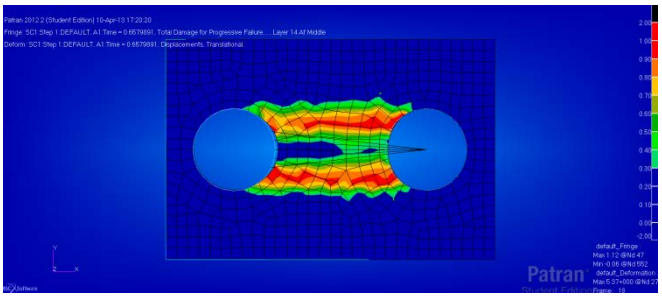

f) 65 % of total displacement

Figure B.6: Damage propagation for Puck failure criterion with gradual stiffness degradation.

20mm laminate

Puck failure criterion

Immediate degradation

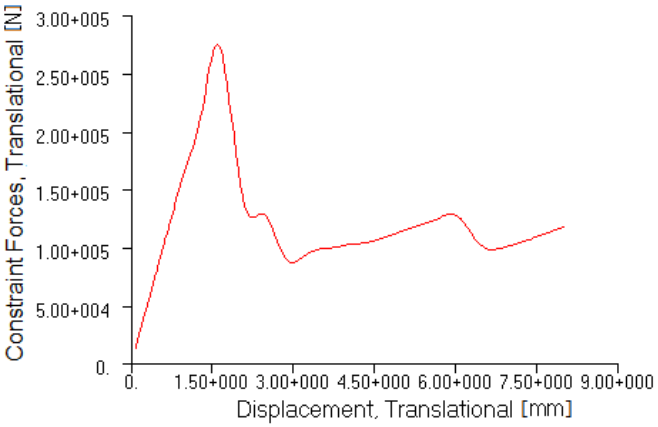

Figure B.7: Constraint force verses displacement for Puck failure criterion with immediate degradation.

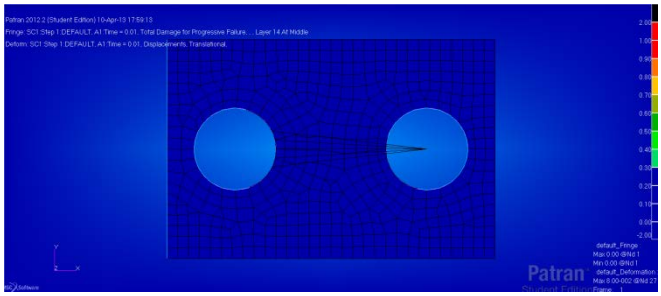

a) 0 % of total displacement

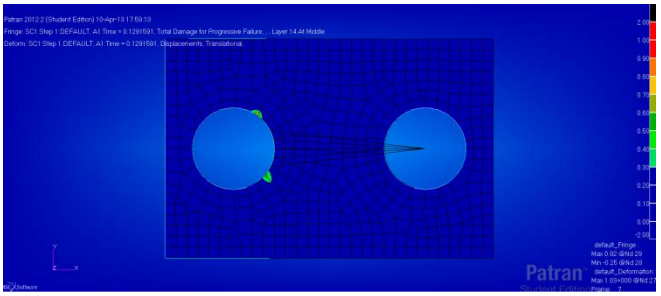

b) 13 % of total displacement

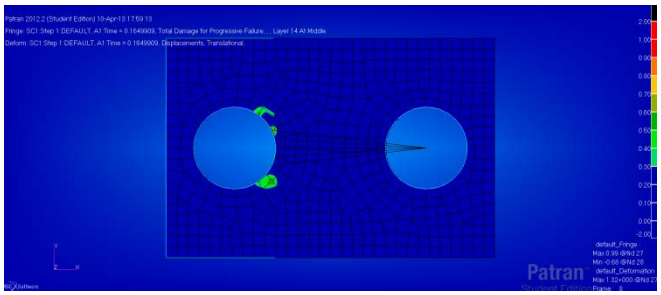

c) 16 % of total displacement

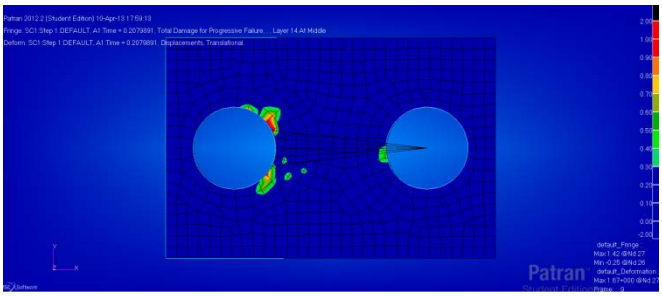

d) 20 % of total displacement

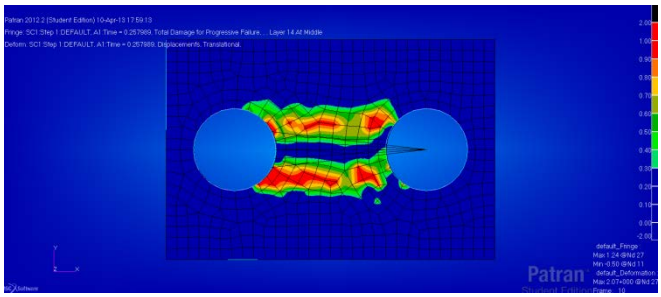

e) 26 % of total displacement

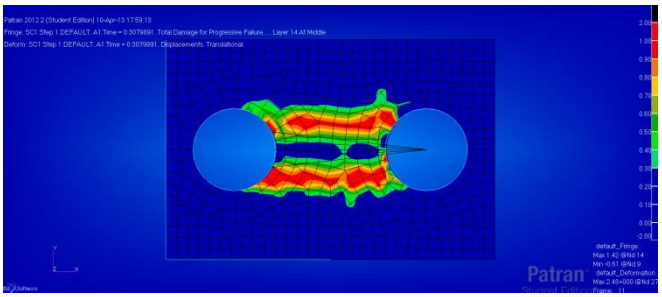

f) 31 % of total displacement

Figure B.8: Damage propagation for Puck failure criterion with immediate stiffness degradation.

30mm laminate

Hashin failure criterion

Gradual degradation

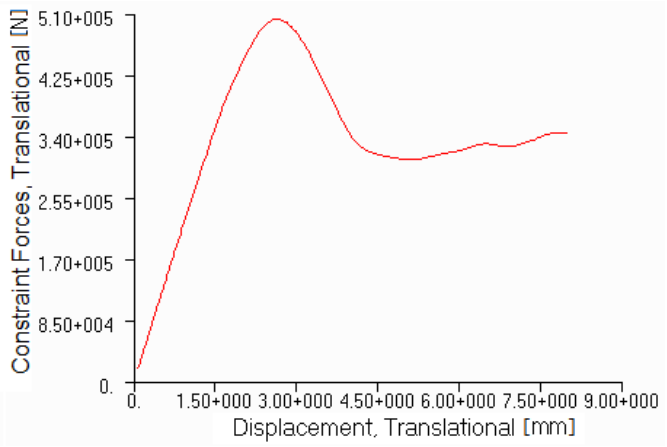

Figure B.9: Constraint force verses displacement for Hashin failure criterion with gradual degradation.

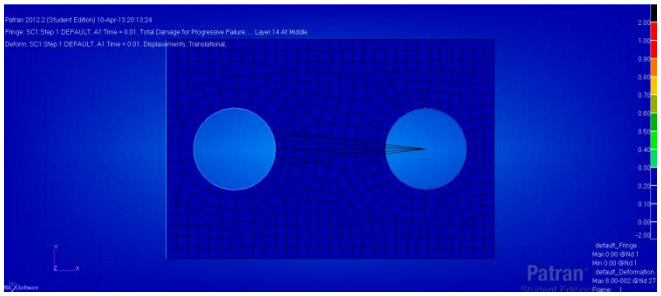

a) 0 % of total displacement

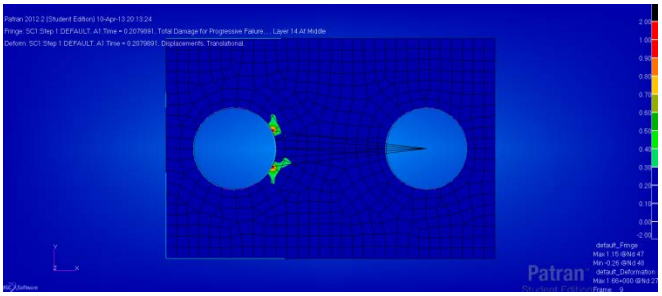

b) 20 % of total displacement

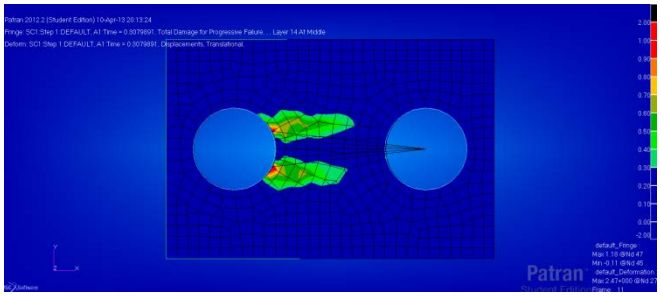

c) 30 % of total displacement

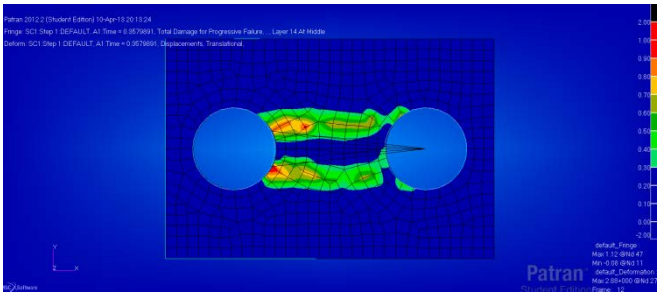

d) 35 % of total displacement

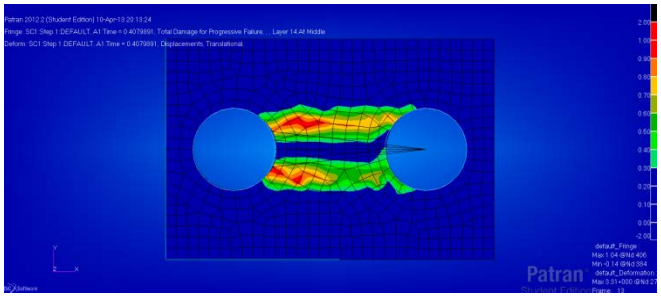

e) 40 % of total displacement

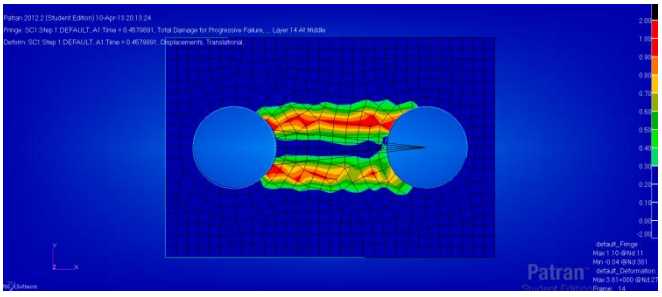

f) 45 % of total displacement

Figure B.10: Damage propagation for Hashin failure criterion with gradual stiffness degradation.

30mm laminate

Hashin failure criterion

Immediate degradation

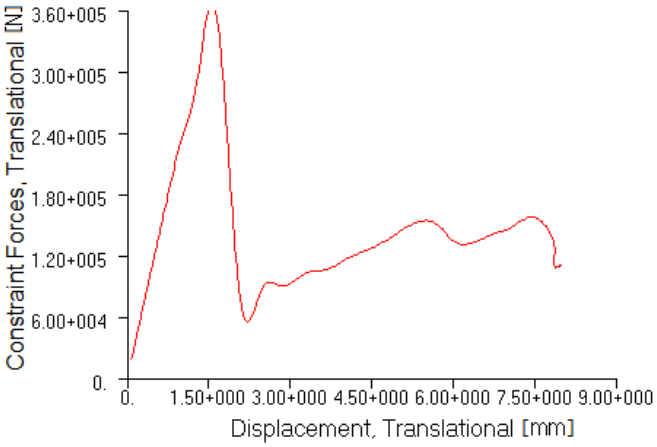

Figure B.11: Constraint force verses displacement for Hashin failure criterion with immediate degradation.

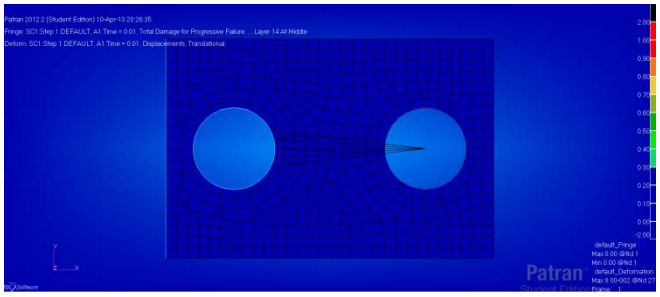

a) 0 % of total displacement

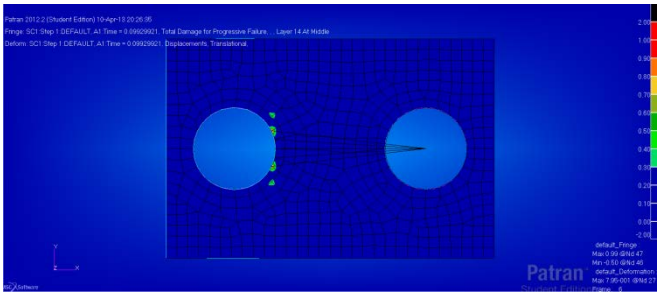

b) 10 % of total displacement

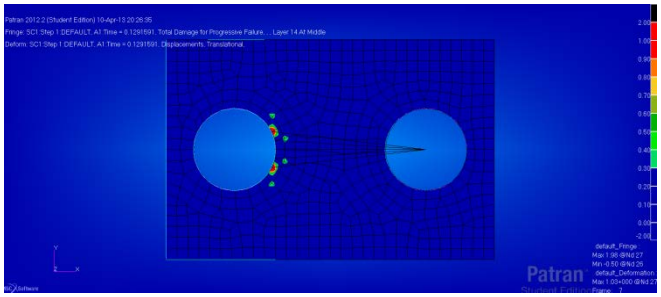

c) 13 % of total displacement

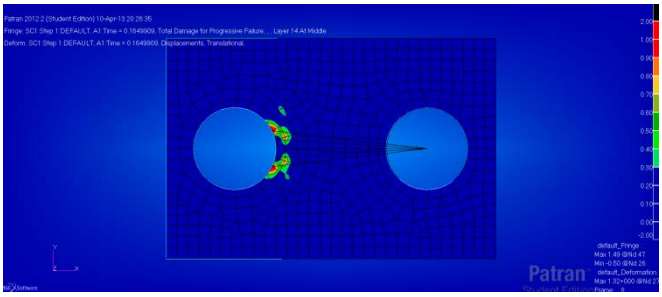

d) 16 % of total displacement

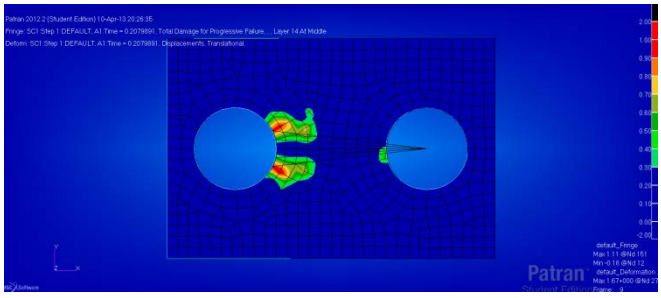

e) 21 % of total displacement

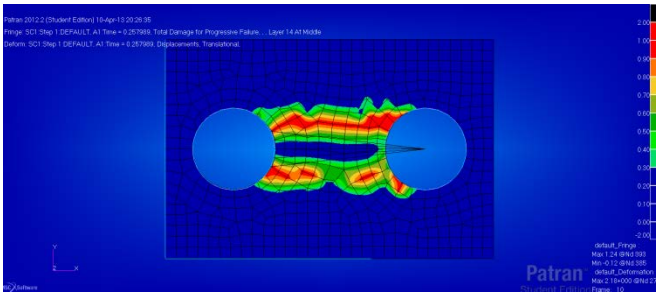

f) 26 % of total displacement

Figure B.12: Damage propagation for Hashin failure criterion with immediate stiffness degradation.

30mm laminate

Puck failure criterion

Gradual degradation

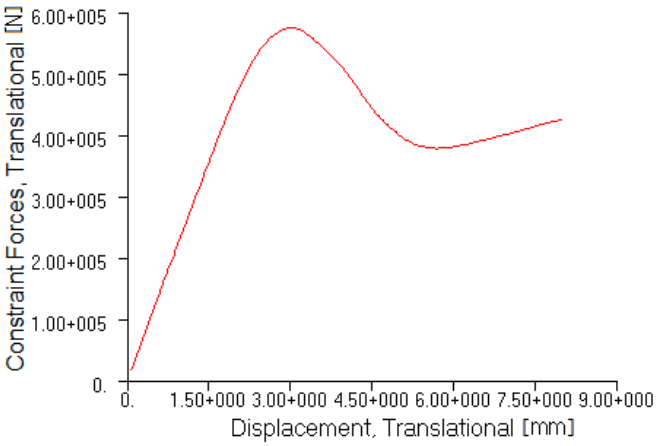

Figure B.13: Constraint force verses displacement for Puck failure criterion with gradual degradation.

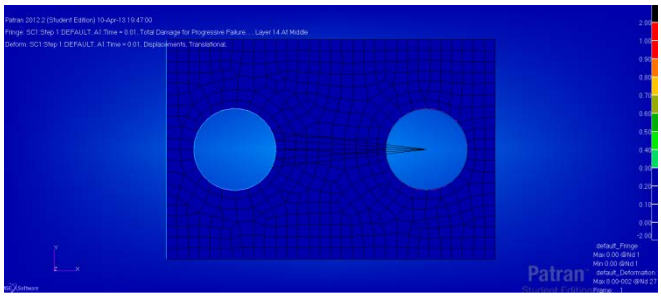

a) 0 % of total displacement

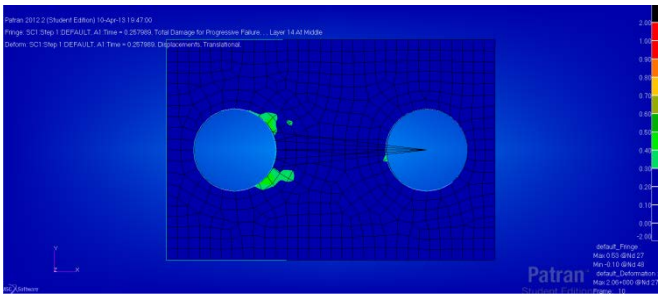

b) 26 % of total displacement

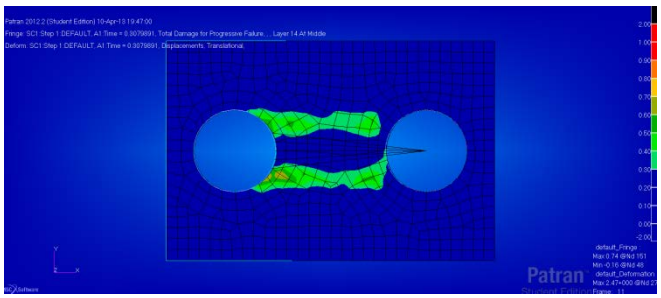

c) 30 % of total displacement

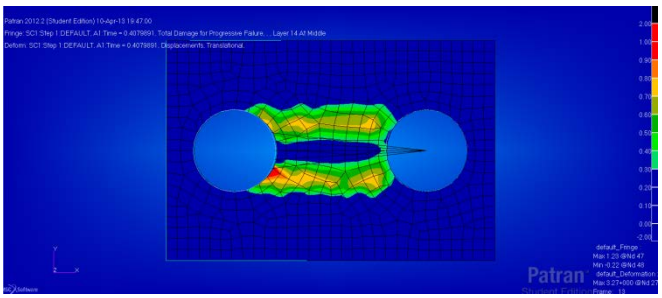

d) 40 % of total displacement

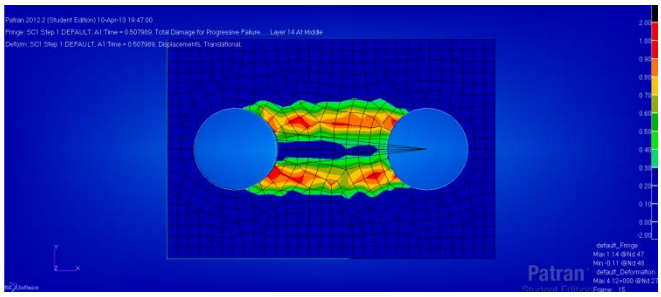

e) 51 % of total displacement

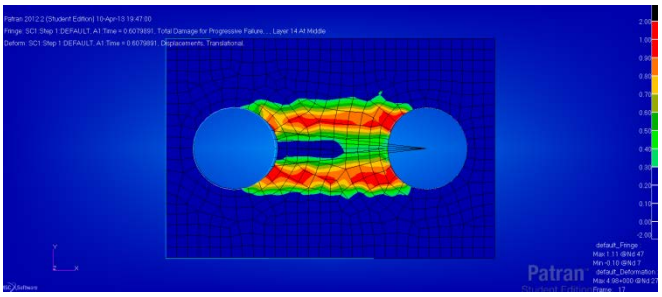

f) 61 % of total displacement

Figure B.14: Damage propagation for Puck failure criterion with gradual stiffness degradation.

30mm laminate

Puck failure criterion

Immediate degradation

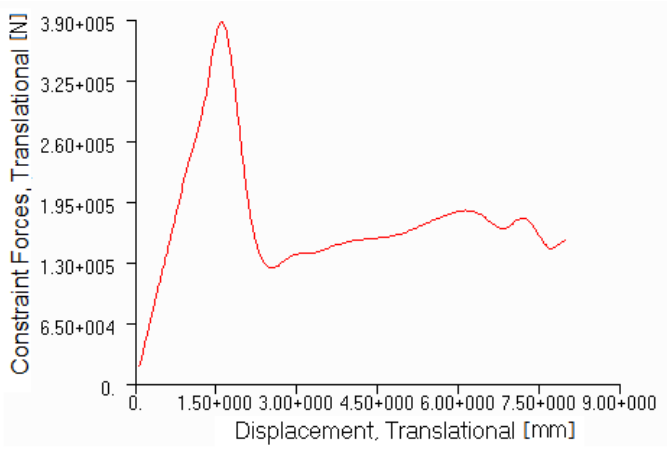

Figure B.15: Constraint force verses displacement for Puck failure criterion with immediate degradation.

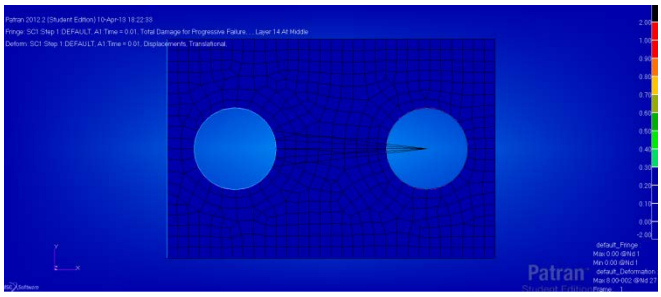

a) 0 % of total displacement

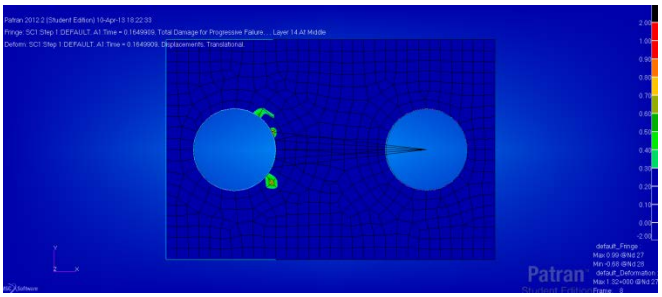

b) 17 % of total displacement

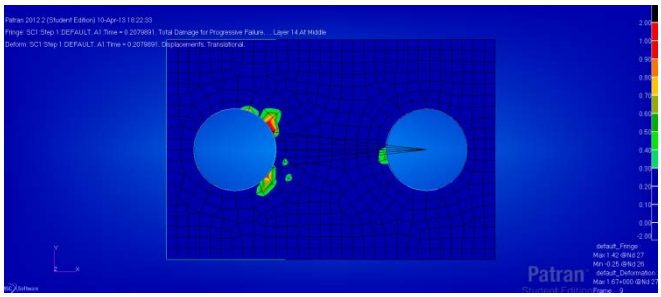

c) 20 % of total displacement

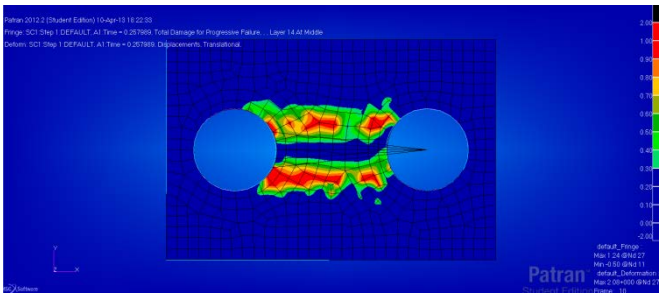

d) 26 % of total displacement

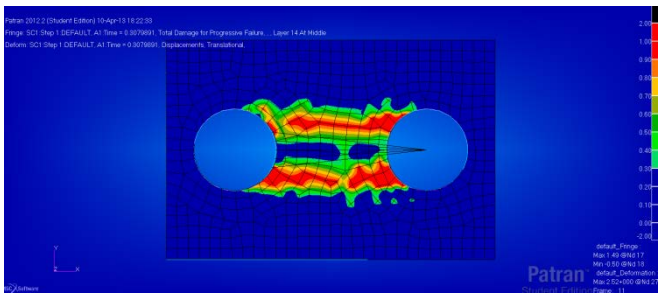

e) 30 % of total displacement

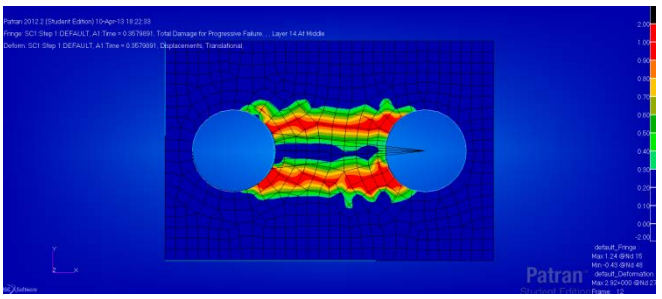

f) 36 % of total displacement

Figure B.16: Damage propagation for Puck failure criterion with immediate stiffness degradation.

40mm laminate

Hashin failure criterion

Gradual degradation

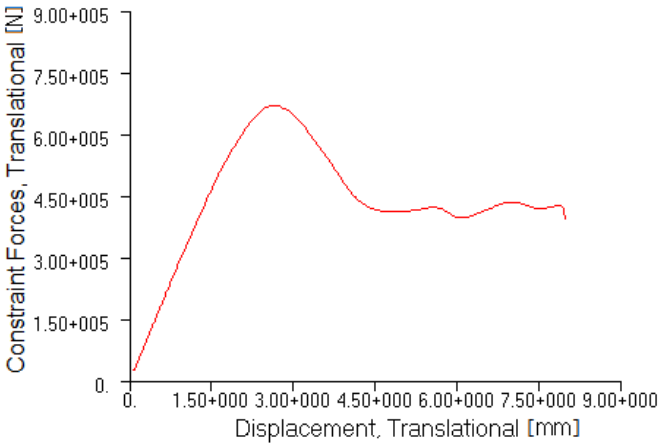

Figure B.17: Constraint force verses displacement for Hashin failure criterion with gradual degradation.

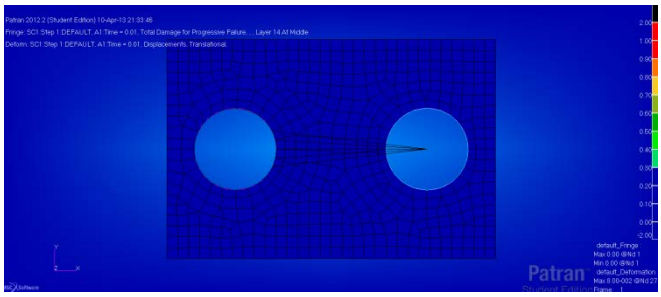

a) 0 % of total displacement

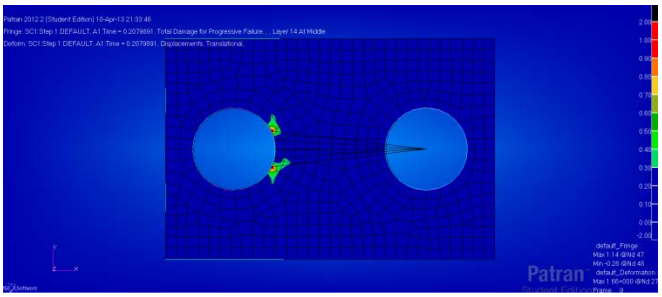

b) 30 % of total displacement

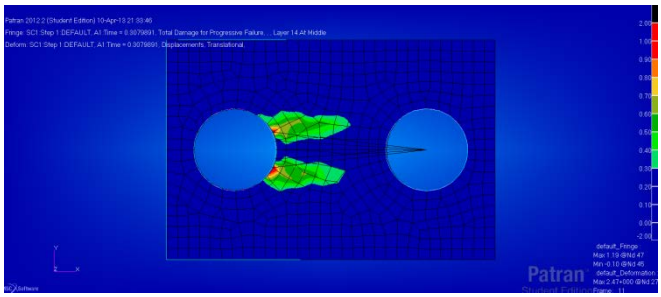

c) 35 % of total displacement

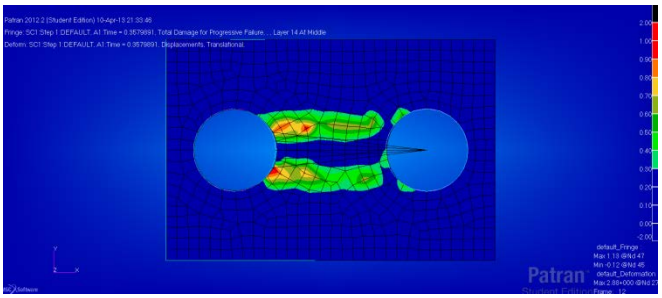

d) 45 % of total displacement

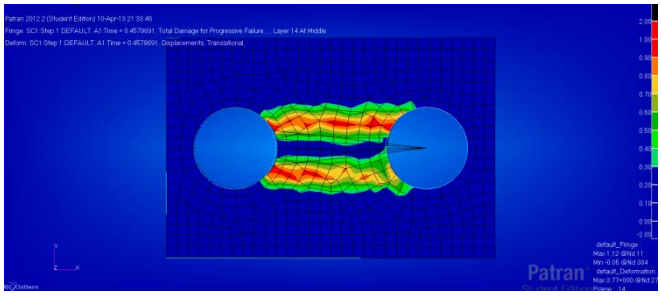

e) 55 % of total displacement

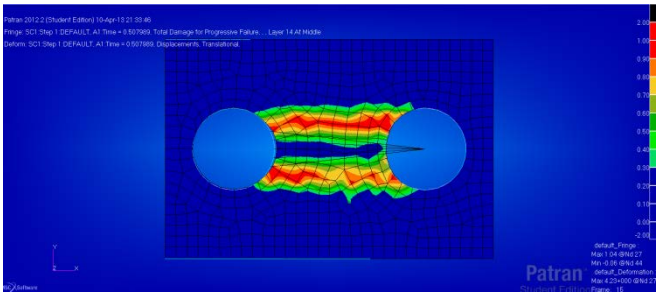

f) 65 % of total displacement

Figure B.18: Damage propagation for Hashin failure criterion with gradual stiffness degradation.

40mm laminate

Hashin failure criterion

Immediate degradation

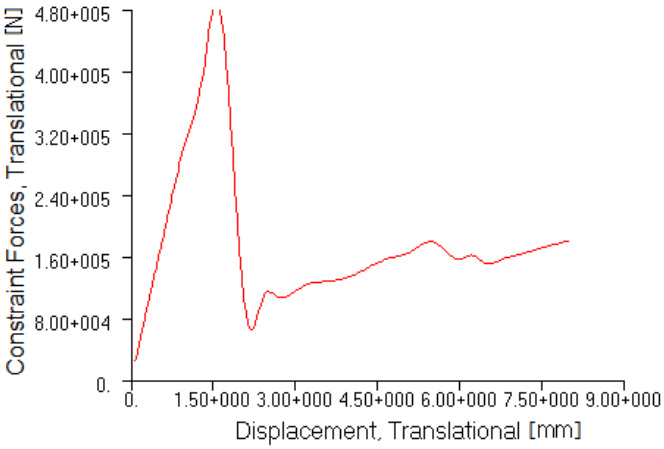

Figure B.19: Constraint force verses displacement for Hashin failure criterion with immediate degradation.

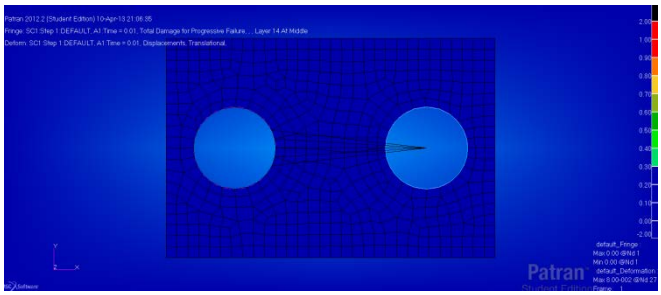

a) 0 % of total displacement

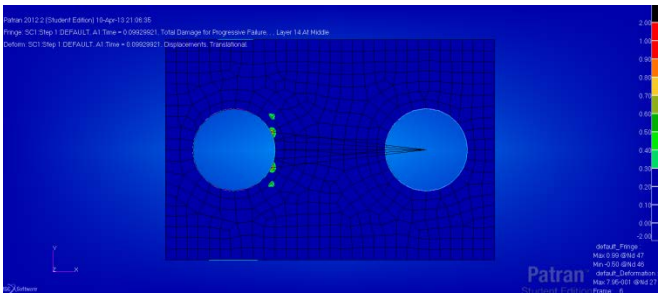

b) 10 % of total displacement

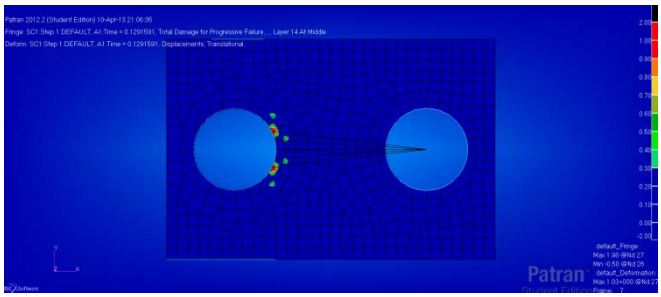

c) 13 % of total displacement

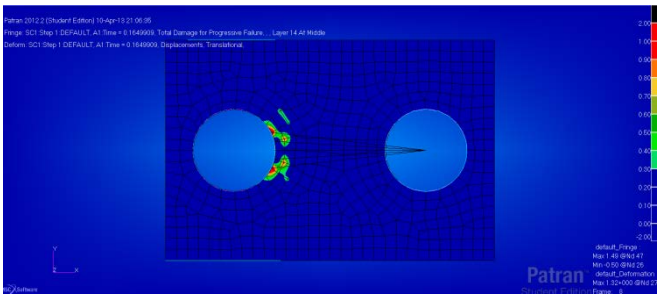

d) 17 % of total displacement

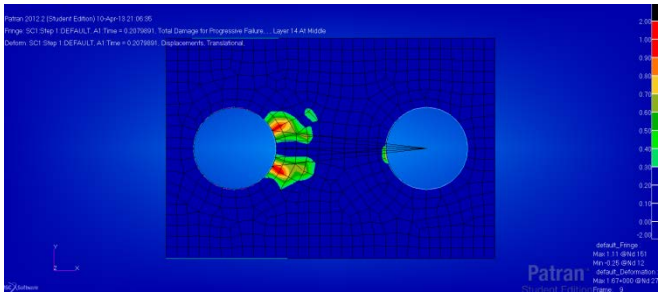

e) 21 % of total displacement

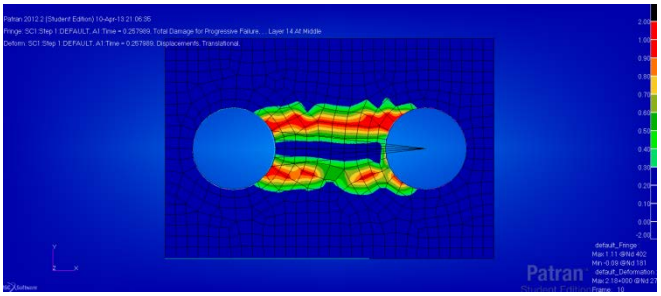

f) 26 % of total displacement

Figure B.20: Damage propagation for Hashin failure criterion with immediate stiffness degradation.

40mm laminate

Puck failure criterion

Gradual degradation

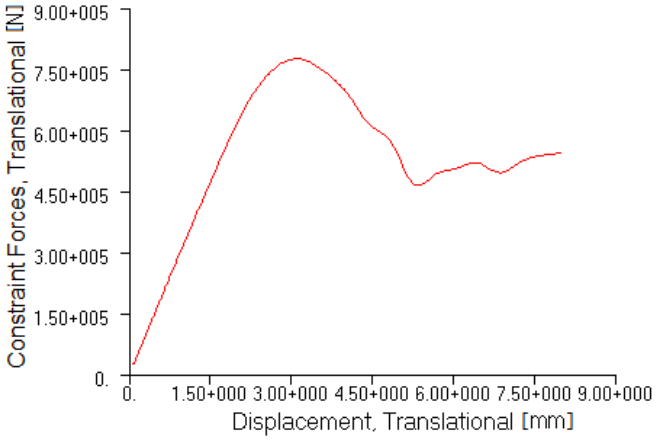

Figure B.21: Constraint force verses displacement for Puck failure criterion with gradual degradation.

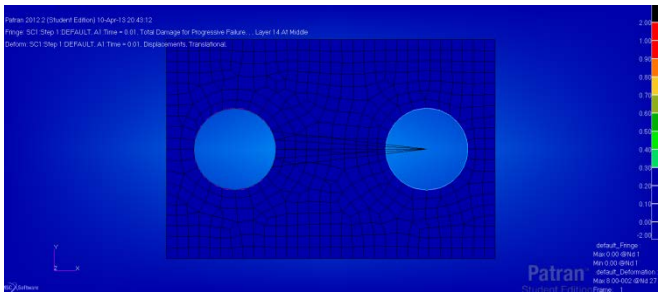

a) 0 % of total displacement

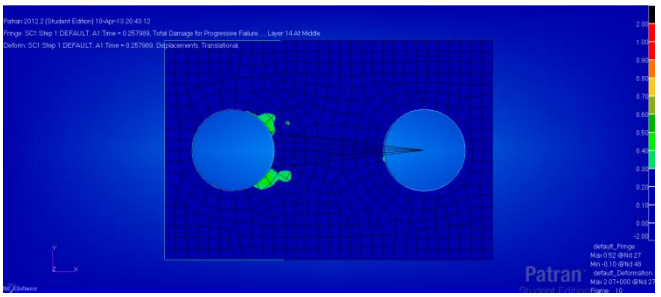

b) 26 % of total displacement

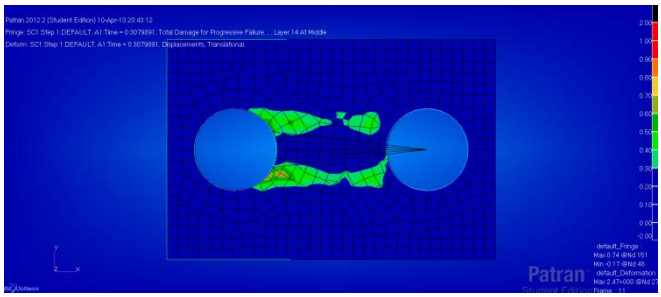

c) 30 % of total displacement

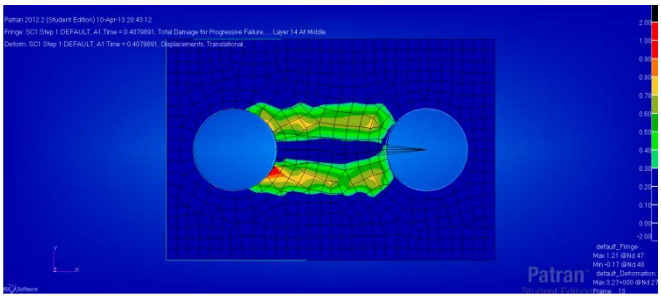

d) 40 % of total displacement

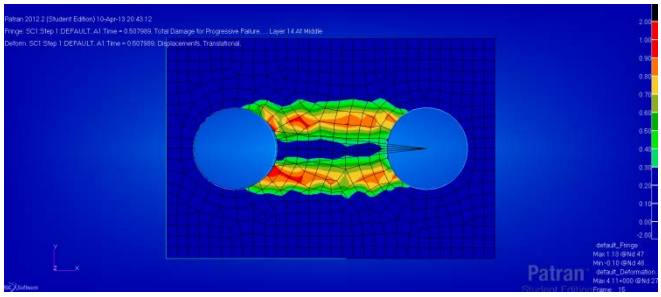

e) 50 % of total displacement

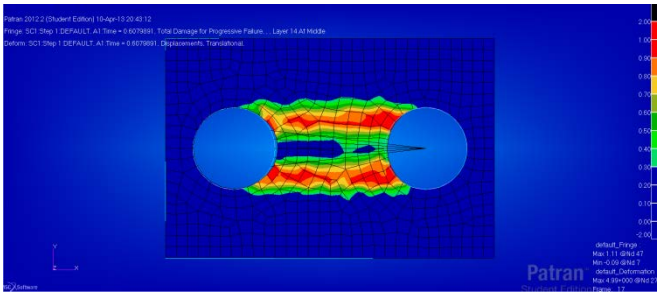

f) 60 % of total displacement

Figure B.22: Damage propagation for Puck failure criterion with gradual stiffness degradation.

40mm laminate

Puck failure criterion

Immediate degradation

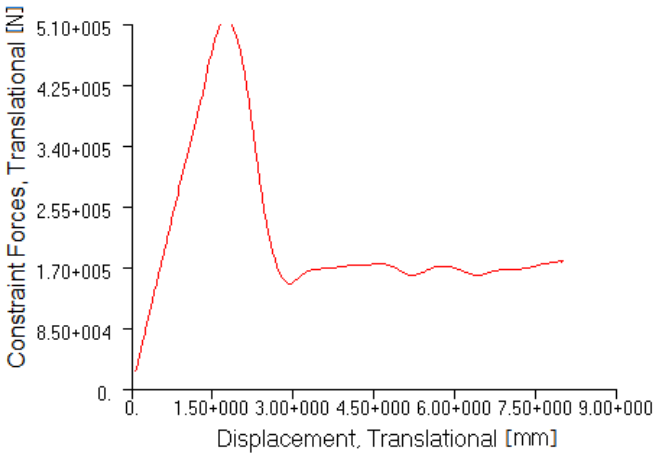

Figure B.23: Constraint force verses displacement for Puck failure criterion with immediate degradation.

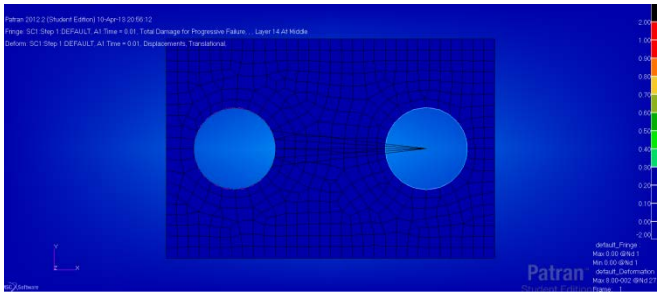

a) 0 % of total displacement

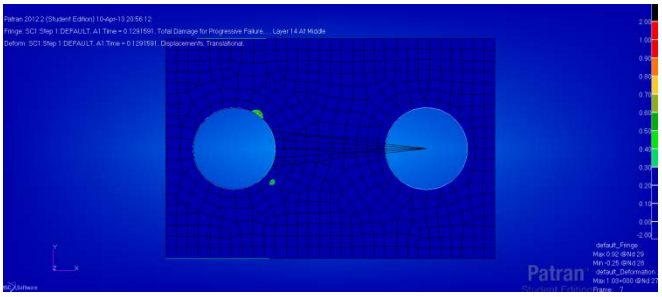

b) 13 % of total displacement

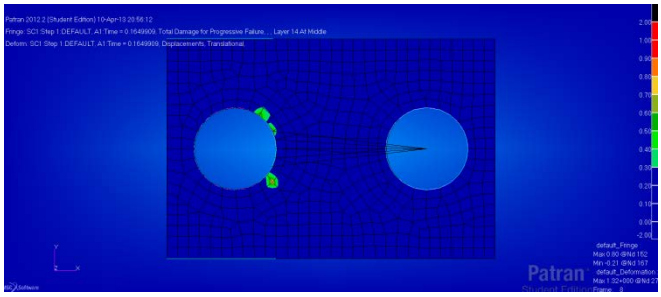

c) 17 % of total displacement

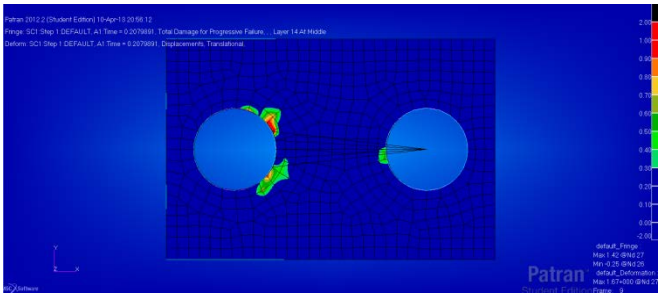

d) 21 % of total displacement

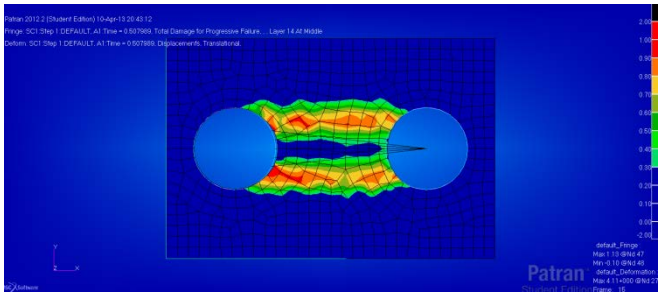

e) 26 % of total displacement

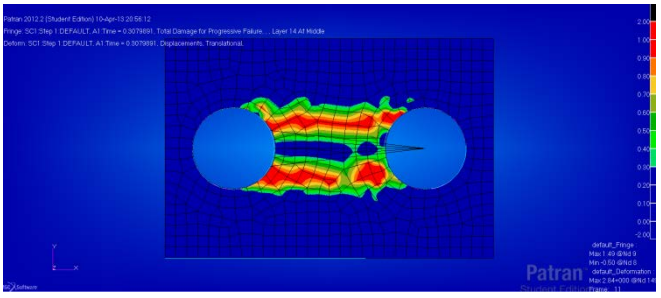

f) 31 % of total displacement

Figure B.24: Damage propagation for Puck failure criterion with immediate stiffness degradation.

Summary for Case 1

The result from the FE analysis is gathered in Table B.1 and shown in Figure B.25. The result is the peak value of the graph, which indicates the maximum load the GRP lift point can withstand before ultimate failure.

Table B.1: Finite element analysis results of break load of lift point for Case 1.

Failure Criteria and degradation model	Break Load [*Te*] for 20mm laminate	Break Load [*Te*] for 30mm laminate	Break Load [*Te*] for 30mm laminate
Hashin with Gradual	36.0	51.0	68.0
Hashin with Immediate	27.0	36.0	48.0
Puck with Gradual	45.*0*	59.0	77.0
Puck with Immediate	28.0	39.0	51.0

The result from the finite element results for Case 1, summarized in table B.1 is presented in figure B.25. The graph includes the breaking capacity for the three laminate thicknesses, 20, 30 and 40mm.

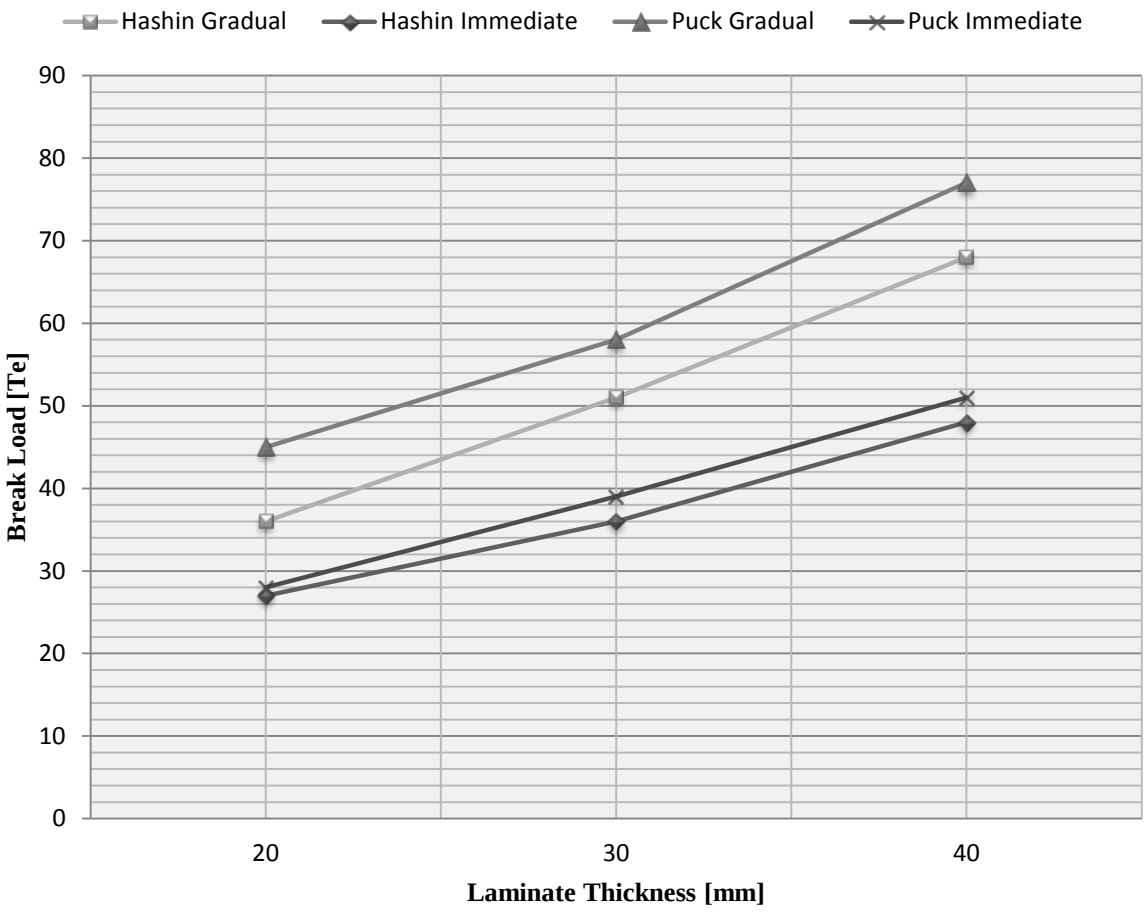

Figure B.25: Finite element results of Case 1.

Appendix C

Case 2

Finite element analysis

Failure criterion and degradation model:

- Hashin failure criterion with gradual degradation
- Hashin failure criterion with immediate degradation
- Puck failure criterion with gradual degradation
- Puck failure criterion with immediate degradation

20mm laminate

Hashin failure criterion

Gradual degradation

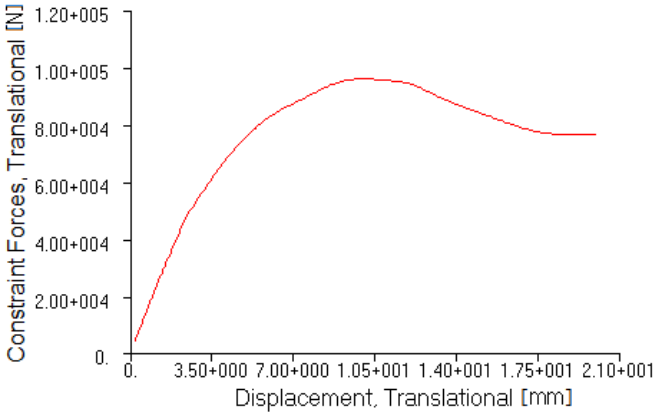

Figure C.1: Constraint force verses displacement for Hashin failure criterion with gradual degradation.

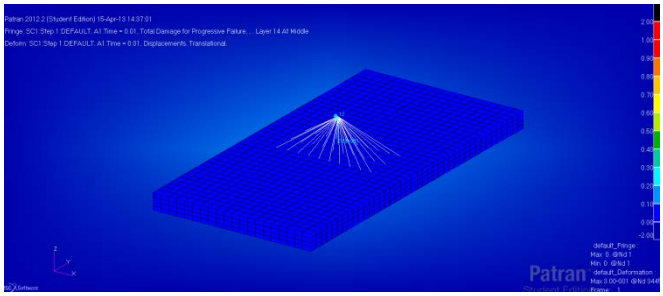

a) 0 % of total displacement

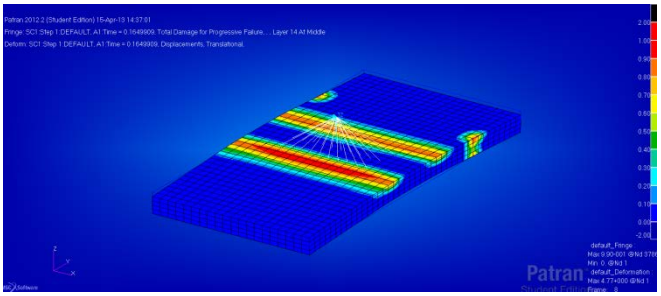

b) 16 % of total displacement

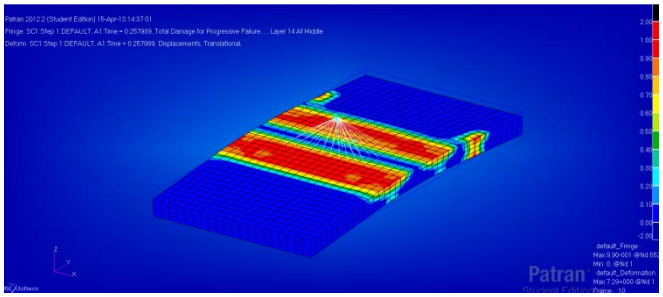

c) 26 % of total displacement

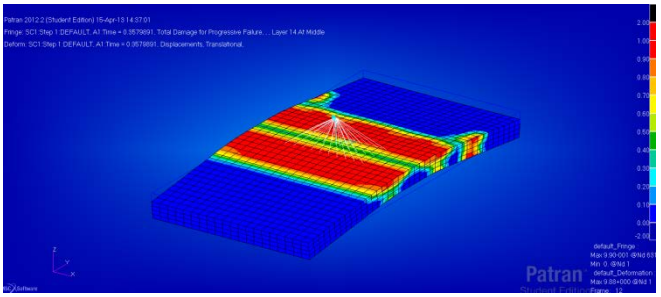

d) 35 % of total displacement

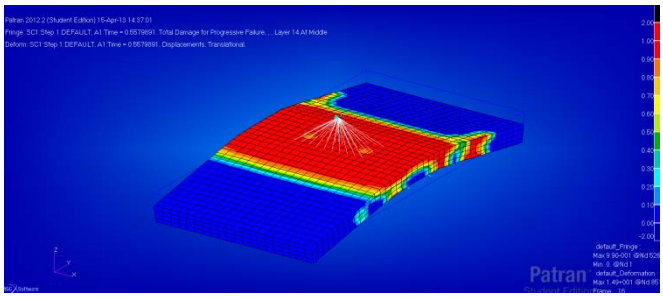

e) 55 % of total displacement

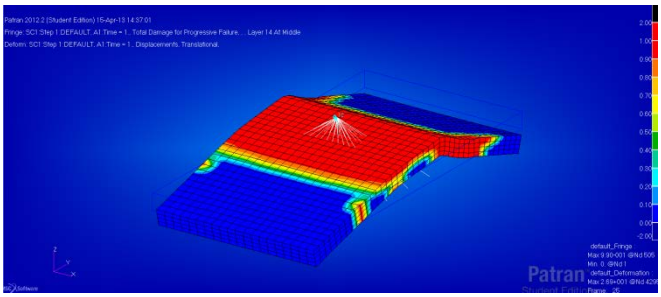

f) 100 % of total displacement

Figure C.2: Damage propagation for Hashin failure criterion with gradual stiffness degradation.

20mm laminate

Hashin failure criterion

Immediate degradation

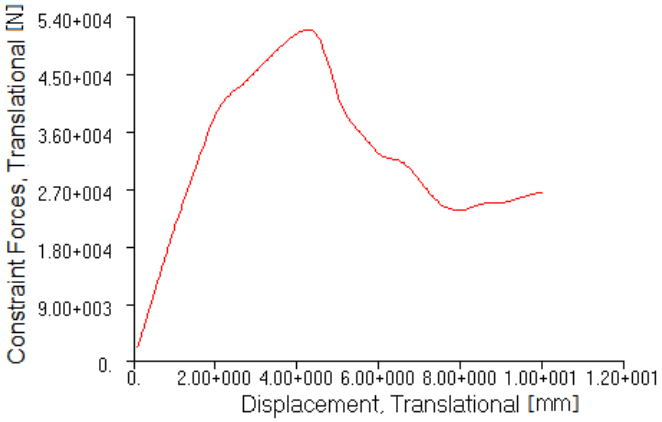

Figure C.3: Constraint force verses displacement for Hashin failure criterion with immediate degradation.

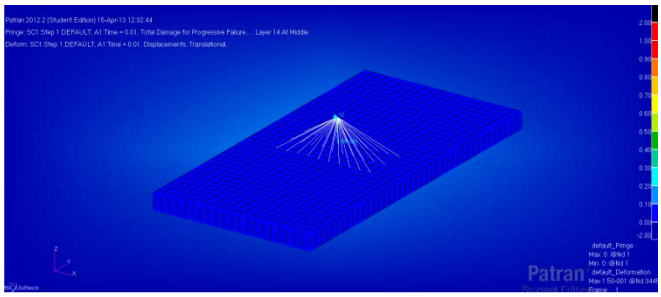

a) 0 % of total displacement

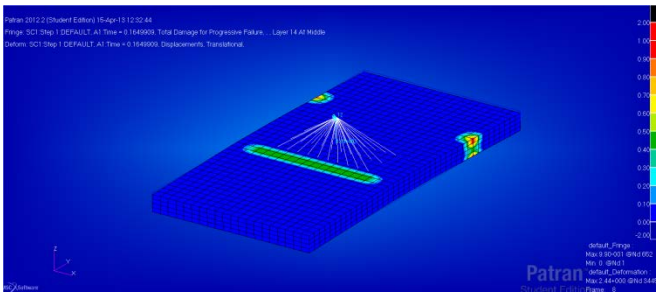

b) 16 % of total displacement

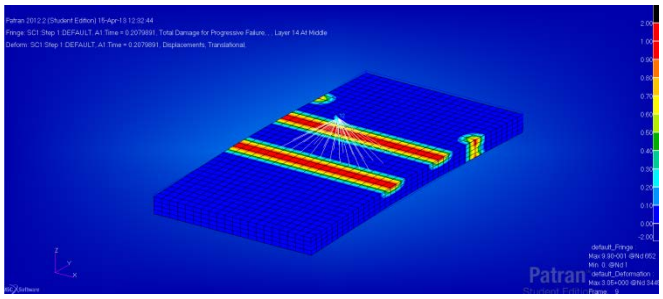

c) 20 % of total displacement

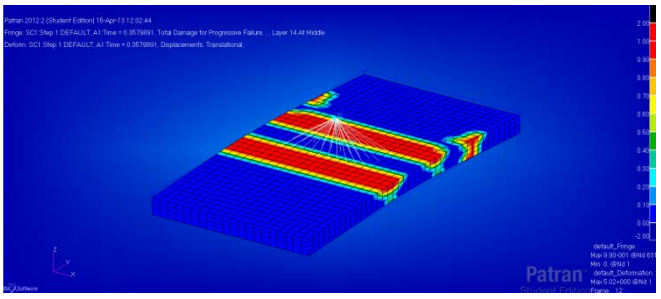

d) 35 % of total displacement

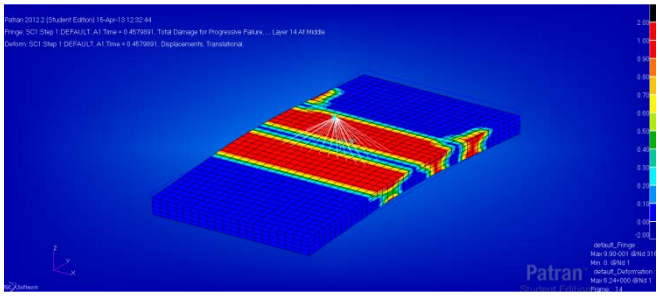

e) 45 % of total displacement

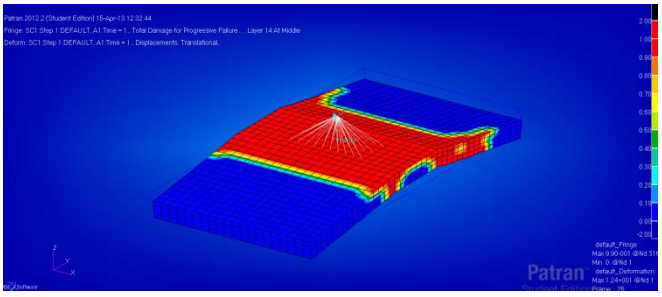

f) 100 % of total displacement

Figure C.4: Damage propagation for Hashin failure criterion with immediate stiffness degradation.

20mm laminate

Puck failure criterion

Gradual degradation

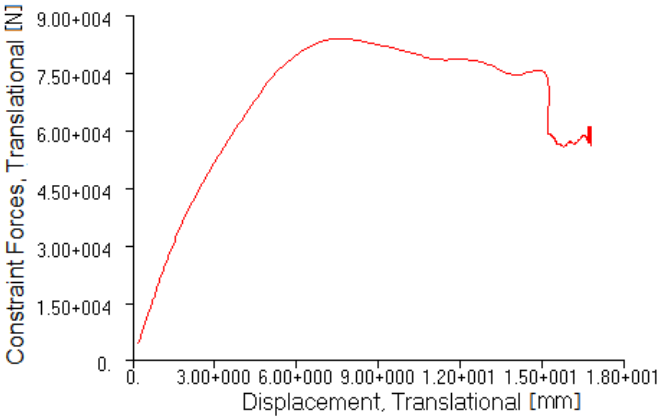

Figure C.5: Constraint force verses displacement for Puck failure criterion with gradual degradation.

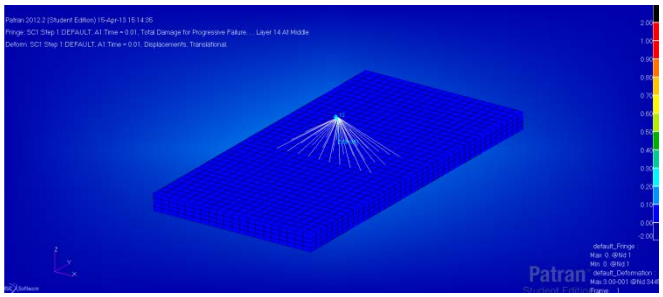

a) 0 % of total displacement

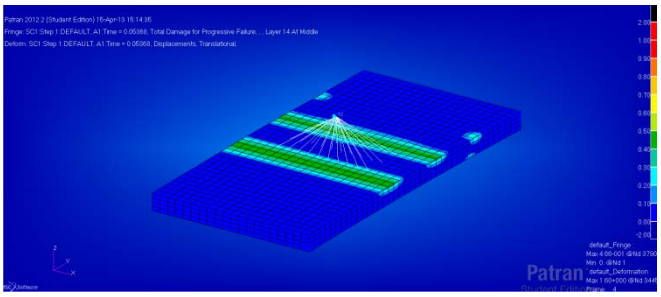

b) 06 % of total displacement

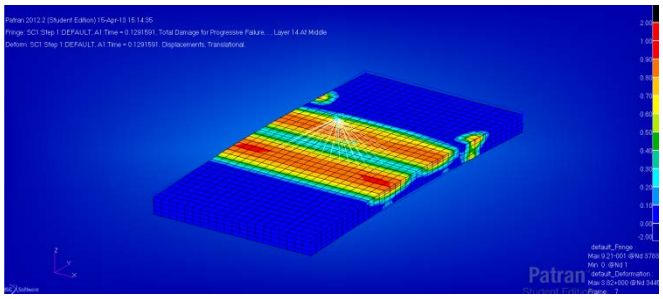

c) 12 % of total displacement

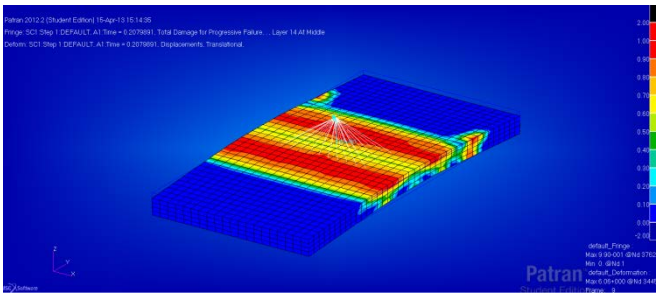

d) 20 % of total displacement

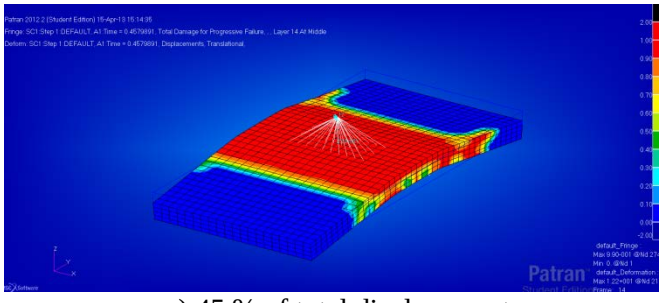

e) 45 % of total displacement

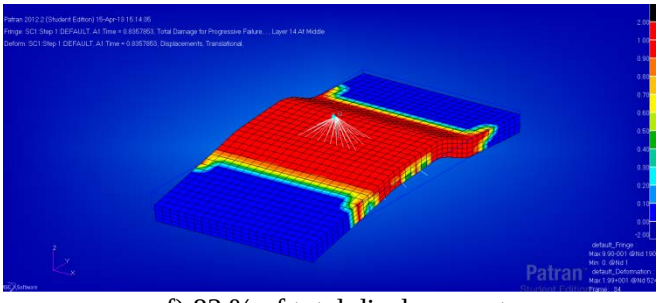

f) 83 % of total displacement

Figure C.6: Damage propagation for Puck failure criterion with gradual stiffness degradation.

20mm laminate

Puck failure criterion

Immediate degradation

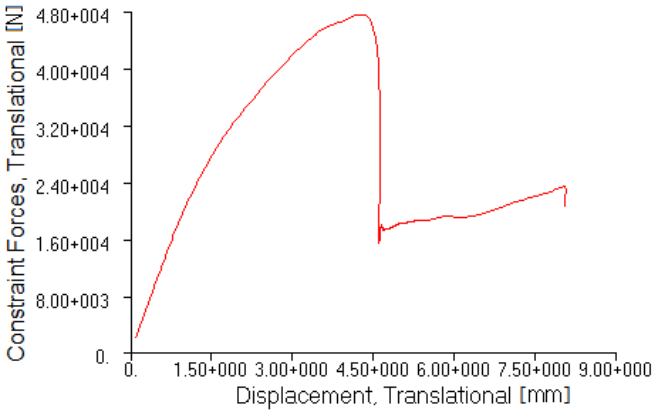

Figure C.7: Constraint force verses displacement for Puck failure criterion with immediate degradation.

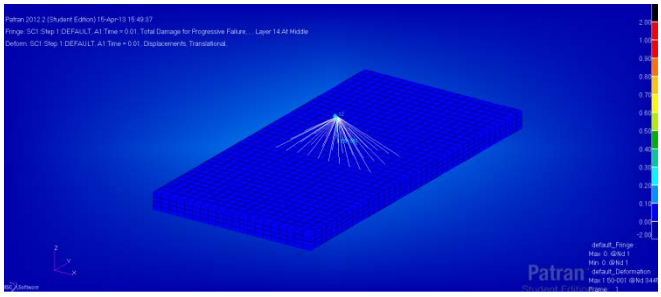

a) 0 % of total displacement

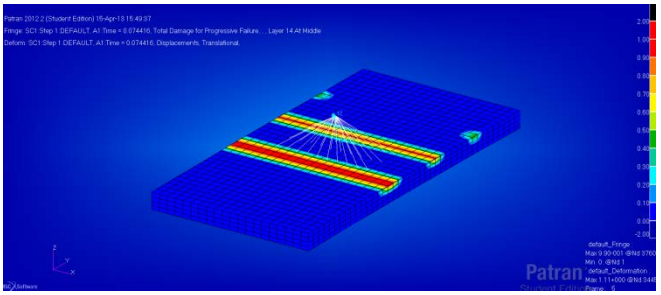

b) 07 % of total displacement

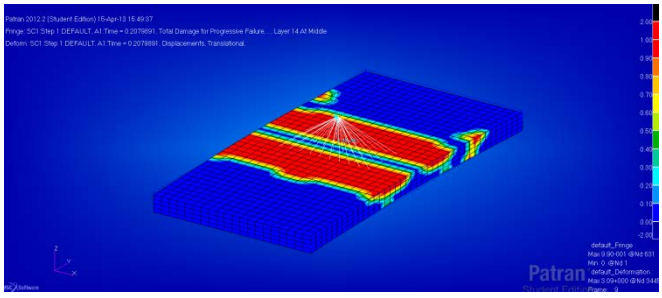

c) 20 % of total displacement

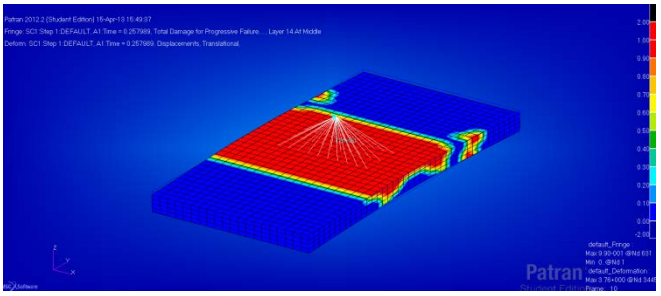

d) 25 % of total displacement

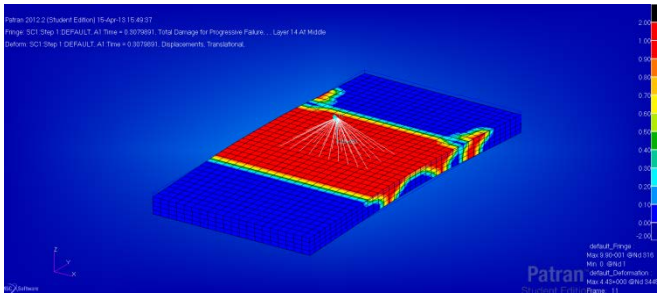

e) 30 % of total displacement

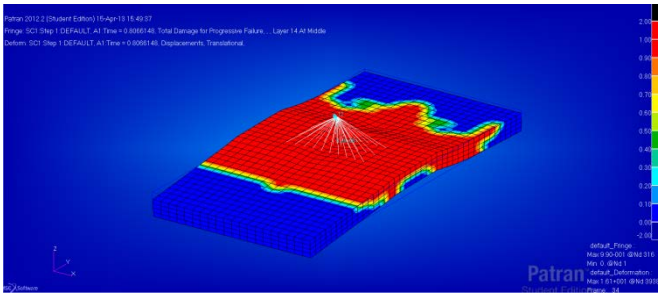

f) 80 % of total displacement

Figure C.8: Damage propagation for Puck failure criterion with immediate stiffness degradation.

30mm laminate

Hashin failure criterion

Gradual degradation

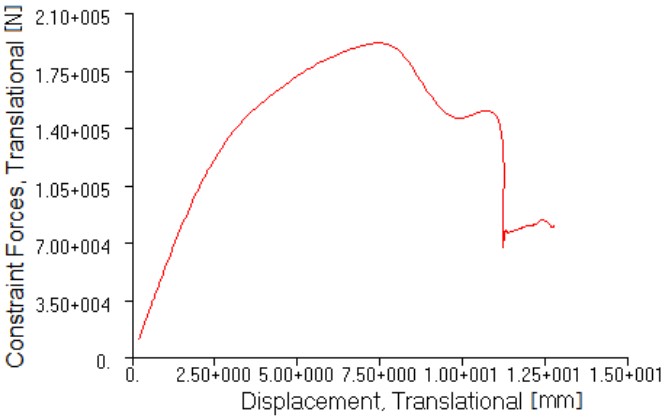

Figure C.9: Constraint force verses displacement for Hashin failure criterion with gradual degradation.

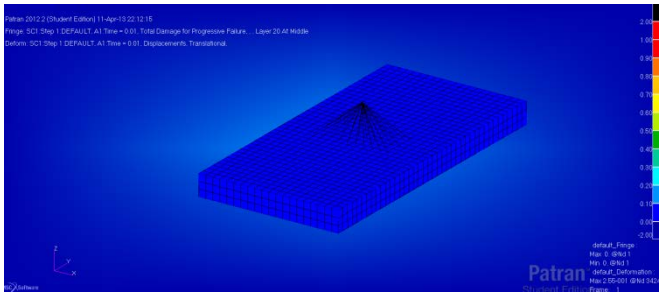

a) 0 % of total displacement

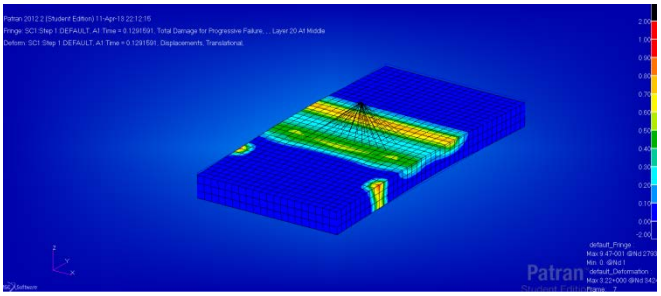

b) 12 % of total displacement

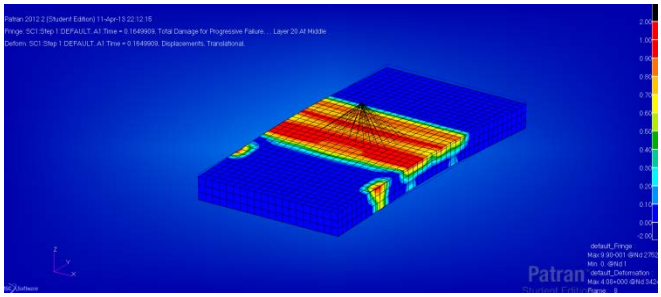

c) 16 % of total displacement

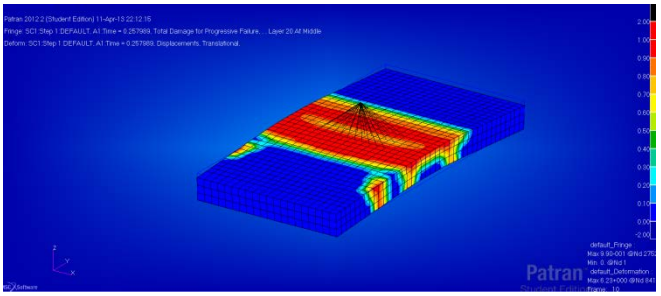

d) 25 % of total displacement

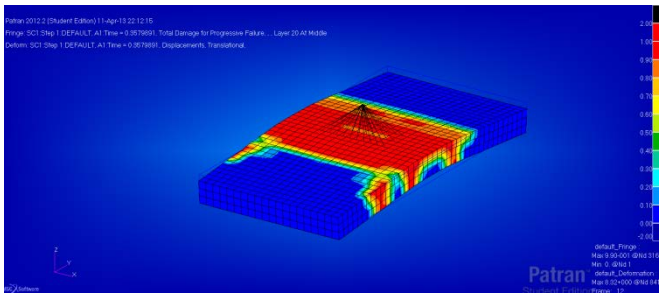

e) 35 % of total displacement

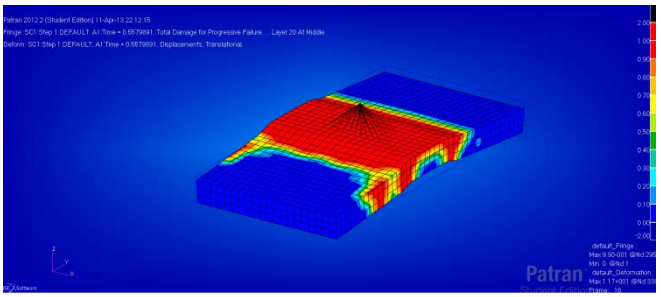

f) 55 % of total displacement

Figure C.10: Damage propagation for Hashin failure criterion with gradual stiffness degradation.

30mm laminate

Hashin failure criterion

Immediate degradation

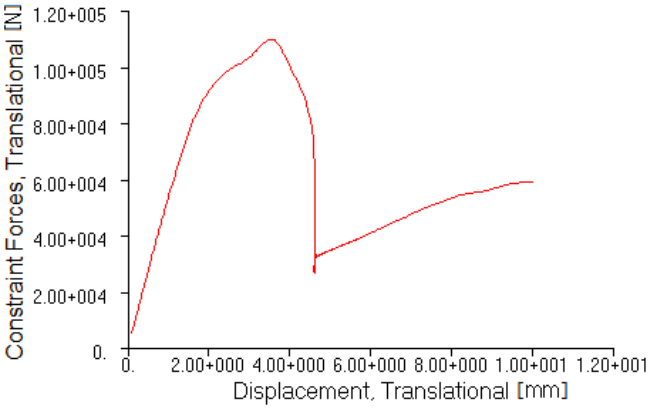

Figure C.11: Constraint force verses displacement for Hashin failure criterion with immediate degradation.

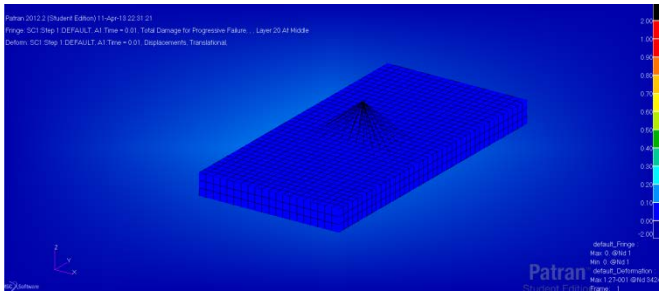

a) 0 % of total displacement

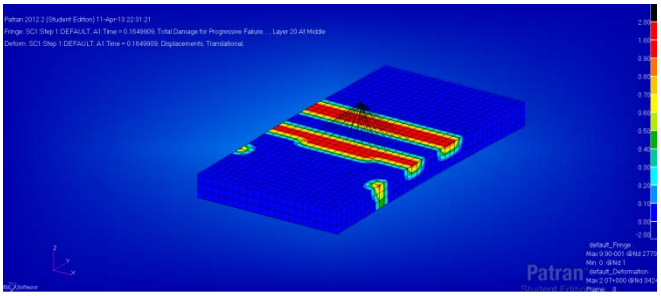

b) 16 % of total displacement

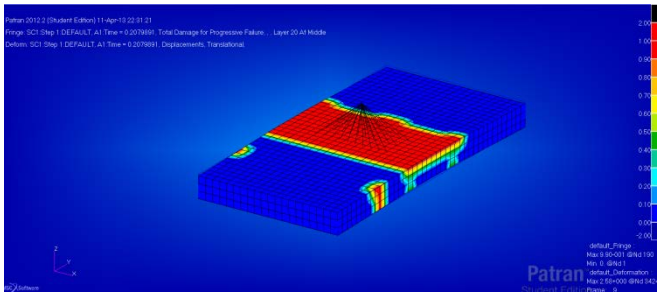

c) 20 % of total displacement

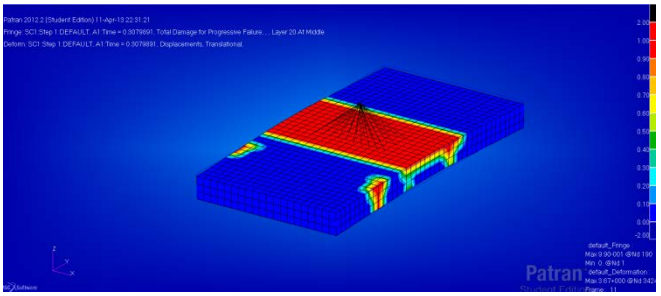

d) 30 % of total displacement

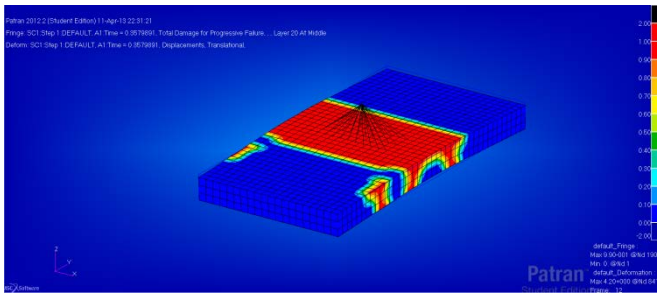

e) 35 % of total displacement

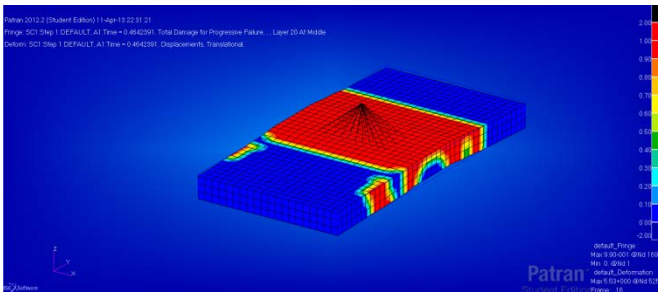

f) 45 % of total displacement

Figure C.12: Damage propagation for Hashin failure criterion with immediate stiffness degradation.

30mm laminate

Puck failure criterion

Gradual degradation

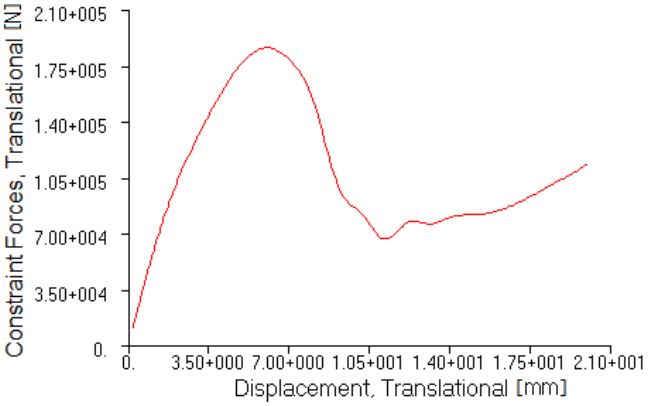

Figure C.13: Constraint force verses displacement for Puck failure criterion with gradual degradation.

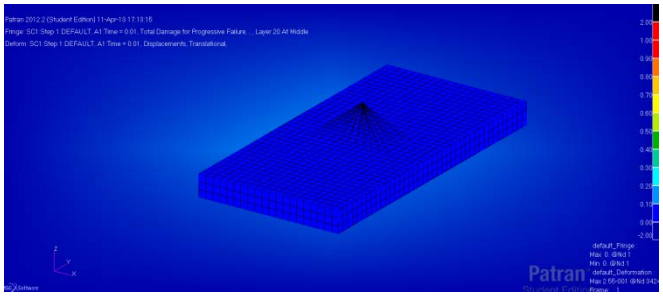

a) 0 % of total displacement

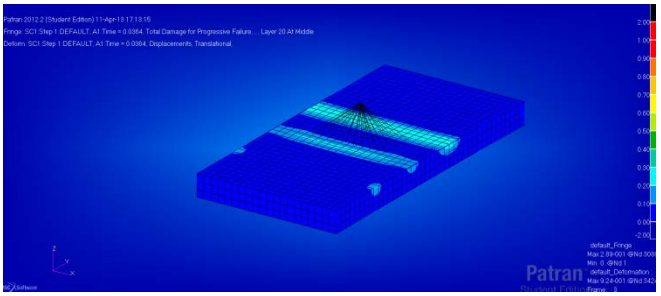

b) 03 % of total displacement

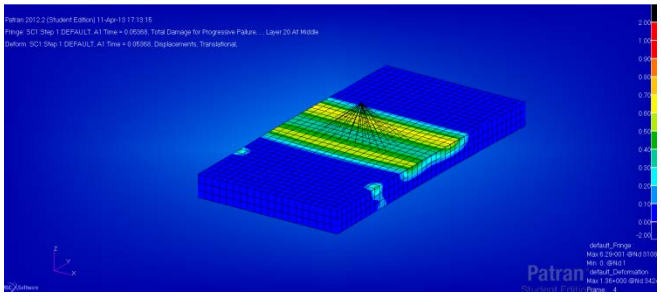

c) 05 % of total displacement

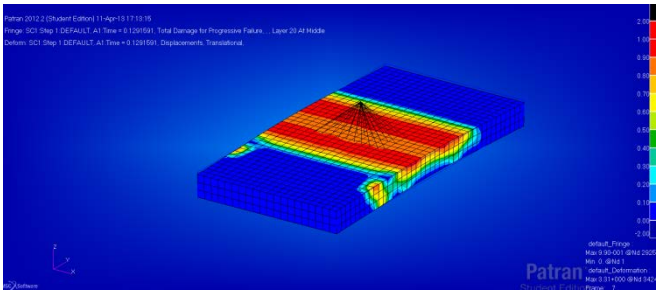

d) 12 % of total displacement

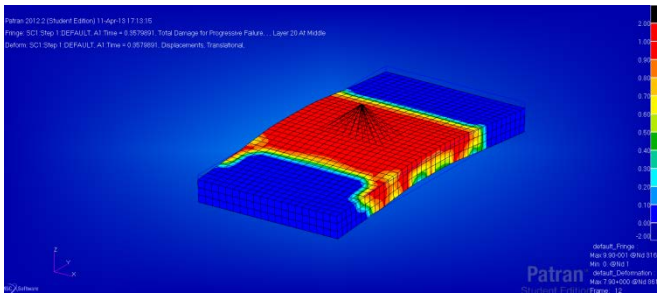

e) 35 % of total displacement

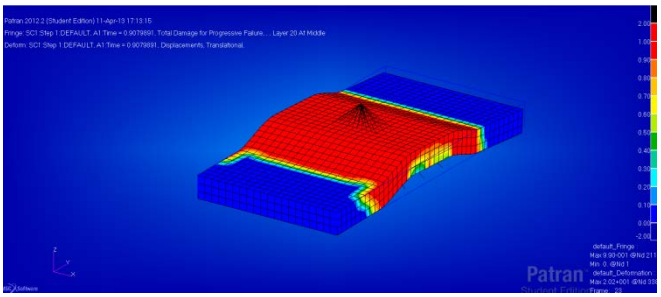

f) 90 % of total displacement

Figure C.14: Damage propagation for Puck failure criterion with gradual stiffness degradation.

30mm laminate

Puck failure criterion

Immediate degradation

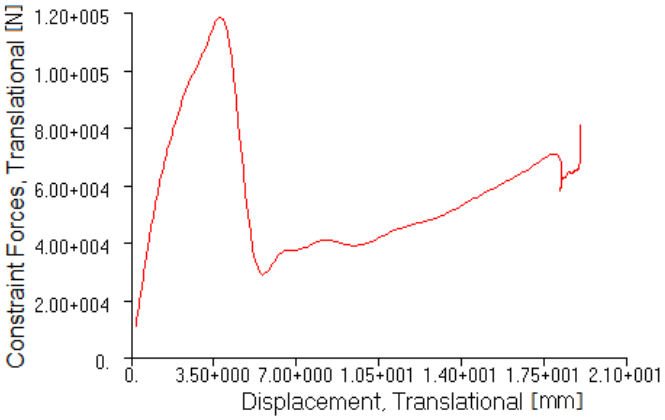

Figure C.15: Constraint force verses displacement for Puck failure criterion with immediate degradation.

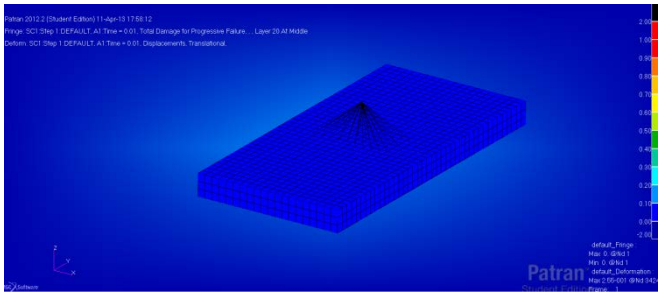

a) 0 % of total displacement

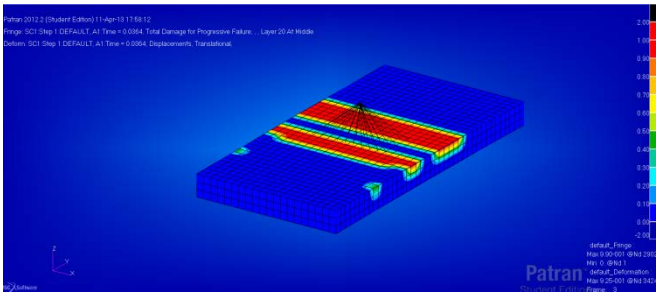

b) 03 % of total displacement

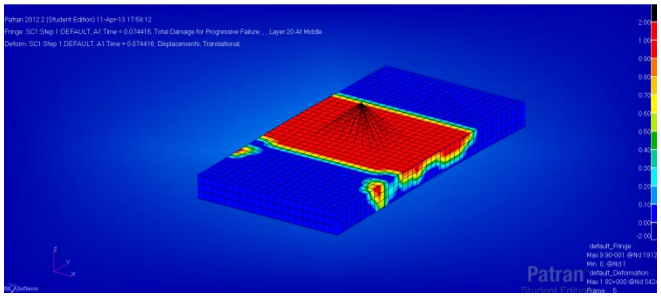

c) 07 % of total displacement

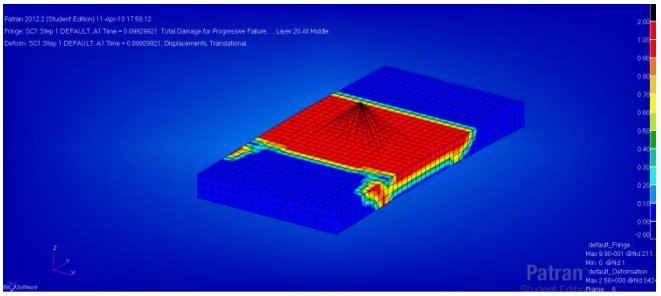

d) 10 % of total displacement

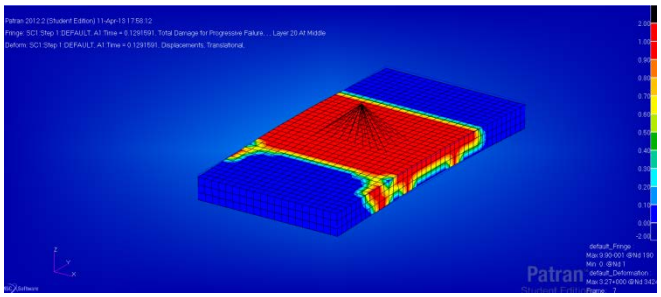

e) 12 % of total displacement

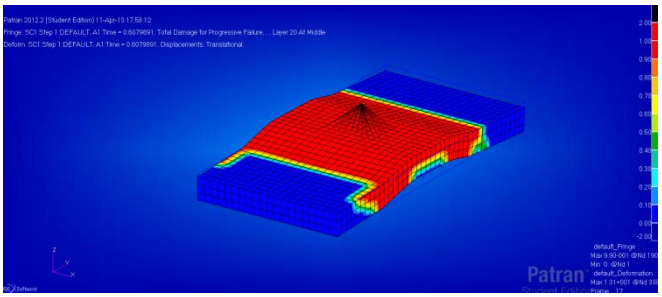

f) 60 % of total displacement

Figure C.16: Damage propagation for Puck failure criterion with immediate stiffness degradation.

40mm laminate

Hashin failure criterion

Gradual degradation

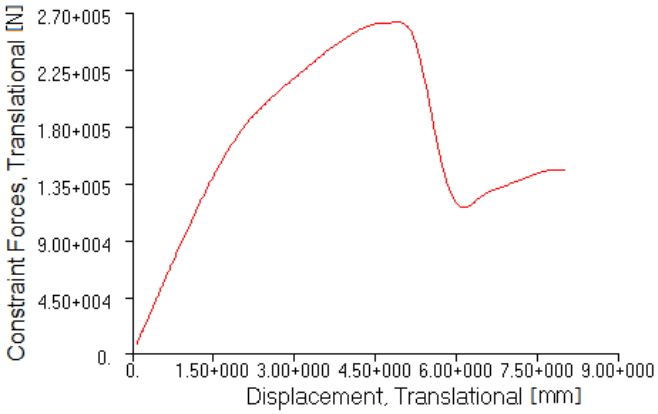

Figure C.17: Constraint force verses displacement for Hashin failure criterion with gradual degradation.

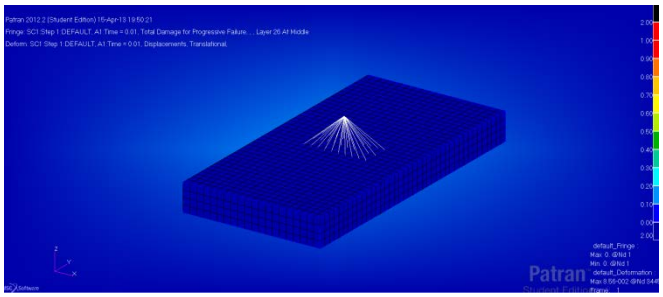

a) 0 % of total displacement

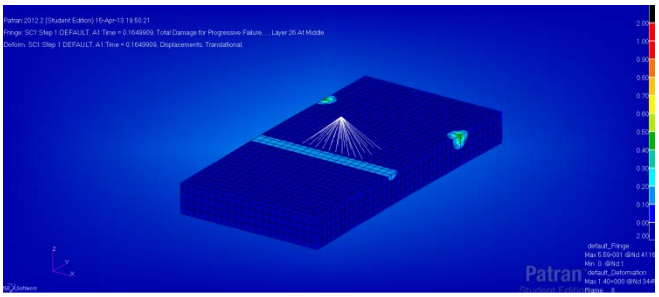

b) 16 % of total displacement

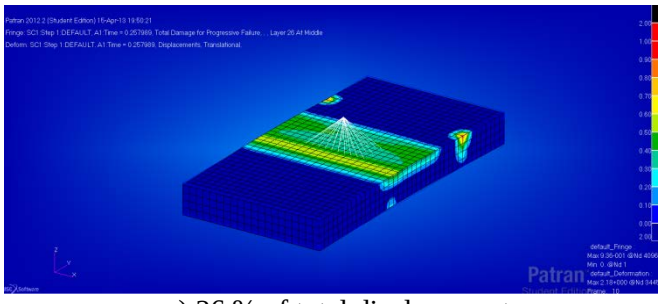

c) 26 % of total displacement

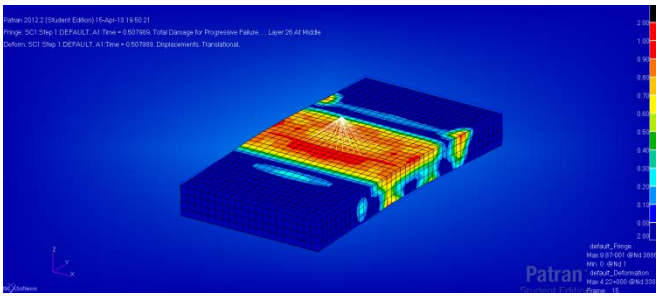

d) 50 % of total displacement

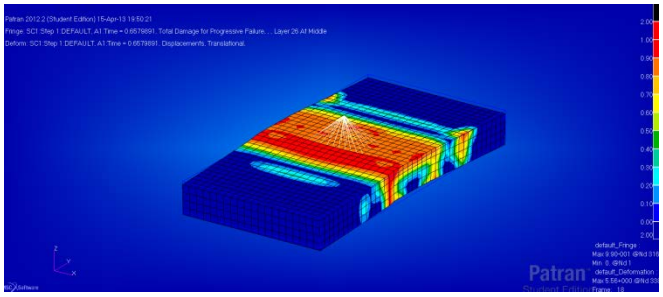

e) 65 % of total displacement

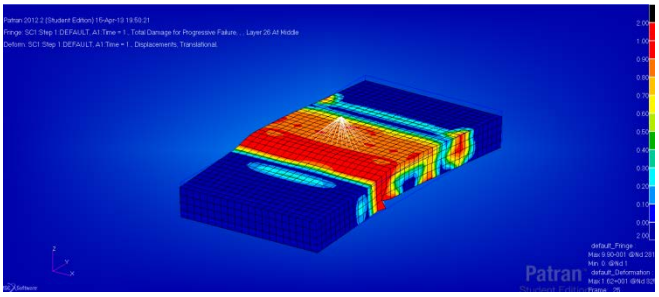

f) 100 % of total displacement

Figure C.18: Damage propagation for Hashin failure criterion with gradual stiffness degradation.

40mm laminate

Hashin failure criterion

Immediate degradation

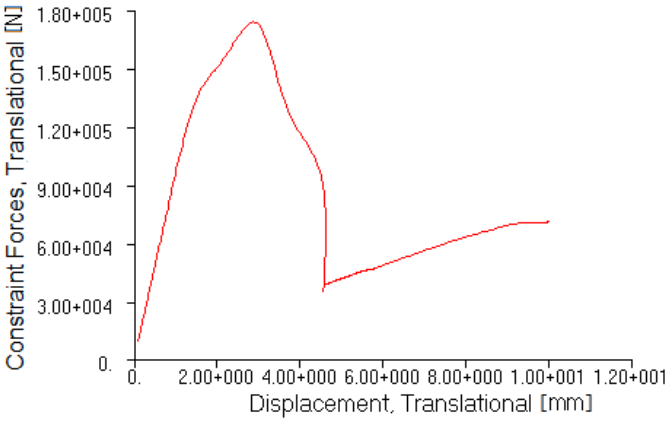

Figure C.19: Constraint force verses displacement for Hashin failure criterion with immediate degradation.

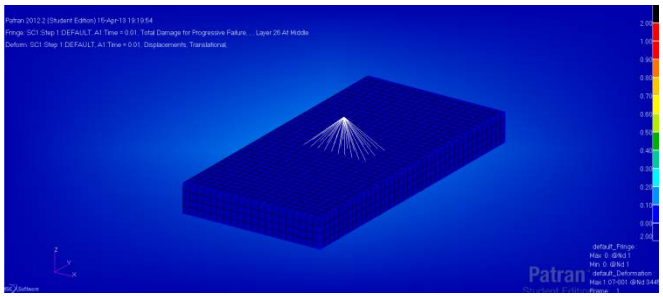

a) 0 % of total displacement

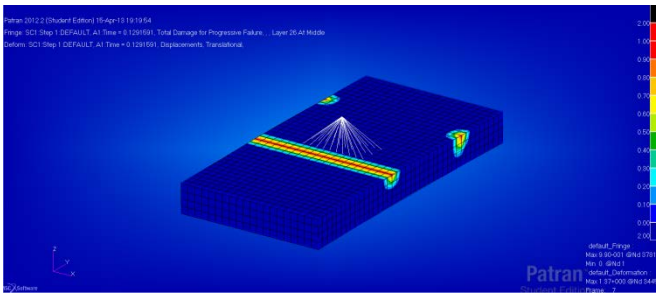

b) 13 % of total displacement

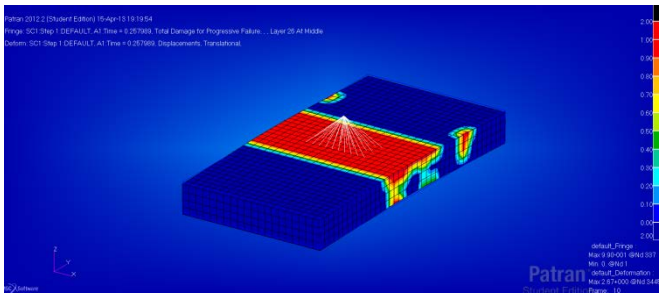

c) 26 % of total displacement

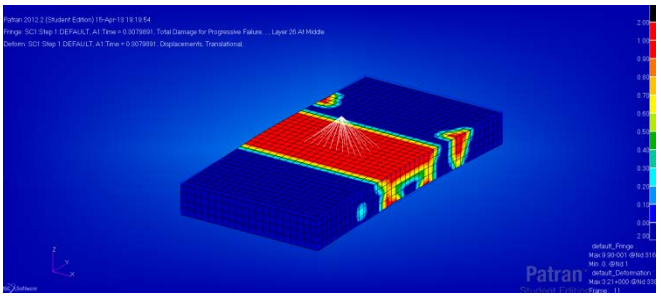

d) 30 % of total displacement

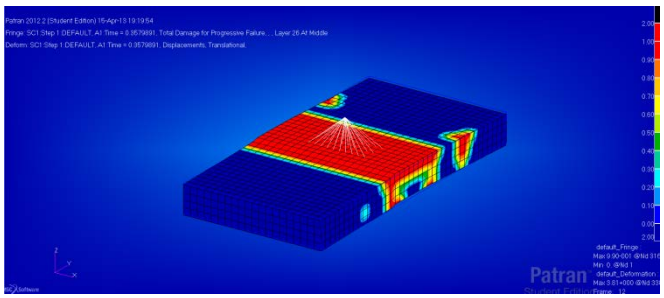

e) 35 % of total displacement

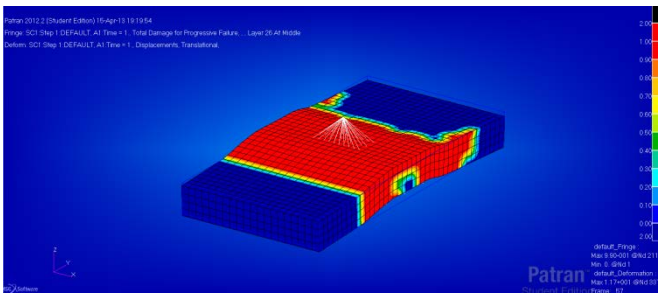

f) 100 % of total displacement

Figure C.20: Damage propagation for Hashin failure criterion with immediate stiffness degradation.

40mm laminate

Puck failure criterion

Gradual degradation

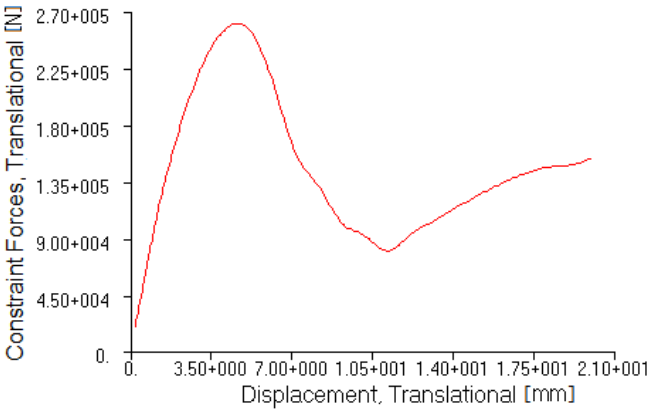

Figure C.21: Constraint force verses displacement for Puck failure criterion with gradual degradation.

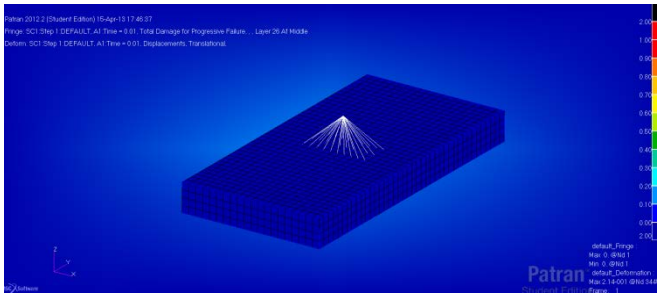

a) 0 % of total displacement

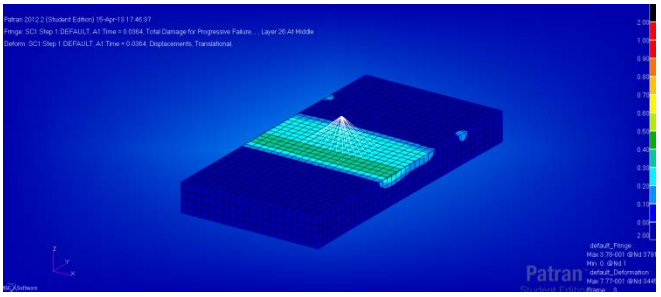

b) 03 % of total displacement

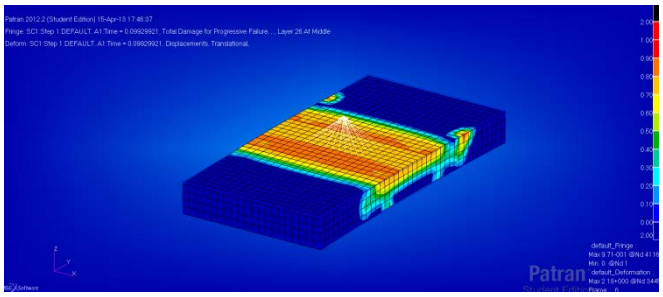

c) 10 % of total displacement

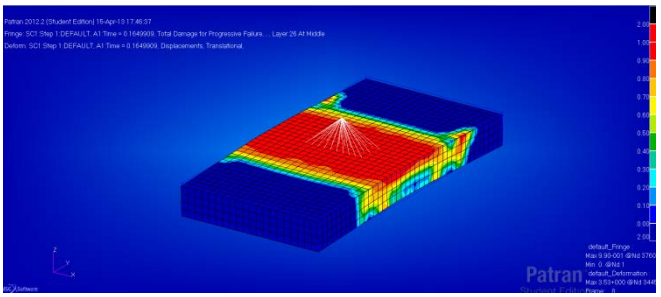

d) 16 % of total displacement

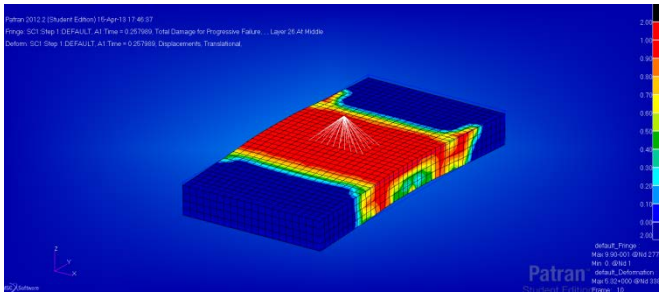

e) 25 % of total displacement

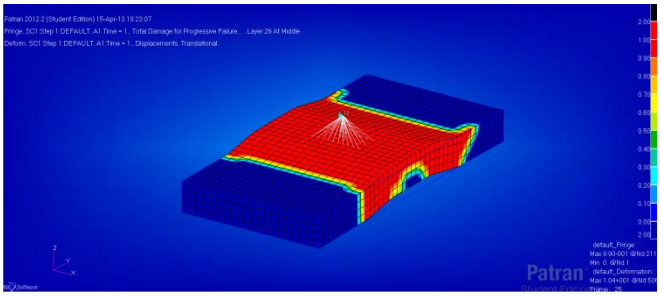

f) 100 % of total displacement

Figure C.22: Damage propagation for Puck failure criterion with gradual stiffness degradation.

40mm laminate

Puck failure criterion

Immediate degradation

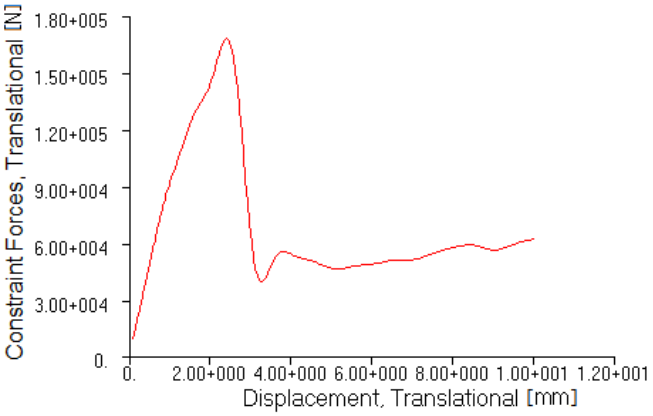

Figure C.23: Constraint force verses displacement for Puck failure criterion with immediate degradation.

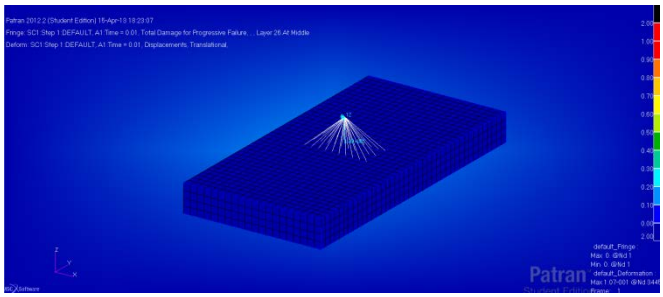

a) 0 % of total displacement

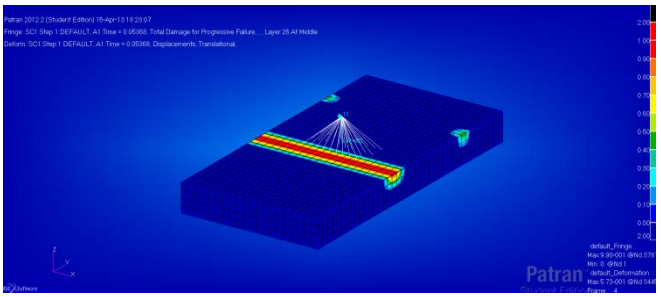

b) 05 % of total displacement

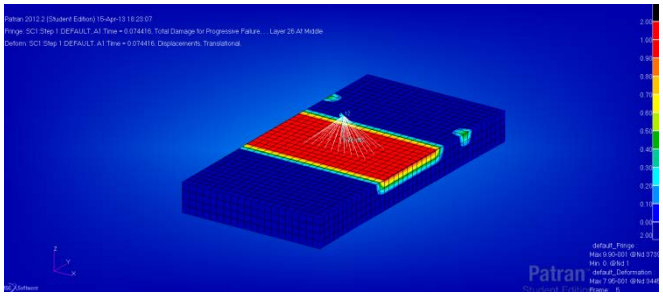

c) 07 % of total displacement

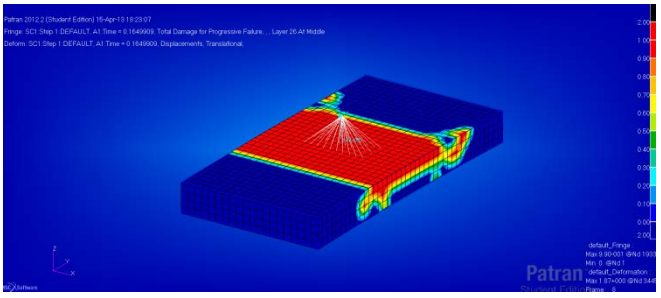

d) 16 % of total displacement

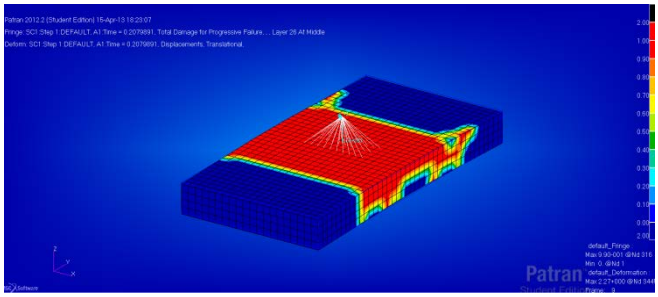

e) 20 % of total displacement

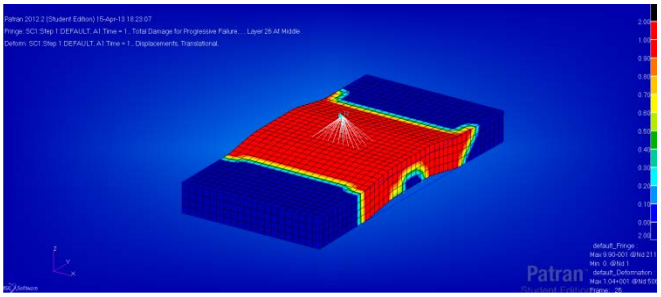

f) 100 % of total displacement

Figure C.24: Damage propagation for Puck failure criterion with immediate stiffness degradation.

Summary for Case 2

The result from the finite element results for Case 2, summarized in table C.1 is presented in figure C.25. The graph includes the breaking capacity for the three laminate thicknesses, 20, 30 and 40mm.

Table C.1: Finite element results of break load for lift point for Case 2.

Failure Criteria and degradation model	Break Load [*Te*] for 20mm laminate	Break Load [*Te*] for 30mm laminate	Break Load [*Te*] for 30mm laminate
Hashin and Gradual	9.5	19.3	26.1
Hashin and Immediate	5.4	11.0	17.4
Puck and Gradual	8.3	18.9	26.0
Puck and Immediate	4.8	12.0	16.8

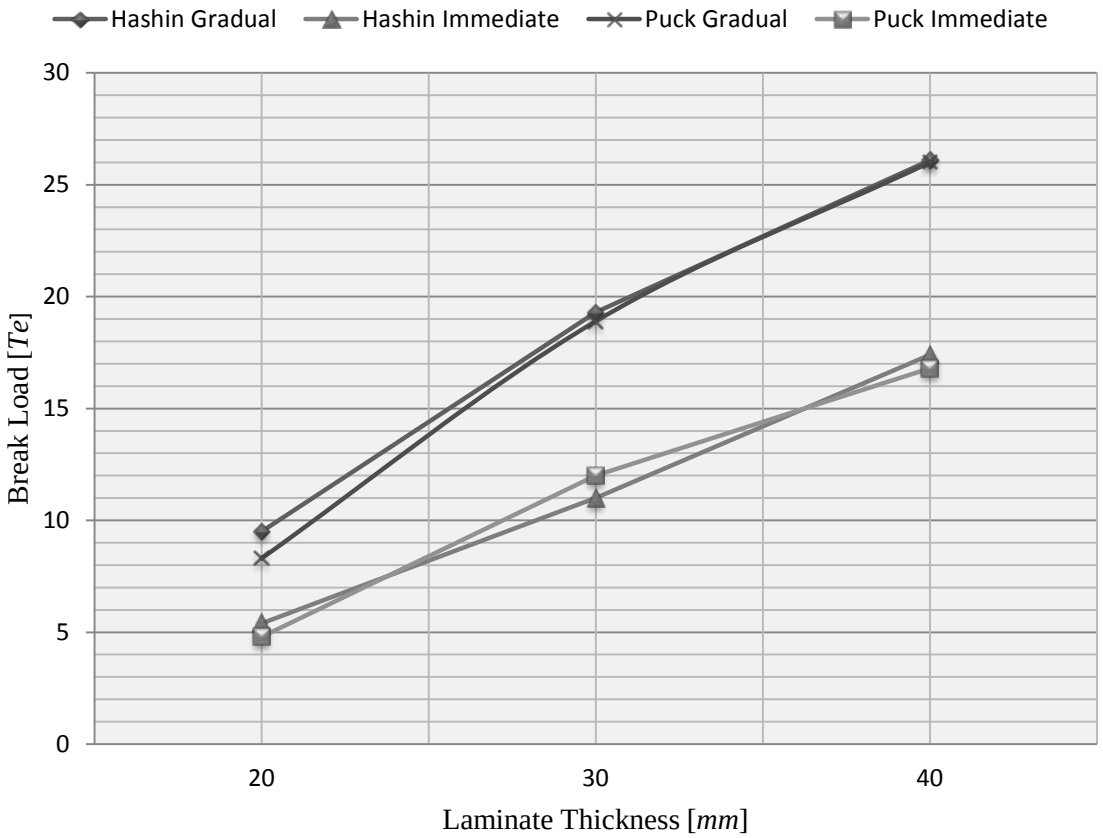

Figure C.25: Finite element analysis results of Case 2

Appendix D

Case 3

Geometric Approach

Lifting point capacity as a function of out-of-plane angle

Mathcad Sheet
Lift point capacity as a function of out-of-plane angle

Calculation of lift point capacity for 20mm

The maximum values chosen below represent the best analytical results compared to the testing.

$Te := 1000kg$

Maximum out-of-plane-load : (Hashin - Gradual from Test 2) $F_{z.20} := 9.5Te$

Maximum in-plane load : (Puck - Gradual from Test 1) $F_{p.20} := 45Te$

Lift point capacity function: $f_{20}(\theta) := \min\left(\frac{F_{z.20}}{\sin(\theta)}, \frac{F_{p.20}}{\cos(\theta)}\right)$

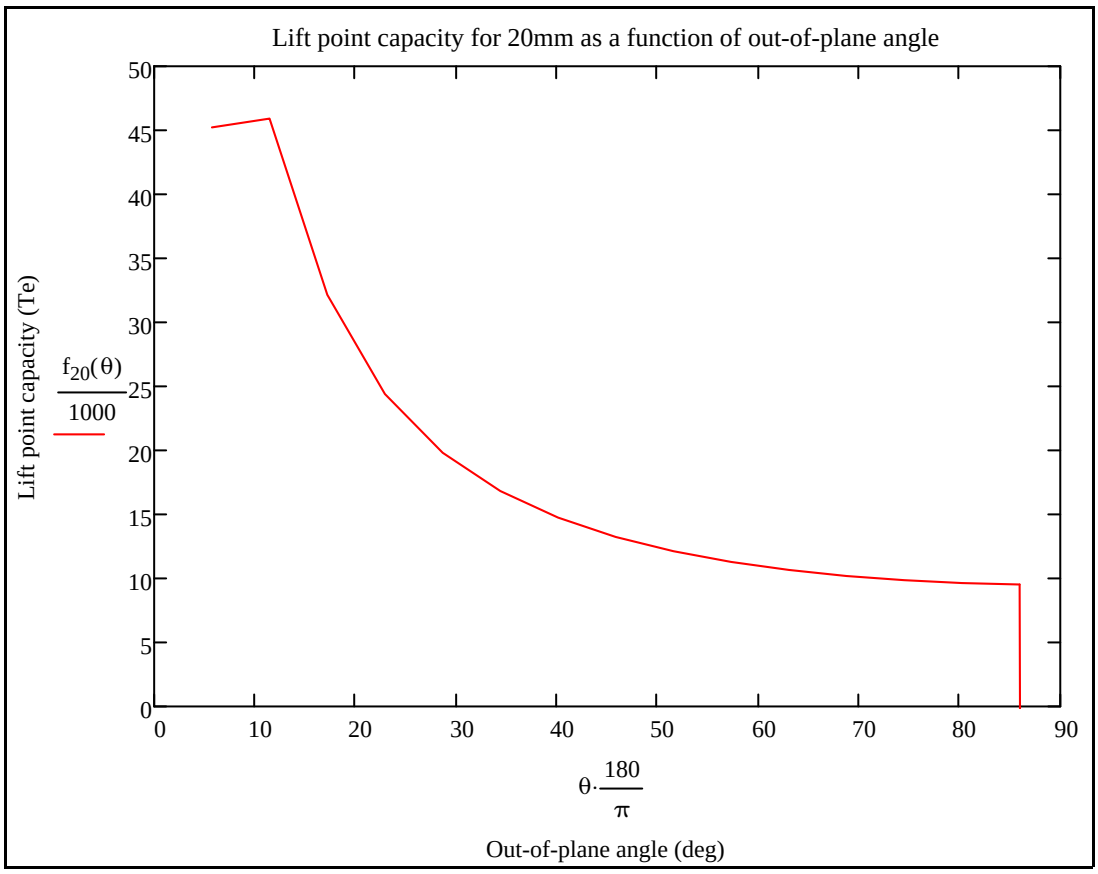

Lift point out-of-plane angle: $\theta_{20} := 45deg$

Lift point capacity: $f_{20}(\theta_{20}) = 13.4 \cdot Te$

Mathcad Sheet
Lift point capacity as a function of out-of-plane angle

Calculation of lift point capacity for 30mm

The maximum values chosen below represent the best analytical results compared to the testing.

Maximum out-of-plane-load :
(Hashin - Gradual from Test 2)

$F_{z.30} := 19.3Te$

Maximum in-plane load :
(Puck - Gradual from Test 1)

$F_{p.30} := 58Te$

Lift point capacity function:

$$f_{30}(\theta) := \min\left(\frac{F_{z.30}}{\sin(\theta)}, \frac{F_{p.30}}{\cos(\theta)}\right)$$

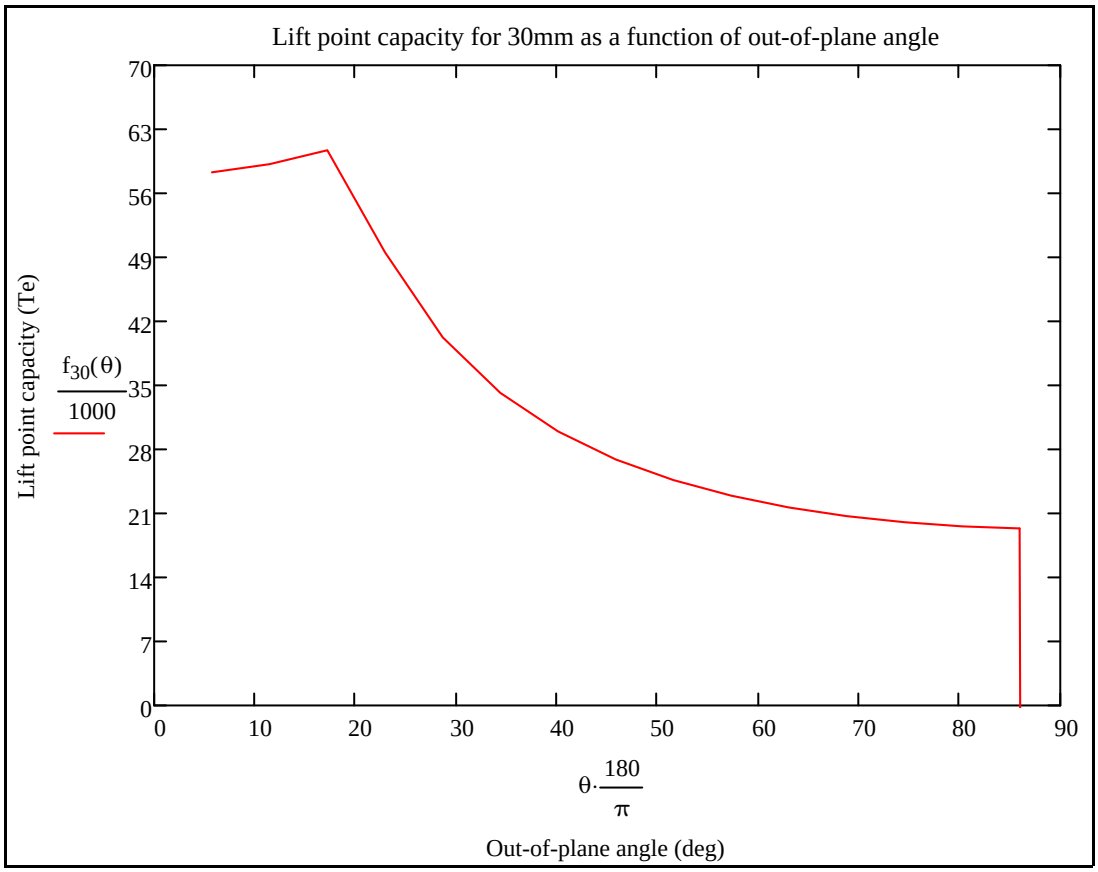

Lift point out-of-plane angle:

$\theta_{30} := 45deg$

Lift point capacity:

$f_{30}(\theta_{30}) = 27.3 \cdot Te$

Mathcad Sheet
Lift point capacity as a function of out-of-plane angle

Calculation of lift point capacity for 40mm

The maximum values chosen below represent the best analytical results compared to the testing.

Maximum out-of-plane-load :
(Hashin - Gradual from Test 2)

$F_{z.40} := 26.1Te$

Maximum in-plane load :
(Puck - Gradual from Test 1)

$F_{p.40} := 77Te$

Lift point capacity function:

$$f_{40}(\theta) := \min\left(\frac{F_{z.40}}{\sin(\theta)}, \frac{F_{p.40}}{\cos(\theta)}\right)$$

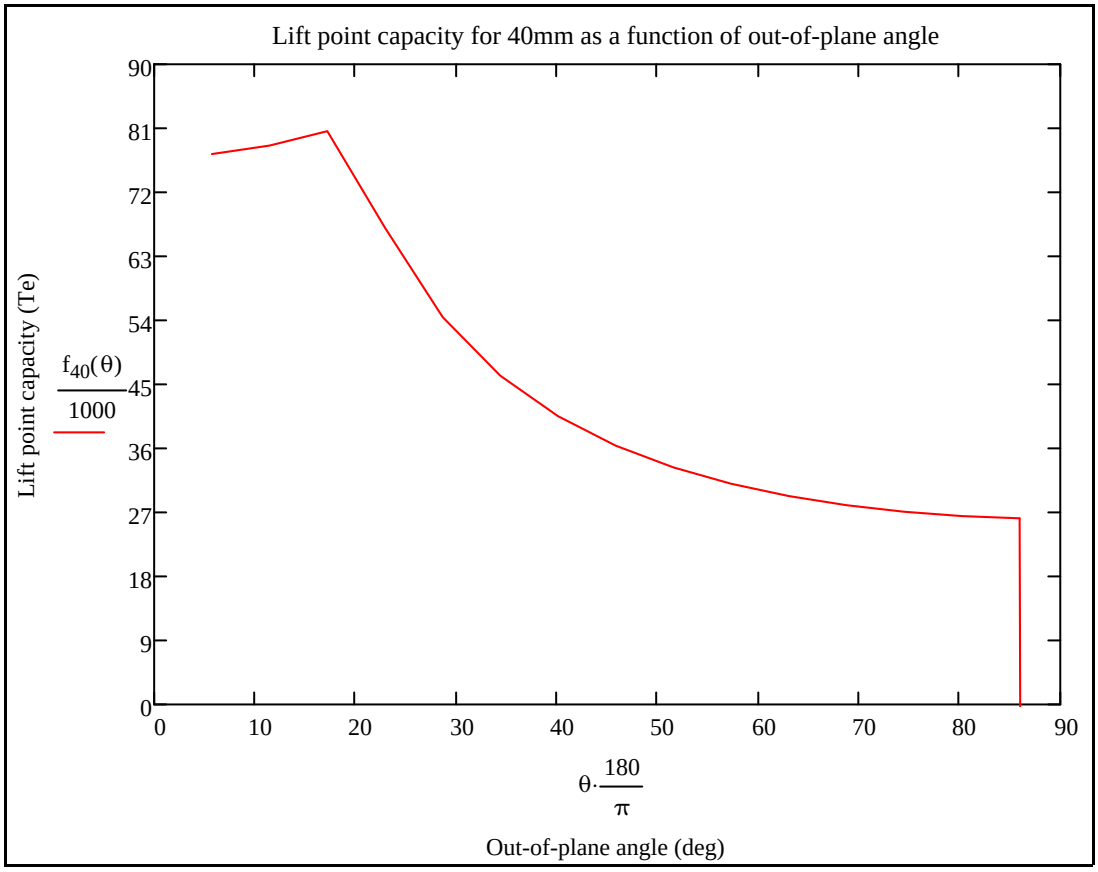

Lift point out-of-plane angle:

$\theta_{40} := 45deg$

Lift point capacity:

$f_{40}(\theta_{40}) = 36.9 \cdot Te$

Summary for Case 3

The result from the Mathcad Sheet is gathered in Table D.1 .The result the value at the approximate 45 degree range, which indicates the maximum load the GRP lift point can withstand before ultimate failure at Test 3.

The result from the capacity function appears in form of a graph based on the out of plane angle, and shows the ultimate break load for any given angle. The beauty of the graph is that it contains a lot of information, but is able to present them in a very delicate way. By using this graph for a specific laminate thickness one can find the capacity for any given angle and for any situation. It leads to a fast and effective way to fin the capacity.

Table D.1: Result for a representative of angles in the range of 35 to 45 degree.

Laminate Thickness [*mm*]	Break Load [*Te*] at angle $\theta = 35°$	Break Load [*Te*] at angle $\theta = 40°$	Break Load [*Te*] at angle $\theta = 45°$
20.0	16.6	14.8	13.4
30.0	33.6	30.0	27.3
40.0	45.5	40.6	36.9